

2013

## **Computational Material Modeling For Mechanical Properties Prediction And A Methodology For Mie Gruneisen Equation Of State Characterization Via Molecular/Nano Scale Cementitious Material Constituents**

Ahmed Mohamed

*North Carolina Agricultural and Technical State University*

Follow this and additional works at: <https://digital.library.ncat.edu/dissertations>



Part of the [Computational Engineering Commons](#), and the [Nanoscience and Nanotechnology Commons](#)

---

### **Recommended Citation**

Mohamed, Ahmed, "Computational Material Modeling For Mechanical Properties Prediction And A Methodology For Mie Gruneisen Equation Of State Characterization Via Molecular/Nano Scale Cementitious Material Constituents" (2013). *Dissertations*. 114.  
<https://digital.library.ncat.edu/dissertations/114>

This Dissertation is brought to you for free and open access by the Electronic Theses and Dissertations at Aggie Digital Collections and Scholarship. It has been accepted for inclusion in Dissertations by an authorized administrator of Aggie Digital Collections and Scholarship. For more information, please contact [iyanna@ncat.edu](mailto:iyanna@ncat.edu).

Computational Material Modeling for Mechanical Properties Prediction and a  
Methodology for Mie Gruneisen Equation of State Characterization via Molecular/Nano  
Scale Cementitious Material Constituents

Ahmed Mohamed

North Carolina A&T State University

A dissertation submitted to the graduate faculty  
in partial fulfillment of the requirements for the degree of

DOCTOR OF PHILOSOPHY

Department: Computational Science & Engineering

Major: Computational Science & Engineering

Major Professor: Dr. Ram Mohan

Greensboro, North Carolina

2013

School of Graduate Studies  
North Carolina Agricultural and Technical State University  
This is to certify that the Doctoral Dissertation of

Ahmed Mohamed

has met the dissertation requirements of  
North Carolina Agricultural and Technical State University

Greensboro, North Carolina  
2013

Approved by:

---

Dr. Ram Mohan  
Major Professor

---

Dr. Ajit Kelkar  
Committee Member

---

Dr. Sameer Hamoush  
Committee Member

---

Dr. Miguel Picornell  
Committee Member

---

Dr. Marwan Bikdash  
Department Chair

---

Dr. Kenneth Flurchick  
Committee Member

---

Dr. Sanjiv Sarin  
Dean, The Graduate School



### Biographical Sketch

Ahmed Mohamed was born on May 20, 1969 in Alexandria, Egypt. He is the first born in the family of Mr. Nabil Mohamed and Mrs. Samira Metawee. Ahmed is the husband of Mrs. Riem Rostom, and the proud father of Adam Mohamed. Ahmed has one younger brother Dr. Mohamed Nabil, PhD. Ahmed graduated from El Abassia High School in 1986 and attended Alexandria University in Egypt where he earned a Bachelor of Science degree in Civil Engineering in 1992.

After graduating from college, Ahmed worked as a construction engineer in Egypt until 1997. He started his own general contracting company and successfully delivered residential and commercial projects until 1999.

In December 1999, Ahmed immigrated to the United States of America and worked in engineering firms in New York until 2006. He then moved to North Carolina and worked in a land development design company. By 2008 he decided to continue his education and earned a masters degree in Civil Engineering.

After earning the master degree, Ahmed became interested in the new PhD program in the computational science and engineering department and opted to continue his studies combining engineered materials and computational modeling.

## Dedication

This dissertation is dedicated to the memory of my father. It is also dedicated to my mother, my lovely wife, my wonderful son, my brother, and to all my family and friends who supported and helped me accomplish my goal in attaining higher education.

## Acknowledgements

First of all, I would like to thank almighty God for granting me the opportunity and providing me with the strength to accomplish this goal.

I gratefully acknowledge Dr. Ram Mohan my major advisor for his supervision, advice, and support. Without his support and persistence, this research would not have been possible. I would also like to thank him for the many academic conversations, from which I will benefit for the rest of my life.

I would like to thank my Committee Members from Civil Engineering Department Dr. Sameer Hamoush, Dr. Miguel Picornell, and from Computational Science and Engineering Department Dr. Marwan Bikdash, Dr. Kenneth Flurchick, and from Nano Engineering Department Dr. Ajit Kelkar for their help, advice, useful discussions from the beginning of my work and research to the end, and as my teachers throughout my graduate school experience. I will always be grateful for everything I learned from all of them. I also would like to thank Dr. John Rivas for all his technical support.

The support from U.S. Army Research Office under a Partnership in Research Transition (PIRT) cooperative agreement award contract W911NF-11-2-0043 (CAM: Dr. Joe Myers, ARO; Co-CAM: Mr. Wayne Hodo, ERDC). Technical discussions with Mr. Wayne Hodo are gratefully acknowledged. Thanks are also due to University of Mississippi, Oxford researchers for technical discussions in the early stages.

Finally, special thanks go to the Computational Science and Engineering Department and Joint School of Nanoscience and Nanoengineering professors, staff, and students for helping me throughout my graduate school experience.

## Table of Contents

List of Figures .....	xii
List of Tables .....	xv
Abstract .....	2
CHAPTER 1 Introduction.....	3
1.1 Cementitious Materials Molecular Level Constituents.....	4
1.1.1 Unhydrated cement constituents. ....	4
1.1.2 Hydrated cement products.....	6
1.2 Cement Molecular Structure .....	8
1.3 Computational Modeling .....	12
1.3.1 Quantum scale level. ....	15
1.3.2 Nano scale level.....	15
1.4 Mechanical Properties of Cementitious Materials – Literature Review .....	16
1.5 Mechanical Properties Prediction via MD for Cementitious Materials –Current Literature and State of Art .....	18
1.6 MD Mechanical Properties Prediction at Higher Pressures .....	19
1.7 Shock Wave Propagation .....	20
1.8 Equation of State Models .....	21
1.9 MD Modeling of Shock Wave Effects on Materials.....	22
1.10 Dissertation Organization.....	22



CHAPTER 2 Molecular Dynamics Background .....	24
2.1 Accelrys Materials Studio .....	26
2.2 Force Field.....	27
2.2.1 Bonded terms.....	29
2.2.1.1 Bond stretching term.....	29
2.2.1.2 Bond angle bending term.....	30
2.2.1.3 Bond angle rotation term.....	30
2.2.1.4 Out of plane angle term.....	31
2.2.2 Non-bonded terms.....	31
2.2.2.1 Van der Waals forces term.....	31
2.2.2.2 Electrostatic forces term.....	33
2.2.3 Cross terms.....	33
2.3 Molecular Dynamics .....	33
2.3.1 Energy minimization.....	34
2.3.2 Dynamic simulation.....	36
2.3.2.1 Euler algorithm.....	37
2.3.2.2 Modified Euler algorithm.....	38
2.3.2.3 4th order Runge-Kutta method (RK4) algorithm.....	38
2.3.2.4 Verlet algorithm.....	38
2.3.2.5 Velocity Verlet and Leapfrog algorithms.....	39

2.3.2.6 Predictor Corrector algorithm.....	40
2.3.3 Mechanical properties calculation.....	41
2.4 Dynamic Run Parameters.....	42
2.4.1 Periodic boundary conditions (PBC).....	42
2.4.2 Statistical ensembles.....	43
2.4.3 Temperature control methods.....	44
2.4.3.1 Velocity scaling.....	44
2.4.3.2 Berendsen method.....	44
2.4.3.3 Nose method and Nose-Hoover method.....	45
2.4.3.4 Andersen method.....	45
2.4.4 Pressure control methods.....	45
2.4.4.1 Andersen method.....	45
2.4.4.2 Berendsen method.....	46
2.4.4.3 Parrinello-Rahman method.....	46
2.4.5 Time step.....	46
2.4.6 Dynamic time.....	47
2.4.7 Cutoff distance.....	47
2.5 Analysis Details.....	48
CHAPTER 3 Mechanical Properties Prediction.....	50
3.1 Mechanical Properties.....	51

3.2 MD Simulation Parameters for Initial Analysis .....	53
3.3 Comparison of Mechanical Properties Predicted from Different MD Analysis Time Durations .....	54
3.4 Influence of Different Molecular Cell Sizes on the Predicted Mechanical Properties .....	56
3.5 MD Modeling Analysis for Mechanical Property Predictions .....	58
3.5.1 Comparison of MD analysis predicted mechanical properties for C <sub>3</sub> S and C <sub>2</sub> S .....	58
3.5.2 Hydrated cement CH mechanical properties comparison. ....	61
3.5.3 C-S-H MD predicted mechanical properties and comparison to literature values .....	62
3.6 Property Predictions at Higher Pressure States via MD Analysis .....	65
3.6.1 C <sub>3</sub> S MD analysis of mechanical properties at high pressures. ....	66
3.6.2 C <sub>2</sub> S MD analysis predicted mechanical properties at different pressures .....	66
3.6.3 MD analysis of mechanical properties for CH at different ensemble pressures. ....	67
3.6.4 C-S-H Jennite MD analysis predicted mechanical properties at various ensemble pressure states .....	68
3.6.5 MD analysis for predictive mechanical properties for C-S-H Tobermorite 14 at different ensemble pressure states .....	68
3.6.6 Poisson's ratio at different ensemble pressure states. ....	69
3.7 Computational Resources .....	70
3.8 Concluding Remarks .....	71

CHAPTER 4 MD Methodology for Mie-Gruneisen EOS Characterization .....	72
4.1 Shock Wave Propagation Theory.....	73
4.1.1 Continuum mechanics equations.....	75
4.1.2 Jump equations.....	77
4.1.3 Equation of state.....	79
4.2 Hugoniot Curves .....	82
4.2.1 Pressure-specific volume Hugoniot.....	83
4.2.2 Longitudinal stress-specific volume Hugoniot.....	83
4.2.3 Proposed material model.....	85
4.3 Prior MD Modeling Analysis.....	87
4.4 Current MD Analysis Methodology.....	89
4.4.1 MD#1 Isothermal compression MD modeling analysis.....	89
4.4.2 MD#2 Estimation of Gruneisen parameter MD modeling analysis.....	91
4.4.3 MD#3 Estimation of ultimate shear strength MD modeling analysis.....	93
4.5 Concluding Remarks.....	95
CHAPTER 5 MD Prediction of Mie-Gruneisen EOS Model for C-S-H Jennite .....	96
5.1 MD#1 Isothermal Compression Modeling Analysis.....	97
5.2 MD#2 Estimation of Gruneisen Parameter MD Modeling Analysis .....	99
5.3 MD#3 Estimation of Shear Strength MD Modeling Analysis .....	102
5.4 Longitudinal Stress vs. Specific Volume Hugoniot Curve .....	105

5.5 MD#1 Modeling Analysis for Larger C-S-H Jennite Structure .....	105
5.6 Concluding Remarks .....	109
CHAPTER 6 Conclusion .....	110
6.1 Concluding Remarks .....	110
6.3 Future Directions.....	111
References.....	112
<i>Appendix A</i> .....	116

## List of Figures

Figure 1.1 Cementitious materials hierarchical structure. ....	3
Figure 1.2 Compressive strength of Portland cement compounds. ....	5
Figure 1.3 Hydration process over time.....	7
Figure 1.4 Representation of $C_3S$ molecular structure.....	8
Figure 1.5 Representation of $C_2S$ molecular structure.....	9
Figure 1.6 Representation of CH molecular structure. ....	9
Figure 1.7 Representation of C-S-H Jennite mineral.....	11
Figure 1.8 Representation of C-S-H Tobermorite mineral. ....	12
Figure 1.9 Different scale levels, time scales, and applicable computational modeling methods.	14
Figure 2.1 Bond stretching term. ....	29
Figure 2.2 Bond angle bending term.....	30
Figure 2.3 Dihedral angle rotation term.....	31
Figure 2.4 Out of plane angle. ....	31
Figure 2.5 Van der Waals forces attractive and repulsive. ....	32
Figure 2.6 Molecular dynamics analysis process. ....	34
Figure 2.7 Periodic boundary conditions illustration.....	43
Figure 2.8 Cutoff distance.....	48
Figure 3.1 Predicted mechanical properties from MD analysis employing different dynamics time durations.....	55
Figure 3.2 Mechanical properties for different cell sizes. ....	57
Figure 3.3 $C_3S$ mechanical properties results comparison.....	59
Figure 3.4 $C_2S$ mechanical properties results comparison.....	60

Figure 3.5 CH mechanical properties comparison.....	62
Figure 3.6 C-S-H Jennite mechanical properties comparison. ....	63
Figure 3.7 Tobermorite 14 mechanical properties comparison. ....	64
Figure 3.8 C <sub>3</sub> S modulus results at higher pressures.....	66
Figure 3.9 C <sub>2</sub> S properties vs. pressure values (0.0001-2.0) GPa.....	67
Figure 3.10 MD analysis of predicted properties for CH at various ensemble pressure range. ...	67
Figure 3.11 C-S-H Jennite mechanical properties vs. pressure. ....	68
Figure 3.12 C-S-H Tobermorite properties vs. pressure.....	68
Figure 3.13 Poisson's ratio at different pressure value. ....	69
Figure 4.1 Representation of shock wave propagation through medium. ....	73
Figure 4.2 Reference and current configurations of a body.....	75
Figure 4.3 Shock transition between uniform states.....	77
Figure 4.4 Material model flow chart. ....	86
Figure 4.5 Shear test at the molecular scale.....	88
Figure 4.6 Shear stress – strain variation [69]. ....	88
Figure 4.7 Schematic of NPT dynamic pressure profile for MD#1.....	90
Figure 4.8 Flow Chart: MD #1 - Isothermal compression MD modeling analysis. ....	91
Figure 4.9 Flow Chart: MD#2 - Gruneisen parameter MD modeling analysis. ....	92
Figure 4.10 Schematics of shear deformation.....	94
Figure 4.11 Flow Chart: MD #3 -Ultimate shear strength MD modeling analysis. ....	95
Figure 5.1 C-S-H Jennite crystalline structure.....	96
Figure 5.2 Isothermal pressure specific curve relationship. ....	98
Figure 5.3 Isothermal energy vs. specific volume relationship. ....	98

Figure 5.4 Determination of Gruneisen parameter. ....	99
Figure 5.5 Comparison of Gruneisen parameter. ....	101
Figure 5.6 Hugoniot pressure vs. specific volume. ....	101
Figure 5.7 Comparison between Isothermal and Hugoniot pressure vs. specific volume. ....	102
Figure 5.8 Shear stress-strain curves for different pressure increment structures. ....	104
Figure 5.9 C-S-H Jennite longitudinal stress - specific volume Hugoniot curve. ....	105
Figure 5.10 Four unit cells C-S-H Jennite molecular structure. ....	106
Figure 5.11 Isothermal pressure vs. specific curve relationship. ....	107
Figure 5.12 Isothermal energy vs. specific curve relationship. ....	107
Figure 5.13 Isothermal pressure vs. specific volume relation for C-S-H Jennite structures modeled using 1x1x1 unit cell and 4x4x4 unit cell. ....	108
Figure 5.14 Isothermal internal energy vs. specific volume relation for C-S-H Jennite structures modeled using 1x1x1 unit cell and 4x4x4 unit cell. ....	108



## List of Tables

Table 1.1 Portland Cement Compounds, Chemical Formulas, and Shorthand Notations .....	5
Table 1.2 ASTM C 150 Portland Cement Types[6] .....	6
Table 1.3 Some Hydrated Cement Products, their Chemical Formulas, and Mineral Phases .....	7
Table 1.4 Scale and Size Levels in Materials and Computational Methods.....	14
Table 3.1 Crystalline Structures Dimensions.....	54
Table 3.2 Poisson's Ratio at Different Dynamics Time Durations .....	56
Table 3.3 Predicted Poisson's Ratio from MD Analysis with Different Cell Sizes.....	57
Table 3.4 Mechanical Properties Results.....	58
Table 3.5 C <sub>3</sub> S MD Analysis Predictions and Available Literature Data .....	59
Table 3.6 C <sub>2</sub> S MD Analysis Predictions and Available Literature Data .....	60
Table 3.7 CH MD Analysis Predictions and Literature Data .....	61
Table 3.8 Jennite C-S-H MD Analysis Mechanical Properties and Literature Data .....	63
Table 3.9 C-S-H Tobermorite 14 Mechanical Properties Comparison.....	64
Table 3.10 Computing Time for Different Pressures.....	70
Table 3.11 Computing Time for Different Cell Sizes and Dynamic Time Models.....	71
Table 5.1 C-S-H Jennite Ultimate Shear Strength Values for Different Molecular Structures ..	103

## Abstract

Cementitious materials have complex hierarchical structures with random features that range from nanometer (*nm*) to millimeter (*mm*) scale. Processes occurring at the nanometer scale affect the performance at larger length scales. The present work employs molecular dynamics (MD) simulations as the computational modeling methodology to predict mechanical properties for both hydrated and unhydrated cementitious materials at the molecular/nano scale level. A detailed study on the effect of increasing MD simulation cell size, dynamics time duration on the predicted mechanical properties was performed. Further studies focused on understanding the effect of higher thermodynamic pressure states on predicted mechanical properties using MD based material modeling.

High strain rate behavior of materials undergoing shocks, detonations and other dynamic failure modes are characterized via an Equation of State (EOS) and Hugoniot curves to account for the associated adiabatic effects. A MD modeling methodology for the characterization of Mie Gruneisen EOS and Hugoniot curves based on molecular structures is developed and presented. This method is demonstrated for cement hydrated product (C-S-H Jennite) and the associated adiabatic longitudinal stress – specific volume relationship is developed. This method is based on the assumption that cementitious molecular constituents are confined and subjected to plane longitudinal shock waves. This allows their response to be investigated based on the estimation of shock Hugoniot curves.

## CHAPTER 1

### Introduction

Cement is the most used manufactured material world wide[1]. The world production of cement in the year 2010 was 3,300 million ton [2]. Cementitious materials are cement based materials such as cement paste, mortar, and concrete [3]. Cementitious materials have complex hierarchical structures with random features that range from nanometer (*nm*) to millimeter (*mm*) scale and beyond with each length scale representing a new random composite.

Figure 1.1 shows different cementitious materials structures with their corresponding scale levels[4]. Level-I is the molecular scale and presents individual molecular components, for example, calcium Silicate Hydrate (C-S-H) crystals. Level-II is the meso scale and represents cement paste which includes C-S-H, Calcium Hydrate (CH), water and some unhydrated cement. Level-III is the micro scale and represents mortar that consists of cement paste and granulated sand. Level-IV is the macro scale and represents concrete consisting of mortar and aggregates.

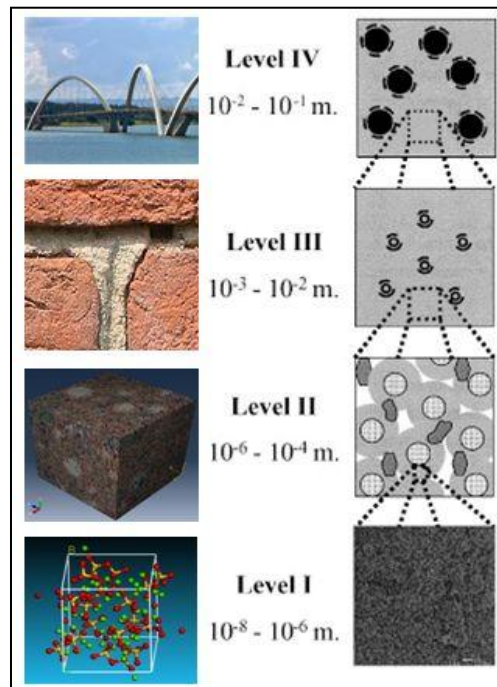


Figure 1.1 Cementitious materials hierarchical structure.

Cement paste is the binder for all cementitious materials and plays a very important role in their overall strength. It is also believed that the formation of C-S-H gel during the hydration and curing of cement-water mix controls the strength of cement paste [5]. Hydration process govern the development of hydrated cement molecular structures and the associated nanometer/molecular length features impacting their strength and characteristic behavior

Clearly, processes occurring at the nanometer scale affect the performance at larger length scales which makes it important to understand not only the phenomena and the behavior at the nano/molecular level but also how these changes build up to the macro level. This material science level understanding is essential to build towards improved cementitious materials design, their associated structures and their enhancements.

## **1.1 Cementitious Materials Molecular Level Constituents**

At nano/molecular scale level, there are two phases of cementitious materials: unhydrated or dry cement constituents, and hydrated cement products. Cement powder in its raw material form consists of unhydrated constituents, while the hydrated constituents are formed during the hydration process of water-cement mixture.

**1.1.1 Unhydrated cement constituents.** The most common cement form, Portland cement is formed by combining five raw materials: calcium oxide (CaO), silica (SiO<sub>2</sub>), alumina (Al<sub>2</sub>O<sub>3</sub>), iron oxide (Fe<sub>2</sub>O<sub>3</sub>), and calcium sulfate (CaSO<sub>4</sub>). Heating these raw materials at 1400 to 1600°C in a kiln results in chemical reactions to reproduce clinkers that include four key compounds shown in Table 1.1[3]. Throughout this dissertation the notation commonly followed in the cementitious material community is employed; C refers to CaO; S refers to SiO<sub>2</sub>, A refers to Al<sub>2</sub>O<sub>3</sub>, F refers to Fe<sub>2</sub>O<sub>3</sub>, and H refers to H<sub>2</sub>O.

Table 1.1

*Portland Cement Compounds, Chemical Formulas, and Shorthand Notations*

Name	Chemical formula	Shorthand notation
Tri-Calcium silicate (alite)	$3\text{CaO}\cdot\text{SiO}_2$	$\text{C}_3\text{S}$
Di-calcium silicate (belite)	$2\text{CaO}\cdot\text{SiO}_2$	$\text{C}_2\text{S}$
Tri-calcium aluminate	$3\text{CaO}\cdot\text{Al}_2\text{O}_3$	$\text{C}_3\text{A}$
Tetra-calcium aluminoferrite	$4\text{CaO}\cdot\text{Al}_2\text{O}_3\cdot\text{Fe}_2\text{O}_3$	$\text{C}_4\text{AF}$

The type of Portland cement depends on the proportions of these four main compounds plus calcium sulfate. ASTM C150 classifies Portland cement types by chemical components proportions as shown in Table 1.2 and performance measurements. One performance measurement is compressive strength as shown in Figure 1.2 [6]. The compressive strength depends on the composition of individual constituents resulting in different Portland cement types.

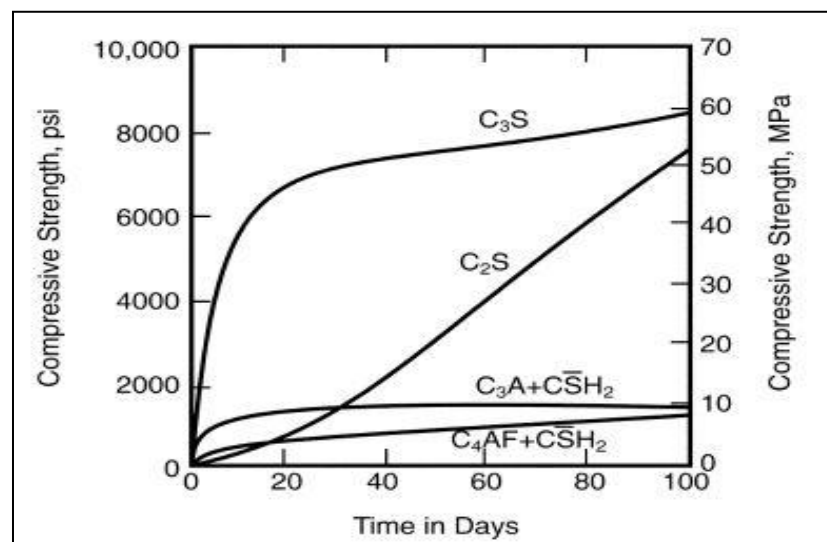


Figure 1.2 Compressive strength of Portland cement compounds.

Table 1.2

*ASTM C 150 Portland Cement Types[6]*

Cement Type	ASTM C 150	C <sub>3</sub> S %	C <sub>2</sub> S %	C <sub>3</sub> A %	C <sub>4</sub> AF %	Fineness m <sup>2</sup> /kg
I	General purpose	55	19	10	7	370
II	Moderate sulfate resistance (moderate heat of hydration)	51	24	6	11	370
III	High early strength	56	19	10	7	540
IV	Low heat of hydration	28	49	4	12	380
V	Sulfate resistant	38	43	4	9	380

For all five Portland cement types, C<sub>3</sub>S and C<sub>2</sub>S represent approximately 75% of the total cement mass [6], and comprise the key molecular constituents considered in the present work for unhydrated cement components.

**1.1.2 Hydrated cement products.** Hydration of cement is a chemical reaction between cement compounds and water that are mixed together to form the cement paste. This reaction causes hardening of the cement resulting in hydrated cement constituents that impact strength to cement paste. Hydration is a very complicated process and produces complex hydrated material constituents. The most important hydrated cement products are Calcium Hydroxide (CH) and Calcium Silicate Hydrate (C-S-H) [3].

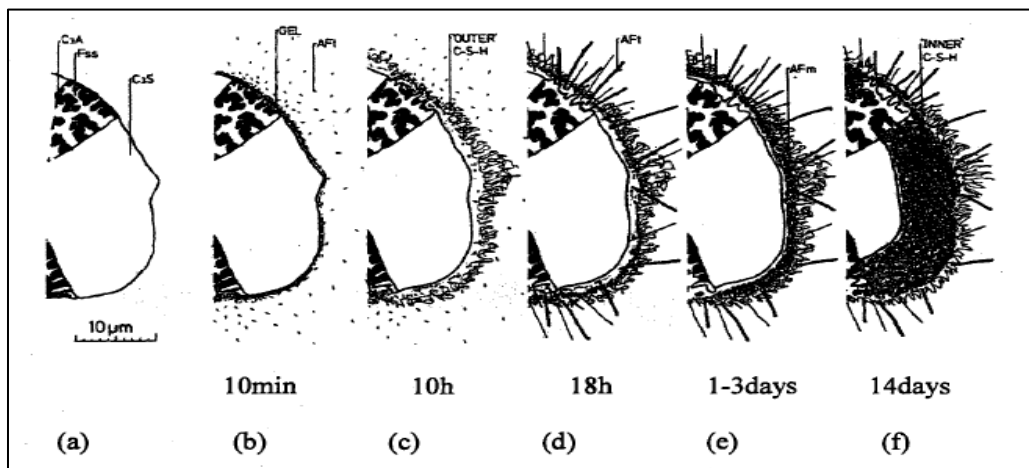
Table 1.3 shows some examples of the hydrated cement products along with their chemical formulas and mineral phases [3].

Table 1.3

*Some Hydrated Cement Products, their Chemical Formulas, and Mineral Phases*

Hydrated Product	Chemical Formula	Name or Mineral Phase
CH	$\text{Ca(OH)}_2$ or $\text{CaO.H}_2\text{O}$	Calcium hydroxide
C-S-H	$2(\text{CaO}).\text{SiO}_2.0.9-1.25(\text{H}_2\text{O})$ , and/or; $\text{CaO.SiO}_2.1.1(\text{H}_2\text{O})$ , and/or; $0.8-1.5(\text{CaO}).\text{SiO}_2.1.0-2.5(\text{H}_2\text{O})$	Calcium Silicate Hydrate
C-A-H	More complex than C-S-H	Calcium Aluminate Hydrate
AFt	Shorthand notation is $\text{C}_3\text{AS}_3\text{H}_{30-32}$	Aluminate Ferrite trisulfate
AFm	Shorthand notation is $\text{C}_2\text{ASH}_{12}$	Aluminate Ferrite
$\text{C}_3\text{AH}_6$	$3\text{CaO.A}_2\text{O}_3.6(\text{H}_2\text{O})$	Hydrogarnet

Figure 1.3 shows the hydration process occurs over time through chemical reaction of unhydrated components continually increasing the amount of formed C-S-H [7]. The formation of C-S-H and morphological regions of C-S-H evolve over a period of time from the chemical interaction of unhydrated components and surrounding water.



*Figure 1.3 Hydration process over time.*

## 1.2 Cement Molecular Structure

As noted earlier, molecular structure represents the nanometer/molecular scale features of the material system. In the present work with an emphasis on nanometer / molecular material scale, the focuses for unhydrated cement constituents are on  $C_3S$  and  $C_2S$ . The focuses for hydrated cement are on CH and C-S-H gel. A discussion of molecular structures for these unhydrated and hydrated constituents is presented next. For all molecular structures, green atoms represent calcium atoms, red atoms represent oxygen atoms, gold atoms represent silicon atoms, and white atoms represent hydrogen atoms.

There are a few proposed crystalline structures of tri-calcium silicate  $C_3S$ , for example Kazuyori Urabe et al [8] and Golovastikov et al [9]. In the present work, Golovastikov's triclinic  $C_3S$  crystalline structure with cell size (11.67x14.24x13.72) Å, and angles ( $\alpha = 105.5$ ,  $\beta = 94.33$ ,  $\gamma = 90$ ) was employed. Figure 1.4 shows  $C_3S$  molecular structure.

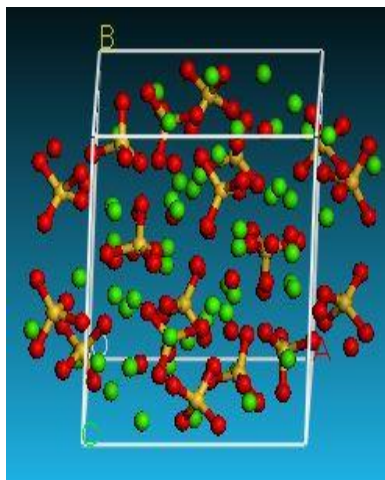


*Figure 1.4* Representation of  $C_3S$  molecular structure.

The crystalline structure of  $C_2S$  followed the proposed crystalline structure by CM Mideley et al [10] with cell size (5.48x6.76x9.28) Å, and angles ( $\alpha = 90$ ,  $\beta = 94.33$ ,  $\gamma = 90$ ) as shown in Figure 1.5.



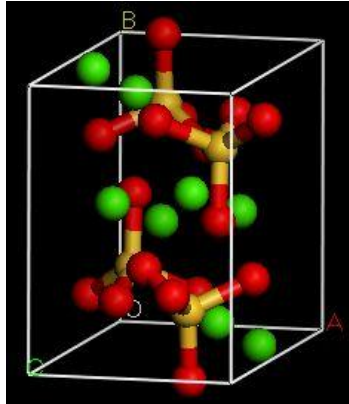


*Figure 1.5* Representation of  $C_2S$  molecular structure.

For hydrated cement products, Harutynuyan et al [11] investigated and studied early growth of calcium hydroxide (CH) crystal using x ray transmission microscopy imaging. Evaluating crystalline growth rate was done by analyzing the hydration process images. CH crystalline structure used in the present work built upon Harutynuyan's investigations, and proposed by D.M. Henderson [12] was obtained from the American Mineralogist Crystalline Structure Database [13]. Figure 1.6 shows CH crystalline structure with cell size (3.59x3.59x4.9) Å, and angles ( $\alpha = 90$ ,  $\beta = 90$ ,  $\gamma = 120$ ).

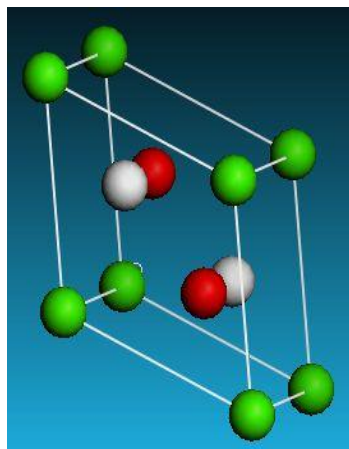


*Figure 1.6* Representation of CH molecular structure.

C-S-H gel is a very complicated hydration product. The complexity of this structure is due to the different mix proportions between calcium, silicon, and water leading to distinct

chemical formulas with corresponding structures. Even now, the molecular structure of C-S-H is still debatable and consensus of the correct molecular / nano scale representation does not exist although there have been several studies to find a close molecular structure representation.

Allen et al [1], measured the composition and density of nanoscale C-S-H gel. They determined the mean chemical formula of C-S-H gel as  $(\text{CaO})_{1.7}(\text{SiO}_2)(\text{H}_2\text{O})_{1.80}$  presenting a Ca-Si ratio of 1.7 and mass density of  $2.604 \text{ g/cm}^3$ .

Selvam et al [5, 14], studied C-S-H at the atomic level in order to enhance macroscopic mechanical properties. They proposed an amorphous structure of C-S-H that was based on the crystalline structure of mineral Tobermorite. Their findings demonstrated functionalizing the C-S-H gel improved mechanical properties. Their method relied on computational simulations involving two models. The first model limited the silicate chain length. The second model introduced porosity by using a packing factor of 0.69. Their results were claimed to be in good agreement with the experimental results.

Thomas et al [15], developed a hypothetical phase of C-S-H with the following three components,  $\text{CaO-SiO}_2\text{-H}_2\text{O}$ , C/S molar ratio was 1.0, and water solid ratio was 0.5. Their study compared their hypothetical configuration with C-S-H Tobermorite and Jennite minerals based on factors that included composition, mass density, and atomic packing density. They found that the atomic density is higher for their C-S-H phase than both Tobermorite and Jennite. As well, they found that if C-S-H is cured at  $80 \text{ }^\circ\text{C}$  it will result in lower atomic packing density. Finally, when  $\text{C}_3\text{S}$  is hydrated at  $40 \text{ }^\circ\text{C}$  the produced C-S-H has lower water content and higher density than their hypothetical phase of C-S-H. They validated their conclusions through comparison between the  $\text{C}_3\text{S}$ ,  $\text{C}_2\text{S}$  and published experimental chemical shrinkage results of cement paste.

Dolado et al [16], developed a nano structure of C-S-H gel. They studied the formation of C-S-H clusters by polymerization of  $\text{Si}(\text{OH})_4$  in the presence of solvated calcium  $\text{Ca}(\text{OH})_2 \cdot 4\text{H}_2\text{O}$  with Ca to Si ratio of 1.7, developing their C-S-H molecular structure based on a series of molecular dynamics simulations that predicted the formation of a branched three dimensional solid C-S-H solid network. These simulation based structure was found to reflect observations of features through small angle neutron scattering (SANS) and other techniques.

Bonaccorsi et al [17], analyzed the triclinic crystalline structure of Jennite using X ray diffraction. In this structure, the triclinic refined unit cell were ( $a = 10.576$ ,  $b = 7.265$ ,  $c = 10.931$ ) Å,  $\alpha = 101.30$ ,  $\gamma = 109.65$ ,  $\beta = 96.98$ . The crystalline chemical formula of Jennite is  $\text{Ca}_9\text{Si}_6\text{O}_{18}(\text{OH})_6 \cdot 8\text{H}_2\text{O}$ . They concluded that Jennite transforms to metajennite at  $70\text{-}90^\circ\text{C}$  by losing four water molecules. Figure 1.7 shows Jennite mineral molecular structure.

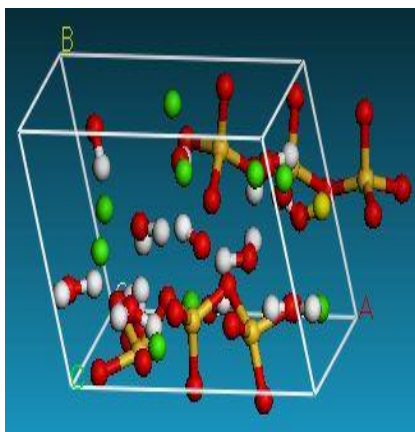


*Figure 1.7* Representation of C-S-H Jennite mineral.

Bonaccorsi et al [18], studied the crystalline structure of Tobermorite  $14\text{Å}$ , also known as Plombierite. Three different Tobermorite phases were categorized by basal spacing. These phases had sizes of  $9.3$ ,  $11.3$ , and  $14\text{Å}$ . They solved the crystal structure of Tobermorite 14A using order-disorder theory and refined it with synchrotron radiation diffraction data. According to Bonaccorsi, Tobermorite  $14\text{Å}$  has B11b space group symmetry and cell parameters of  $a =$

6.735Å,  $b=7.425\text{Å}$ ,  $c=27.987\text{Å}$ , and  $\gamma = 123.25^\circ$ . The associated chemical formula is  $\text{Ca}_5\text{Si}_6\text{O}_{16}(\text{OH})_2 \cdot 7\text{H}_2\text{O}$ . Figure 1.8 shows Tobermorite mineral molecular structure.

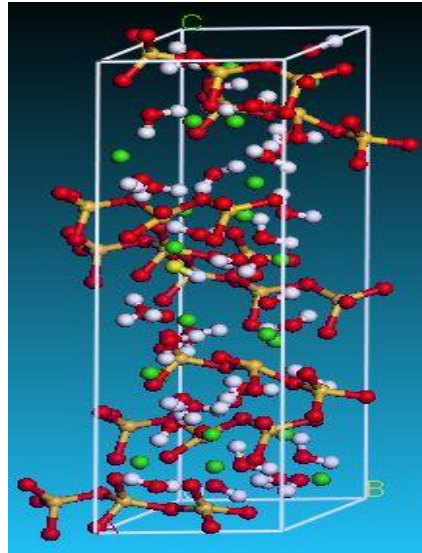


*Figure 1.8* Representation of C-S-H Tobermorite mineral.

In the present work, Jennite [17] and Tobermorite 14 [18] minerals were used as a representation for C-S-H.

### 1.3 Computational Modeling

Direct experimentation is inefficient and impractical at molecular scale level. Computational modeling provides a potentially effective method to study the behavior of cementitious materials at the molecular level.

Computational modeling has now become a third method of investigation in several sciences and engineering disciplines. Scientists and engineers are now using computational models to investigate and predict future system characteristics and behavior under different conditions. Computational models along with both experimental investigation and theoretical studies are useful when conducting experiments is cost prohibitive and impractical.

Computational Materials Science (CMS) is the fastest growing area in materials research because

of the availability of increased computational power, advances in physics and chemistry, and economic viability [19]. CMS approaches based on robust modeling representations are clearly needed for material development and understanding their characteristics.

Researchers are now taking advantage of the computational modeling capability to simulate, predict, and study properties of materials. The molecular material configuration is an important factor in these CMS modeling studies, and majority of literature are concentrating on model creation rather than designing new materials. This would allow setting the rules for creating an accurate model representative of the material structure, and it will facilitate analysis of existing materials as well as in the theoretical development of new materials and their structures with the desired properties.

Current computational power is enabling extensive analysis to be performed at the nano scale level (atomistic level) even for complex, large molecular material systems. The challenge is to create accurate computational models and methods, which can represent the cementitious materials molecular structures, and predict the mechanical properties of cement at the nano/molecular scale [20].

There are multiple spatial and /or temporal scales associated with materials and computational modeling methods. Small scales features affect and determine the behavior and properties at larger scales in multi-scale material systems such as cement [21]. Different scale levels that exist in materials and their corresponding modeling approaches that have been employed are shown in Figure 1.9. Scale levels in materials are features at quantum, nano, micro, meso, and macro scales and the corresponding modeling methods vary at each of these length scales.

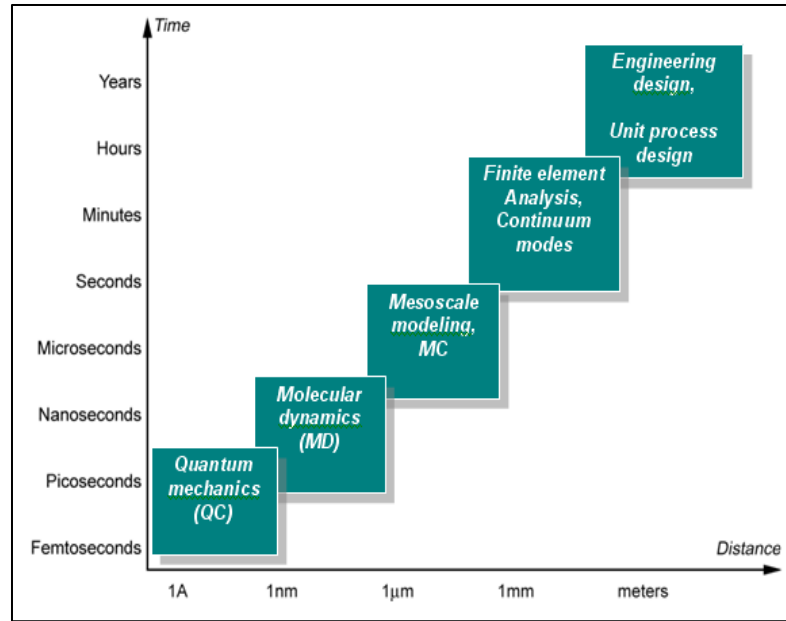


Figure 1.9 Different scale levels, time scales, and applicable computational modeling methods.

Table 1.4 shows the scale and size levels in materials, the associated computational methods, size, length, and time ranges of their applicability. Brief discussions of different time and length scale methods are presented in the next section.

Table 1.4

*Scale and Size Levels in Materials and Computational Methods*

Scale	Size Level	Method	Length (m)	Time (s)
Quantum	Electron	Quantum mechanics	$10^{-10}:10^{-9}$	pico-femto $10^{-12}:10^{-15}$
Nano	Atoms	Molecular dynamics	$10^{-9}:10^{-6}$	nano-pico $10^{-9}:10^{-12}$
Meso	Segment	Meso scale dynamics	$10^{-6}:10^{-3}$	micro-nano $10^{-6}:10^{-9}$
Micro	Grids	Finite element analysis	$10^{-3}:10^{-1}$	s-min
Macro	Engineering design	Unit process design	$10^{-2}:10^2$	hours-years

**1.3.1 Quantum scale level.** It is applicable at the electron size level, where the model equation used is the time-dependent Schrodinger equation accounting for the electron level movement and resolution [22].

$$i\hbar \frac{\partial}{\partial t} \psi (r, t) = \frac{-\hbar^2}{2m} \nabla^2 \psi (r, t) + V (r, t) \psi (r, t) \quad (1.1)$$

where:

$\psi$  is the wave function,

m is the mass,

V is the potential energy, and

$\nabla^2$  is the Laplacian operator

At the quantum scale level, it is inefficient to create an accurate model for large and complex material systems that can be modeled and analyzed with the current available computational power.

**1.3.2 Nano scale level.** The possible material configurations at this scale are at the atomic and molecular scale and the corresponding molecular dynamics modeling methods are applicable. The individual electron degrees of freedom are simplified and are included in the potential energy function via electrostatic energy terms that governs the interaction between the atomic nuclei. Current computational power allows solving larger models at the nano scale level as molecular scale models neglecting movement of individual electrons are computationally simpler to solve than quantum scale models.

The computational methodology employed at such molecular scales is molecular dynamics MD modeling methodology that is based on Newton equation of motion describing the movement of individual atoms in a molecular material system. The general form of this equation is given by

$$F_i = m_i a_i = m_i \frac{dv_i}{dt} = m_i \frac{d^2 r_i}{dt^2} \quad (1.2)$$

where:

$m_i$  is atom mass,

$v_i$  is atom velocity,

$r_i$  is atom position, and

$F_i$  is total force acting on a particular atom. Though, the discrete differential equations are applied for each atom, the force term that is defined as the gradient of the potential energy includes the effect of all the atoms, bonded and non-bonded interactions in the molecular structure. Further details are presented in a later section.

The challenge is to create accurate computational models that represent the material structure as well as their associated energy. This energy accounts for all possible bonded and non-bonded atom movements as well as the electrical charges associated with the molecular system.

#### **1.4 Mechanical Properties of Cementitious Materials – Literature Review**

Molecular Dynamics methods are effective in predicting mechanical and physical properties of material systems based on their molecular structures. The time dynamic molecular structural changes are employed in such analysis and have been employed in several material systems. In particular, of interest in the present work is the prediction of mechanical properties of cementitious material molecular structures.

Several studies have been conducted to study the mechanical properties and behavior of cementitious materials at both micro and macro scales. In this section a brief review on these studies will be presented.



Garboczi et al [23], used computer simulation and percolation theory to study the microstructure of Portland cement based materials. Their study focused on the micro structural changes that occur during the hydration process.

Boumiz et al [24, 25], studied the effect of time and degree of hydration on mechanical properties of cement paste and mortar at early stages. They followed a method based on transmission of ultrasonic short pulse through the samples. They used water/cement ratio of 0.35 and 0.4 samples to obtain the mechanical properties. Their compressive strength results for 1, 2, 7, and 28 days were 19.4, 36.2, 54.4, and 64.8 MPa respectively.

Ulm et al [4], analyzed the effect of two types of C-S-H (low and high density) on the elasticity of cement-based materials using nanoindentation and micromechanical modeling. Their results were elastic modulus 22 GPa, bulk modulus 15 GPa, shear modulus 9 GPa, and Poisson's ratio 0.25.

Haecker et al [26], used a combination of CEMHYD3D and finite element computations to obtain the linear elastic properties of Portland cement paste constituents. CEMHYD3D is a chemical analysis program that can numerically determine the cement paste microstructure. Their results for  $C_3S$  were elastic modulus 135 GPa, and Poisson's ratio 0.31. Their results for  $C_2S$  were elastic modulus 140 GPa, and Poisson's ratio 0.19.

Monteiro et al [27], developed a micro mechanical theory based on the mathematical morphology of concrete and reported an elastic modulus of 73 GPa, bulk modulus of 40 GPa, shear modulus of 16 GPa, and Poisson's ratio of 0.32.

Velez et al [28], used nanoindentation technique to determine the elastic modulus of different cementitious materials. C-S-H properties reported were elastic modulus of 22 GPa, bulk modulus of 15 GPa, shear modulus of 9 GPa, and Poisson's ratio of 0.25. While these are

primarily based on experimental techniques at meso/micro scales, limited MD modeling based on cementitious material molecular structures have been attempted and is discussed next.

### **1.5 Mechanical Properties Prediction via MD for Cementitious Materials –Current Literature and State of Art**

Al-Ostaz et al [29], used Molecular Dynamics (MD) simulations to predict the mechanical properties of hydrated cement products. The most important products by volume were Calcium Silicate Hydrate (C-S-H) and Calcium Hydroxide (CH). In their work, C-S-H, which is about 50-60% of hydrated cement volume, was represented by two different structures: Jennite and Tobermorite 14Å crystals. CH is about 20-25 percent of hydrated cement solid volume was represented by Portlandite crystal. The mechanical properties such as elastic, shear, and bulk modulus were calculated using Materials Studio Accelrys MD modeling analysis code and compared with available values from the literature[4, 28]. MD predicted mechanical properties values were close to the literature values for Jennite and CH. There was a significant disparity for Tobermorite 14Å. They concluded that the positive correlation of the MD mechanical results with the literature makes MD a viable simulation tool. The disparity in the MD model predictions for Tobermorite 14Å results was attributed to the fact that there is no solid rule when choosing the force field and the simulation super cell, which have a great effect on the predicted results from MD simulations.

Weidong et al [7, 30], performed MD simulations to predict the mechanical properties of major Portland cement compounds. Portland cement compounds used in their study were  $C_3S$ ,  $C_2S$ , and  $C_3A$ . COMPASS, Universal force field (UFF), and Dreiding force fields were employed and compared in their MD analysis. A combination of different force fields and different cell sizes were investigated and the results were compared with the data from nano

indentation experiments of cement samples. Their results demonstrated that the choice of the force field has a significant effect while the size of the super cell has a minimal effect on predicted mechanical properties. They also concluded that the COMPASS and Forcite Plus force fields as defined within the Materials Studio Accelrys were effective for  $C_2S$  and  $C_3S$  while Dreiding force field was stated to be more appropriate for  $C_3A$ .

Murray et al [31], used MD to understand the mechanical behavior of cement paste. They used C-S-H low and high density molecular structures. They used MD to model the tensile deformation and obtain stress strain curve model. Also, they estimated elastic modulus for two C-S-H models: C-S-H with continuous silicate chains and C-S-H with dimer silicate chains. Their reported values were 96 GPa for continuous silicate chains and 70 GPa for dimer silicate chains.

A review of the literature on the MD predicted mechanical properties of cementitious materials reveals interest has been limited to atmospheric pressure condition. In the present work, the prediction of mechanical properties was expanded to higher thermodynamic pressure state conditions. MD provides an effective methodology to computationally predict the expected property changes under different thermodynamic state conditions.

## **1.6 MD Mechanical Properties Prediction at Higher Pressures**

Computational MD modeling provides an effective way to understand the expected properties of materials under different thermodynamic pressure and temperature conditions through appropriate ensembles [32]. Further discussions on the MD ensemble and pressure and temperature control methods will be discussed in detail in chapter 2.

Pressure is one of the most important thermodynamic parameters and influences the property, mechanical and molecular structural response of materials at higher pressures

experienced in shock and ballistic loading conditions. One of the focuses of the present dissertation is to study and understand the behavior of materials under higher pressure values, as well as predicting the mechanical properties using MD modeling methods and the cementitious material molecular structures. Another important characteristic of material systems under high strain rate deformation seen in shock waves is the analysis and characterization of adiabatic effects through appropriate equation of state models. Experimental determination of such equation of state models is non-trivial; therefore a potential MD based computational modeling approach for cementitious molecular structures is proposed and presented in this work. Next section provides a brief theoretical background of shock wave propagation and equation of state models.

### **1.7 Shock Wave Propagation**

Shock wave or shock front or simply shock is the resulting pressure when explosions or high speed collisions of solids occur. These explosions or collisions create a huge rate of pressure change in a very short time [33]. The difference between shock wave and sound wave is their effect on the state of the propagating material medium. Shock wave is a nonlinear wave that changes the state of the medium. Sound wave is small amplitude at local sound speed and does not change the state of the propagating material medium.

Materials subjected to a phenomenon like shock wave propagation, detonation, explosions, and other high speed impacts undergo deformation at very high strain rates. In chapter 4, a detailed discussion about plane longitudinal shock wave is presented. High strain rate behavior of materials undergoing shocks, detonations, and other high strain dynamic phenomena are characterized via Equation of State (EOS) to account for the associated adiabatic effects. Literature cites different EOS models for condensed matter such as cementitious

materials. A MD modeling methodology for the characterization of a particular Mie-Gruneisen EOS[34] based on molecular structures is proposed and presented. The main results from this MD modeling methodology are isothermal and Hugoniot axial stress vs. specific volume curves, which are the simple forms of EOS material models.

### 1.8 Equation of State Models

The mathematical relation between the state variables of a material, such as pressure (P), temperature (T), and specific volume ( $v$ ) is represented in an EOS and accounts for the adiabatic changes experienced during high strain rate material deformation. The uses of the EOS of a material along with the Jump equations form a set of equations that can be used to determine the effect of the propagation of a shock through a material. Some of the common EOS material models cited in the literature are.

- Bulk modulus (K) [34], also called incompressibility, which is the ability of the material to withstand changes in volume under isotropic compression at constant temperature. Murnaghan EOS [35] is based on the assumption that the bulk modulus and pressure have a linear relationship.
- The Birch-Murnaghan EOS [36] is considered to be one of the most widely used EOS by mineralogists. It is based on the Eulerian strain ( $f_E$ ). Mazzatesta et al[37], used ultrasonic methodology to find Birch-Murnaghan EOS for cementitious materials.
- Mie-Gruneisen EOS [38] describes the relation between pressure, internal energy, and volume. Mie Gruneisen EOS was selected in the present work for the demonstration of the MD modeling methodology for EOS characterization providing a relation between pressure, internal energy, and volume.

## 1.9 MD Modeling of Shock Wave Effects on Materials

Gurjicic et al[39], used MD analysis and Mie-Gruneisen EOS to analyze the shock wave behavior through soda lime glass molecular structure. A Gruneisen parameter value from literature was employed in their MD analysis.

Other studies to calculate Gruneisen parameter in Mie-Gruneisen EOS for different materials [40-45] used both experimental and theoretical methods.

The principal focus of the present work is to introduce a MD modeling methodology to obtain the parameters that define the Mie-Gruneisen EOS and its corresponding Hugoniot curves based only on the molecular structure model. C-S-H Jennite structure was the material selected for demonstration of the present MD modeling methodology.

## 1.10 Dissertation Organization

The organization of the remainder of this dissertation is as follows.

- Chapter 2, Molecular Dynamic Background, discusses Accelrys Materials Studio, the MD simulation analysis code used in the present work [32], force field used in molecular dynamics simulations, molecular dynamics theory, and molecular dynamics parameters employed in the present study.
- Chapter 3, Mechanical Properties Predictions for Cementitious Materials Constituents, includes a brief discussion about the background of mechanical properties predictions from MD, initial MD parameters, comparisons from MD modeling employing different dynamics analysis times and the associated properties, literature comparisons that show scale effects on the mechanical properties of cementitious materials, high pressure values model results, computational resources required for modeling analysis, and concluding remarks.

- Chapter 4, MD Methodology for Mie-Gruneisen EOS Characterization, briefly describes shock wave propagation theory, Hugoniot curves, prior MD models used to study high strain phenomena, and discusses the proposed MD modeling analysis methodology.
- Chapter 5, MD Prediction of Mie-Gruneisen EOS for C-S-H Jennite, demonstrates the application of the proposed MD modeling methodology. As well, this chapter presents the results of Gruneisen parameter model, ultimate shear strength model, Hugoniot curves, and conclusions.
- Chapter 6 presents concluding remarks, and outlines future work.

## CHAPTER 2

### Molecular Dynamics Background

Experimental techniques for the characterization of materials at the nano/molecular scale level are problematic and impractical. Current tool sets are ineffective for manipulation of materials at the nano/molecular scale even in simpler crystalline material systems. In the few instances that direct experimentation could be performed, cost inefficiency prevents actualization, as well as several artifacts associated with the methods, instrumentation and associated theories employed to determine the principal property values. Computational simulation methods based on quantum mechanics (QM) and molecular dynamics built on classical mechanics at atomistic level present a viable alternative. A background description of molecular dynamics (MD) method employed in this work is presented next for completeness.

QM method is an *ab-initio* method that uses Schrodinger mathematical equation [22]. QM describes the change of the chemical and physical properties of a system with time. Since QM works at the electron level, it can clarify the chemical reaction thereby predicting reactivity of molecules. Because it requires massive numerical calculations, QM is limited to smaller molecular systems. For larger molecular systems, classical mechanics based methods are recommended.

Molecular Mechanics (MM) method is an application of the classical mechanics at the molecular level. MM studies slow particles with speeds much less than the speed of light and heavy particles with mass much higher than the electron mass. Therefore, MM considers atoms, molecular level description of materials, and incorporates the effect of the degrees of freedom associated with the electrons in the interatomic potential energy governing the interaction between the atomic nuclei. MM determines the properties and behavior of molecules by



estimating the motion of atomic nuclei and the change in potential energy of the system of atoms. MM cannot be used to study the chemical reaction or to predict reactivity of molecules. MM is less accurate than QM, but requires fewer numerical calculations that allow MM to be usable in simulations of larger systems.

A common method used at nano/molecular scale of materials is molecular dynamics (MD). MD is a computational method for solving dynamic Newton's equation of motion of interacting atoms and molecules over a period of time. MD method was originally developed in the late 1950s and early 1960s by Alder and Wainwright [46]. Over the years, MD has been employed for predicting the properties of different material systems based on their molecular structures.

Murray et al [31] used MD to understand the mechanical behavior of cement paste. They concluded that maximum tensile and compressive strengths obtained using MD models were several orders of magnitude higher than the tensile and compressive strengths at the macro scale.

Presently, MD is applied in modeling several materials including large biomolecules. It can be used to study and investigate the structure and behavior of interacting atoms in any molecular system. Prior studies have employed MD simulation to investigate shock-wave physics and derivation of the Hugoniot curves for soda-lime glass, a material employed in transparent armor applications [39, 47].

Gurjicic et al [39, 47] studied soda-lime glass which is a material commonly used in transparent armor applications. Their study showed that the effectiveness of computation-based modeling is greatly affected by the ability of the models to realistically describe deformation and fracture response of ballistic glass under high-rate/high-pressure loading conditions encountered during blast/ballistic impact.

Over the years, several MD analysis coding developments have evolved resulting in several open source and commercial MD analysis codes such as GROMACS, CHARMM, LAMMPS, and Accelrys. These codes with varying features, force fields are applicable to several material systems and MD analysis. Accelrys Material Studio, a commercial MD code with a variety of modules and available force fields with a Graphical User Interface (GUI), was used in the present study [32].

This chapter presents a brief discussion about MD analysis code employed, associated force fields, and background of different Molecular Dynamics (MD) parameters defined and used in the computational simulations.

## **2.1 Accelrys Materials Studio**

Accelrys Materials Studio is a suite of commercial MD analysis code that is used in advanced modeling of various materials such as polymers, nano tubes, catalysts, metals, ceramics, etc. [32].

In the present work, Accelrys Materials Studio was employed to model and simulate unhydrated cement product molecular structures ( $C_3S$ ), ( $C_2S$ ) and hydrated cement products (CH), (C-S-H Jennite), (C-S-H Tobermorite 14) molecular structures. Several MD modeling analysis parametric studies were performed to include the following.

- Effect of increasing the dynamic analysis duration on the predicted mechanical properties for both hydrated and unhydrated cementitious materials.
- Effect of increasing simulation cell size on the predicted mechanical properties for both hydrated and unhydrated cementitious materials.
- Predict mechanical properties for both hydrated and unhydrated cementitious materials at atmospheric pressure using selected dynamic analysis duration and simulation cell size.

- Effect of higher pressures on the predicted mechanical properties for both hydrated and unhydrated cementitious materials.
- Model and simulate isothermal volumetric compression loading condition for hydrated cement product C-S-H Jennite representations at the molecular level.
- Model pressure – internal energy relation at constant specific volume for hydrated cement product C-S-H Jennite at the molecular level.
- Model and simulate shear deformation for C-S-H Jennite at the molecular level by geometrically deforming the cell, finding the corresponding stress, and developing the stress strain curve for finding the maximum shear strength.

The last three computational MD modeling studies will culminate in the estimation of the Hugoniot relations, which are simpler forms of Mie-Gruneisen EOS, presenting a potential modeling methodology for the characterization of EOS of materials via their molecular structures. Relevant discussions of various parameters that are defined during MD analysis are presented next.

## **2.2 Force Field**

The Force field (FF) is a collective mathematical representation of total potential energy for a molecular system. The coefficients in the mathematical expressions vary for different molecular types based on the material atoms involved. The FF parameters contributing to the various energy terms in the potential energy can be determined either from experiments or from higher levels quantum mechanics calculations. Recently, a number of force fields have been developed and are being widely used in several MD analysis codes. Examples of these force fields are MM3, MM4, DREIDING, SHARP, VALBON, UFF, CFF93, AMBER, CHARMM,

OPLS, and MMFF. In general, force fields employed in MD analysis follow three different directions [48].

- A general force field that can cover any combination of the periodic table elements. The generalization of this direction requires using simple functional forms that are less accurate. UFF is an example of developments on this direction.
- Material specific force fields that improve the quality of prediction of various molecular properties. Examples of efforts on that direction are COMPASS, AMBER, CHARMM, and OPLS. In this case, simple functional forms with parameters defined for specific materials and their interactions are used.
- More complex functional forms in order to predict highly accurate properties (molecular structures, conformational, vibration frequencies, and heats of formation). Examples of these potentials are MM3, CFF93, and MMFF.

The force field employed in MD analysis impacts the potential energy as well as the force and will affect the dynamic simulation run results as well as the predicted mechanical properties.

For cementitious materials, with the unhydrated and hydrated molecular structures showing crystalline / semi crystalline structure, COMPASS force field has been used [7, 48].

COMPASS force field is one possible choice within Accelrys MD code whose functional form can be represented by:

$$\begin{aligned}
 E_{total}^{compass} &= E_{valence} + E_{crossterm} + E_{non-bond} \\
 &= \sum_b \{K_2(b - b_0)^2 + K_3(b - b_0)^3 + K_4(b - b_0)^4\} \\
 &+ \sum_{\theta} \{H_2(\theta - \theta_0)^2 + H_3(\theta - \theta_0)^3 + H_4(\theta - \theta_0)^4\} \\
 &+ \sum_{\phi} \{V_1\{1 - \cos(\phi - \phi_1^0)\} + V_2\{1 - \cos(2\phi - \phi_2^0)\} + V_3\{1 - \cos(3\phi - \phi_3^0)\}\} \\
 &+ \sum_z K_z X^2 + \sum_b \sum_{b'} F_{bb'}(b - b_0)(b' - b'_0) + \sum_{\theta} \sum_{\theta'} F_{\theta\theta'}(\theta - \theta_0)(\theta' - \theta'_0)
 \end{aligned}$$

$$\begin{aligned}
& + \sum_b \sum_{\theta} F_{b\theta} (b - b_o)(\theta - \theta_o) + \sum_b \sum_{\phi} F_{b\theta} (b - b_o) \{V_1 \cos \phi + V_2 \cos 2\phi + V_3 \cos 3\phi\} \\
& + \sum_{b'} \sum_{\phi} F_{b\theta} (b' - b'_o) \{V_1 \cos \phi + V_2 \cos 2\phi + V_3 \cos 3\phi\} \\
& + \sum_{\theta} \sum_{\phi} F_{b\theta} (\theta - \theta_o) \{V_1 \cos \phi + V_2 \cos 2\phi + V_3 \cos 3\phi\} \\
& + \sum_{\phi} \sum_{\theta} \sum_{\theta'} k_{\phi\theta\theta'} \cos \phi (\theta - \theta_o)(\theta' - \theta'_o) + \sum_{i>j} \frac{q_i q_j}{\epsilon r_{ij}} + \sum_{i>j} \left\{ \frac{A_{ij}}{r_{ij}^9} - \frac{B_{ij}}{r_{ij}^6} \right\}
\end{aligned} \tag{2.1}$$

The functional form of the COMPASS (condensed-phase optimized molecular potentials for atomistic simulation studies) contains three major terms [48]: bonded terms, non-bonded terms, and cross terms.

**2.2.1 Bonded terms.** Bond or valence terms represent the energy associated with bond stretching ( $b$ ), bond angle bending ( $\theta$ ), bond angle rotation ( $\phi$ ), and Out of-plane angle ( $x$ ).

**2.2.1.1 Bond stretching term.** The energy associated with bond stretching is represented by the following mathematical representation

$$E_{\text{stretch}} = \frac{K_s}{2} (L - L_o)^2 \tag{2.2}$$

where:

$K_s$  is the spring constant that depends on the type of atoms and bonds formed,

$L_o$  is the equilibrium bond length, and

$L$  is the current bond length.

Figure 2.1 shows a schematic representation of bonded stretch term.

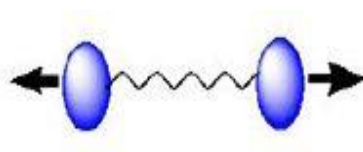


Figure 2.1 Bond stretching term.

**2.2.1.2 Bond angle bending term.** The mathematical representation for bond angle bending is

$$E_{\text{bending}} = \frac{K_{\theta}}{2} (\theta - \theta_0)^2 \quad (2.3)$$

where:

$K_{\theta}$  is the spring constant, and

$\theta_0$  is the equilibrium bond angle.

$\theta$  is the current bond angle.

Figure 2.2 shows a representation of bonded angle bending term.

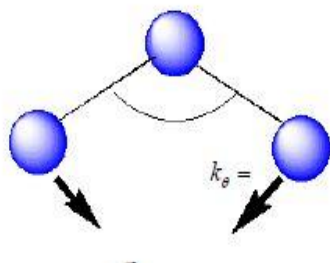


Figure 2.2 Bond angle bending term.

**2.2.1.3 Bond angle rotation term.** The mathematical representation bond angle rotation term in force field is

$$E_{\text{Torsion}} = \frac{V_1}{2} (1 + \cos \phi) + \frac{V_2}{2} (1 + \cos \phi) + \dots \quad (2.4)$$

where:

$V_n$  is the dihedral force constant,

$\phi$  is dihedral angle, and

$n$  is the periodicity.

Figure 2.3 shows a representation of bonded angle rotation term.



Figure 2.3 Dihedral angle rotation term.

**2.2.1.4 Out of plane angle term.** The mathematical representation is

$$E_{out\ of\ plane} = \sum_z K_z X^2 \quad (2.5)$$

where:

$K_z$  is out of plane force constant, and

$X$  is out of plane angle.

Figure 2.4 shows a representation of bonded out of plane angle term.

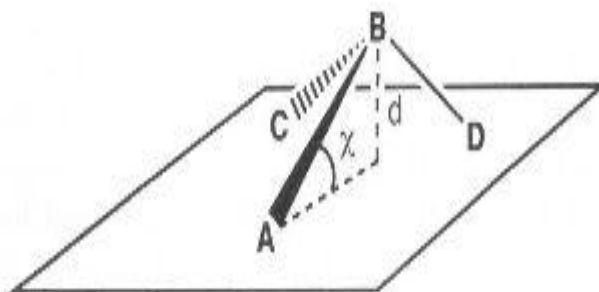


Figure 2.4 Out of plane angle.

**2.2.2 Non-bonded terms.** Non bonded terms consist of Van der Waals forces and electrostatic interaction terms.

**2.2.2.1 Van der Waals forces term.** Van der Waals forces include long range attractive force and short range repulsive force. Both the repulsive and attractive forces can be determined by a mathematically simple model which approximates the interaction between a pair of neutral atoms or molecules. Lennard-Jones potential (L-J) [49] is one such model.

The L-J potential expression given by

$$E_{\text{vdW}} = \frac{A}{r^{12}} - \frac{B}{r^6} \quad (2.6)$$

$$A = -\epsilon\sigma^{12} \quad (2.7)$$

$$B = -2\epsilon\sigma^6 \quad (2.8)$$

where:

A, B are the material constants associated with repulsive and attractive forces respectively,

$\epsilon$  is the depth of the potential well,

$\sigma$  is the finite distance at which the inter-particle potential is zero, and

$r$  is the distance between the two particles.

Figure 2.5 shows a schematic of Lennard-Jones potential term. The L-J energy is at a minimum at the equilibrium distance and asymptotically becomes zero at larger inter-atom distances. To reduce the sphere of influence of LJ potentials and assist in computational efficiency, a cut-off distance is generally used in MD modeling beyond which the LJ energy contribution is neglected.

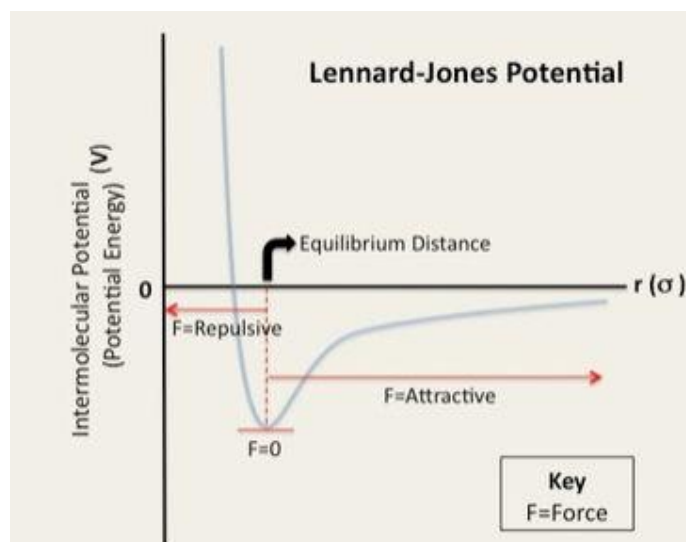


Figure 2.5 Van der Waals forces attractive and repulsive.



**2.2.2.2 Electrostatic forces term.** Electrostatic interaction is the second non-bond term accounting for the electrostatic potential associated with the atoms. It is based on Coulomb's law which describes the force between two point charges. The mathematical representation for electrostatic interaction forces is

$$E_{\text{electro}} = \frac{q_a q_b}{\epsilon_a \gamma_{ab}} \quad (2.9)$$

where:

$q_n$  is the atomic potential charge,

$\epsilon_{ab}$  is the dielectric constant, and

$\gamma_{ab}$  is the inter-atomic distance.

**2.2.3 Cross terms.** Cross terms are important for predicting vibration frequencies and structural variation. Cross terms include the combination of internal coordinates for example bond-bond, bond-angle, and bond-torsion and are included in the COMPASS force field.

Finally, the total potential energy or the so called force field is the summation of all the above energy terms (bond terms, non-bond terms, and cross terms).

$$E_{\text{Total}} = E_{\text{stretch}} + E_{\theta} + E_{\text{Torsion}} + E_{\text{out of plane}} + E_{\text{cross terms}} + E_{\text{vdW}} + E_{\text{Electro}} \quad (2.10)$$

## 2.3 Molecular Dynamics

Molecular dynamics (MD) is a computational methodology that analyzes the dynamic behavior of molecules. It is built upon the application of laws of classical mechanics at the atom/molecular level. Each atom is represented as discrete spheres with mass. The positions and velocity of spheres are obtained over time. Another definition of MD is numerically solving the N-body problem of classical mechanics for positions and velocities. Originally proposed in the 1950s [46], MD method eventually received widespread attention in the 1970s with the advent of digital computers [50].

MD methodology is a combination of [51] molecular modeling, computer simulation, and statistical mechanics. Classical mechanics covers the time dependent behavior of the molecular motion. Different molecular configurations obtained provide the sampling of the configurations, a phase space for the invocation of structural mechanics. As a computational analysis methodology, MD simulation process consists of four key steps in the analysis process [30]; these are static energy minimization, equilibration, dynamics simulation run, and calculation of the mechanical properties employing the atomistic positions and velocities at various dynamic steps and invoking Ergodic hypothesis. Figure 2.6 shows MD analysis steps.

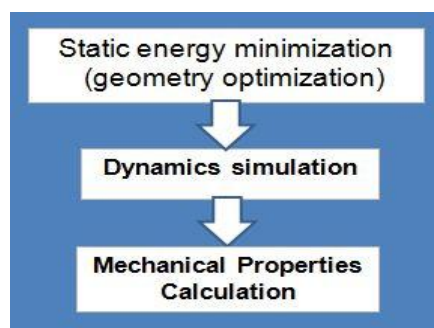


*Figure 2.6* Molecular dynamics analysis process.

**2.3.1 Energy minimization.** The purpose of energy minimization is to find the stable molecular structure configuration which corresponds to the lowest energy for the molecular system. There are several methods to finding the global minimum energy configuration in a static MD analysis. Some common methods that can be used in static minimization and available in many MD analysis codes are:

- steepest descents method,
- conjugate gradient method,
- Newton-Raphson method, and
- Simplex method.

Steepest descents method is a gradient method which depends on the direction of the first derivative and indicates the direction of minimum in a multi-dimensional vector space. In this method the energy of the initial atomic configuration is calculated and then the atoms are moved in the direction of highest energy gradient. As a result, the line search moves perpendicular to the energy gradient. After setting in this point, the search repeats the process until the minimum energy structure is found. This method is relatively slow because the search path zigzags with many orthogonal steps [52].

Conjugate gradient method is also a gradient method. The line search goes in the direction of steepest descent and stops at local minimum before starting in a new search direction. This method is faster than the steepest descent method because the search path is straightforward [52].

In most MD analysis applications, gradient methods are a good choice for large molecular systems, but the convergence of these methods is slow when close to the minimum.

Newton-Raphson method is a Hessian method which depends on the second derivative that indicates the curvature of the function. For a single variable function, this method starts with an initial guess of the function root, and then uses the tangent line to compute the  $x$  intercept. This  $x$  intercept becomes the function root for the next iteration. The process continues until convergence is reached. The following equation shows the iterative process used for a function of a single variable

$$x_{k+1} = x_k - \frac{f'(x_k)}{f''(x_k)} \quad (2.11)$$

where:

$x_k, x_{k+1}$  are values at current and next time step,

$f'(x_k)$  is first derivative, and

$f''(x_k)$  is the second derivative.

For multi variables, the corresponding equation used is

$$x_{k+1} = x_k - G'(x_k)H^{-1}(x_k) \quad (2.12)$$

where:

$G'(x_k)$  is the gradient, and

$H^{-1}(x_k)$  is the inverse of Hessian matrix.

Newton-Raphson is a good choice for smaller molecular system as well as when the molecular structure is near the minimal energy configuration.

Simplex method is different than Gradient and Hessian based methods. It is the least expensive per step but requires the most number of steps. Simplex method chooses three different configurations, reflects the highest energy configuration through the line segment connecting the other two configurations, and repeats this until a minimum energy within tolerance is reached.

The smart minimization method implemented within the MD analysis code Materials Studio – Accelrys uses a combination of the Gradient and Hessian methods. Minimization algorithms are set up for small molecular systems with less than 200 atoms to begin with the steepest descent method, followed by the conjugate gradient method and end with a Newton-Raphson method. Molecular systems larger than 200 atoms begin with the steepest descent method followed by the conjugate gradient method [32].

**2.3.2 Dynamic simulation.** The time dynamic motion of atoms during MD analysis involves the following steps:

- assigning initial atoms velocities,
- scaling the velocities to obtain the desired temperature, and

- solving Newton's equation of motion for the movement of atoms after each time step during the dynamic analysis.

The movements (position and velocities) of atoms after each time step are called trajectories defining the time varying position and velocities of the atoms. These are determined by solving Newton's equation of motion where forces between interacting atoms and potential energy are defined by force fields during MD analysis as defined earlier.

The dynamic movement of atoms is analyzed using time integration algorithms that are used to integrate the equation of motion in most MD analysis codes. Time integration methods are based on finite difference numerical derivative for the time derivative term and can be used to solve the initial value problem (IVP). Common time integration methods for a system of first and second order time derivative equations include:

- Euler Method,
- 2<sup>nd</sup> order Runge-Kutta Method (RK2) or sometimes called Modified Euler Method,
- 4<sup>th</sup> order Runge-Kutta Method (RK4),
- Verlet algorithm,
- Velocity Verlet algorithm, and
- Predictor-Corrector Methods.

**2.3.2.1 Euler algorithm.** This is the simplest numerical method to solve ordinary differential equations (ODEs) and is given by

$$P(t_n + \Delta t) = P(t_n) + \Delta t \cdot \frac{dP(t_n)}{dt} + \text{error } (\Delta t)^2 \quad (2.13)$$

$$\text{or } P_{n+1} = P_n + \Delta t \cdot f(P_n, t_n) + \text{error } (\Delta t)^2 \quad (2.14)$$

The local truncation error is of the order of  $(\Delta t)^2$ , while the global error is of order  $\Delta t$ .

**2.3.2.2 Modified Euler algorithm.** Also called 2<sup>nd</sup> order Runge-Kutta Method (RK2), it was created to improve the accuracy of the numerical approximation by increasing the order of the global error to  $(\Delta t)^2$  or more. The modification takes into account the curvature and depends on the use of function at  $(t+\Delta t/2)$  which will increase the order of the local error to  $(\Delta t)^3$  and also increase the order of the global error to  $(\Delta t)^2$ .

$$K_1 = \Delta t. f(P_n, t_n) \text{ and } K_2 = \Delta t. f(P_n + K_1/2, t_n + \Delta t/2) \quad (2.15)$$

$$P_{n+1} = P_n + \Delta t. f(P_n + K_1/2, t_n + \Delta t/2) + \text{error } (\Delta t)^3 \quad (2.16)$$

**2.3.2.3 4th order Runge-Kutta method (RK4) algorithm.** This method was created to improve the accuracy of the numerical approximation even more than 2<sup>nd</sup> order Runge-Kutta method (RK2). The local truncation error = order of  $(\Delta t)^5$  and the global error is of order  $(\Delta t)^4$

**2.3.2.4 Verlet algorithm.** Though the above methods are good for the solution of a system of first order ODE, a direct solution of the second order time derivative for the atomic positions can be obtained through the use of Verlet algorithm. This is the most commonly used time integration algorithm in molecular dynamics. It utilizes both forward and backward Taylor expansions in the development of the methodology [53].

Forward Taylor expansion follows.

$$r(t + \Delta t) = r(t) + v(t)\Delta t + \frac{1}{2}a(t)\Delta t^2 + \frac{1}{6}b(t)\Delta t^3 + \text{error of order } \Delta t^4 \dots \quad (2.17)$$

Backward Taylor expansion follows.

$$r(t - \Delta t) = r(t) - v(t)\Delta t + \frac{1}{2}a(t)\Delta t^2 - \frac{1}{6}b(t)\Delta t^3 + \text{error of order } \Delta t^4 \quad (2.18)$$

Basic Verlet equation is the product of adding the previous two equations

$$r(t + \Delta t) = 2r(t) - r(t - \Delta t) + a(t)\Delta t^2 + \text{error of order } \Delta t^4 \quad (2.19)$$

where:

$r(t - \Delta t)$  is position at the previous time step,

$r(t)$  is position at current time step, and

$r(t + \Delta t)$  is position at next time step.

Few features of the basic Verlet equation include the following.

- Basic Verlet order of error ( $\Delta t^4$ ) is one order more than 2<sup>nd</sup> order Runge-Kutta Method( $\Delta t^3$ ).
- The acceleration is computed at any time  $t$  step based on the potential energy at this time  $t$  and the atom mass.
- Calculation of the position  $r(t + \Delta t)$  is dependent on the position  $r(t - \Delta t)$  and  $r(t)$ . At the first time step,  $r(\Delta t)$  the position  $r(-\Delta t)$  must be approximated by using the 2<sup>nd</sup> degree Taylor polynomial. The order of error for the first time step is ( $\Delta t^3$ ).
- Basic Verlet equation does not calculate the velocities. The velocities are post-calculated from the atomic positions.

$$v(t) = 1/2\Delta t(r(t + \Delta t) - r(t - \Delta t)) + \text{error of order } \Delta t^2 \quad (2.20)$$

or by using shorter interval to estimate the velocity  $t + \Delta t$

$$v(t + \Delta t) = 1/\Delta t(r(t + \Delta t) - r(t)) + \text{error of order } \Delta t \quad (2.21)$$

The velocities can be directly computed with a modification of the Verlet algorithm called the Velocity Verlet method presented next.

**2.3.2.5 Velocity Verlet and Leapfrog algorithms.** Velocity Verlet and Leapfrog are improvements over basic Verlet algorithm. Both of these improved methods eliminate the limitation of the first step in the Velocity Verlet method. In addition, these methods calculate velocities. Leapfrog algorithm calculates velocities at the half time steps in order to obtain more accurate velocities. Velocity Verlet calculates velocity and position at the time step.

Velocity Verlet algorithm and steps involved in the calculations are presented next.

$$r(t + \Delta t) = r(t) + v(t) \cdot \Delta t + \left(\frac{1}{2}\right) \cdot a(t) \Delta t^2 + \text{error of order } \Delta t^2 \quad (2.22)$$

$$v(t + \Delta t) = v(t) + 1/2(r(t + \Delta t) - r(t)) + \text{error of order } \Delta t \quad (2.23)$$

Calculate the velocity at midpoint.

$$v(t + \Delta t/2) = v(t) + a(t) \cdot (\Delta t)/2 \quad (2.24)$$

Calculate the position at next time step.

$$r(t + \Delta t) = r(t) + v(t + \Delta t/2) \cdot \Delta t \quad (2.25)$$

Calculate the acceleration at next time step.

$$r(t + \Delta t) = F(t + \Delta t)/(m) \quad (2.26)$$

Update the velocity.

$$v(t + \Delta t) = v(t + \Delta t/2) + a(t + \Delta t) \cdot (\Delta t)/2 \quad (2.27)$$

The only difference between Velocity Verlet and Leapfrog is the shifting of velocities by half time. Velocity Verlet is one of the commonly employed methods for dynamic time integration in most MD analysis code developments. Other possibilities for dynamic time integration include Predictor- Corrector methods.

**2.3.2.6 Predictor Corrector algorithm.** The computational methodology followed in this method consists of three steps.

- Predictor step: by knowing the positions, velocities, and acceleration at time  $t$ , and by using Taylor expansion, these values can be predicted at time  $t + \Delta t$ .
- Force evaluation: by calculating the force from the gradient of predicted positions and comparing the results with the predicted acceleration and calculating the difference. This difference is called error signal.
- Corrector step: using the error signal to correct positions and their derivatives.



However, the most commonly used time integration algorithms in molecular dynamics are Verlet algorithm and Predictor Corrector algorithm[32]. This procedure is repeated over a long dynamic analysis period reaching a final molecular structure after the dynamic run. The position and velocities of atoms from the transient dynamic analysis and the molecular structure after the dynamic run is employed for further mechanical properties calculations [51].

**2.3.3 Mechanical properties calculation.** In this section, a brief discussion about mechanical properties calculation is presented. The main idea in calculating any property based on MD analysis is based on the Ergodic hypothesis assumption. Ergodic hypothesis considers ensemble average to be equal to time average. Ensemble average for a system with different possible atomistic configurations is the expected value of all possible atomistic configurations and their probability of occurring. Time average is based on the average value over the time of measurements. Mechanical properties calculation starts after the dynamics simulation. Elastic constants can be determined from the molecular structures using the following equation[54]

$$C_{lmnk} = \frac{\partial \sigma_{lm}}{\partial \varepsilon_{nk}} \Big|_{T, \varepsilon_{nk}} = \frac{1}{V_o} \frac{\partial^2 A}{\partial \varepsilon_{lm} \partial \varepsilon_{nk}} \Big|_{T, \varepsilon_{lm}, \varepsilon_{nk}} \quad (2.28)$$

where:

$C_{lmnk}$  is the fourth order stiffness tensor,

$\varepsilon$  is the strain,

$\sigma$  is the stress,

$A$  is Helmholtz free energy, and

$V_o$  is simulation cell volume.

The internal stress tensor can be used to calculate the elastic stiffness coefficients matrix analytically using the following equation

$$\sigma = -\frac{1}{V_0} \{(\sum_{i=1}^N m_i (v_i v_i^T)) + (\sum_{i<j} r_{ij} f_{ij}^T)\} \quad (2.29)$$

where:

$i$  is the atom number,

$m_i$  is atom mass,

$v_i$  is atom velocity,

$f$  is the force on the atom, and

$V_0$  is the undeformed volume.

Or the elastic stiffness coefficients matrix can be estimated numerically using the following equation

$$\frac{\partial^2 U}{\partial \varepsilon_i \partial \varepsilon_j} = \frac{\partial \sigma_i}{\partial \varepsilon_j} \quad (2.30)$$

where:

$U$  is the potential energy.

A detailed discussion about the mechanical properties and how they were computed will be presented in chapter 3.

## 2.4 Dynamic Run Parameters

Some of the important parameters that are defined and used in the molecular dynamics analysis are periodic boundary conditions (PBC), type of ensemble, pressure control methods, temperature control methods, time step, dynamic time, and cutoff distance. The choice of the values of each of these parameters has a significant effect on the results. This is briefly discussed next.

**2.4.1 Periodic boundary conditions (PBC).** The use of PBC enables the use of smaller molecular configurations representing a bulk system in MD analysis for the prediction of

properties. The relative volume element (RVE) does not feel the existence of the boundary which means the number of atoms inside the central box stays the same. The simulations affect only the atoms in the central box. If one atom moves from the central box another atom from the other side moves in and replaces it. This will keep the number of atoms inside the central box constant [52]. Figure 2.7 shows a representative illustration of PBC.

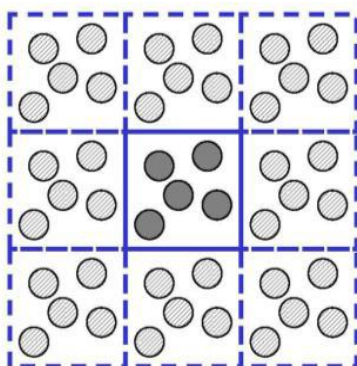


*Figure 2.7* Periodic boundary conditions illustration.

**2.4.2 Statistical ensembles.** In MD analysis, Ensemble is a collection of points / molecular configurations over time satisfying the same macroscopic or thermodynamics properties such as number of atoms (N), pressure (P), temperature (T), volume (V), energy (E), and enthalpy (H). Several statistical ensembles can be generated during the dynamics analysis and material properties can be calculated from these ensembles under the common thermodynamic state conditions.

The most common ensembles used in MD analysis are:

- (NVE) Micro-canonical ensemble,
- (NVT) Canonical ensemble,
- (NPT) Isobaric-Isothermal ensemble, and
- (NPH) Isobaric-Isenthalpic ensemble.

The number of atoms is fixed for all these ensembles. NPT and NPH are usually used for periodic systems because in nonperiodic systems volume is undefined [32].

NVE is a fixed number of atoms, fixed volume, and fixed energy. NVE is not recommended for equilibration but it is good for exploring constant energy configuration. In NVE there is no control on pressure or temperature [32].

NVT is a fixed number of atoms, fixed volume, and fixed temperature. NVT is a good choice when pressure is not a major factor.

NPT is a fixed number of atoms, fixed pressure, and fixed temperature. NPT is a good choice when the pressure and the temperature need to be controlled during the MD analysis.

NPH is a fixed number of atoms, fixed pressure, and fixed enthalpy. NPH can be used during equilibration phase of simulation and there is no temperature control in this ensemble.

**2.4.3 Temperature control methods.** Temperature in MD is a kinetic quantity depending on the atom velocities. Temperature thermodynamic state thus requires several temperature control methods in a MD analysis. There are several temperature control methods or thermostats that are defined in MD codes and used in the analysis. Some of these methods are Velocity scaling, Berendsen, Anderson, and Nose-Hover, and are some of the options available in the MD analysis code Accelrys – Materials Studio employed in the present work.

**2.4.3.1 Velocity scaling.** Velocity scaling method changes atoms velocity to maintain the target temperature. This method is useful initially to bring the structure close to equilibrium. In order to reach final equilibrium an alternate thermostat is adopted.

**2.4.3.2 Berendsen method.** Berendsen method [55] accounts for exchange of thermal energy between system and heat bath by multiplying the velocity by factor  $\lambda$ . This factor can be calculated from the following equation

$$\lambda = \left\{ 1 - \frac{\Delta t}{t} \left( \frac{T - T_0}{T} \right) \right\}^{\frac{1}{2}} \quad (2.31)$$

where:

$\lambda$  is scaling velocity factor,

$t$  is relaxing time,  $\Delta t$  is time step,

$T_0$  is target temperature, and

$T$  is instantaneous temperature.

**2.4.3.3 Nose method and Nose-Hoover method.** Nose method [56] is performing true canonical ensembles with constant temperature. Nose-Hoover [57] eliminates time scaling and has trajectories with even time space. Nose-Hoover is based on an additional degree of freedom representing the interaction of the system and the heat bath. Further details of the method can be found in [32].

**2.4.3.4 Andersen method.** Andersen method has two versions. The first version uses predefined collision period and is based on randomly changing the atoms' velocities. The second version chooses the atom collision times at each time step from a Poisson's distribution. The atoms' velocities are changed according to this distribution. Accelrys Material Studio employs the first version where the predefined collision is proportional to  $N^{2/3}$  and where  $N$  is the number of atoms [32].

**2.4.4 Pressure control methods.** Pressure control methods are used to achieve the target statistical ensembles thermodynamic pressure states. Examples of the pressure control methods that are available for analysis selection in Materials Studio Accelrys are Parrinello, Berendsen, and Anderson [32].

**2.4.4.1 Andersen method.** Andersen method allows the volume of the cell to change while preventing variation in the shape. Andersen method is good for liquid simulations. The

method treats the volume of the cell as a dynamic variable. The kinetic energy term has a user defined mass (M) and a potential term (PV). PV depends on external pressure and the volume of the system [32].

**2.4.4.2 Berendsen method.** Berendsen method couples the system with a pressure bath. Similar to the previous method, volume may change while the cell shape remains. The scaling factor is derived from the following equation [55]

$$\mu = \left(1 + \frac{\Delta t}{t} \gamma (P - P_o)\right)^{1/3} \quad (2.32)$$

where:

$\mu$  is scaling factor,

t is relaxing time constant,

$\gamma$  is the compressibility of the system,

$P_o$  is target pressure, and

P is instantaneous pressure.

**2.4.4.3 Parrinello-Rahman method.** Parrinello-Rahman method [58] is a pressure and stress control method that allows change in both shape and volume. This method is very useful in studying the materials stress-strain relationship. In this method the internal stress can match the external stress applied to the system [32]. One of the most important parameters that this method depends upon is the atomic unit mass. A user defined value, atomic unit mass affects the rate of change of the volume/shape matrix. For large atomic unit mass, the cell will be heavy and slow; for small atomic unit mass, the cell will be fast and the target stress will be reached quickly.

**2.4.5 Time step.** Time step is one of the most important parameters in the dynamic MD simulations. The correct choice of the time step value will lead to stable and accurate results and depends on molecular structure and the various expected atomic motions. In MD analysis

practice the time step should be approximately one tenth of the shortest period of motion of the atoms [7, 52]. Since the vibration range of the atoms in solid lattice is  $10^{-14}$ s, a value of  $10^{-15}$ s (1 fs) will be appropriate as a time step [52]. Though the smaller the time step the more accurate the results but increases the computational requirements.

**2.4.6 Dynamic time.** Total simulation time for the dynamic analysis is also an important parameter in MD runs. If dynamic time is too short the system will not reach a relaxation state and therefore the results will not be reliable and not all possible system configurations are accounted. If MD run time is too long there is also possibility of numerical error accumulation. The range of the MD run is from  $10^3$  to  $10^8$  time steps which are from a few pico seconds to a few hundred nano seconds ( $10^{-9}$ s) [52]. The correct dynamic analysis duration varies across different material systems and several parametric studies are conducted to establish accepted time duration in any MD analysis. Convergence studies of the predicted properties at various dynamic duration analyses is conducted and presented in a subsequent chapter for the cementitious molecular structures.

**2.4.7 Cutoff distance.** During the MD run, most of the computation time involved is to compute the potentials. By using cutoff distance, the long distance interactions become irrelevant. The cutoff distance is a radius of a sphere around each atom where the non-bond interactions outside this sphere are neglected for that atom [52]. This parameter is defined by the user and can vary for different material systems.

Cutoff distance should be smaller than half the unit cell dimension. Further details on the cutoff distances within the context of Materials Studio Accelrys can be found in reference [52].

Figure 2.8 illustrates the meaning of the cutoff distance.

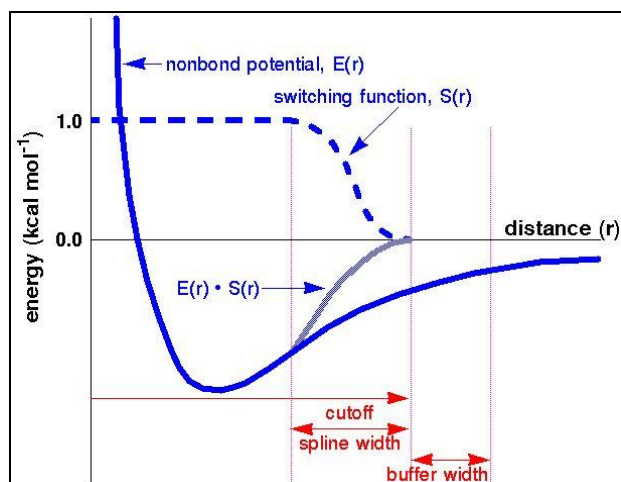


Figure 2.8 Cutoff distance.

## 2.5 Analysis Details

The summary of the analysis parameters discussed above and used in the present MD simulations for the various cementitious material constituents is presented below.

- C<sub>3</sub>S cell size: (11.67x14.24x13.72) Å, and angles are ( $\alpha = 105.5$ ,  $\beta = 94.33$ ,  $\gamma = 90$ )
- C<sub>2</sub>S cell size: (5.48x6.76x9.28) Å, and lattice angles are ( $\alpha = 90$ ,  $\beta = 94.33$ ,  $\gamma = 90$ )
- CH cell size: (5.48x6.76x9.28) Å, and lattice angles are ( $\alpha = 90$ ,  $\beta = 90$ ,  $\gamma = 120$ )
- Jennite cell size: (10.576x7.265x10.931) Å, and lattice angles are ( $\alpha = 101.3$ ,  $\beta = 96.98$ ,  $\gamma = 109.65$ )
- Tobermorite 14 cell size: (6.735x7.425x27.987) Å, and lattice angles are ( $\alpha = 90$ ,  $\beta = 90$ ,  $\gamma = 123.25$ )
- Force field: COMPASS
- Molecular tools: Discover
- Energy minimization: smart minimization
- MD ensemble: NPT
- Temperature: 298K



- Temperature control: Anderson or Nose
- Pressure values: various (GPa)
- Pressure control: Parrinello or Berendsen
- Time step: 1.0 femto second (fs)
- Dynamics time: (100, 200, and 300) pico second (ps)
- Cutoff distance: 12.5 Å
- PBC: on

## CHAPTER 3

### Mechanical Properties Prediction

This chapter focuses on the prediction of mechanical properties of cementitious materials constituents based on their molecular structures. The specific properties predicted through MD simulation are elastic modulus, bulk modulus, shear modulus, and Poisson's ratio. The results for both unhydrated and hydrated cementitious materials are presented.

The organization of this chapter follows.

- Brief discussion and background of the mechanical properties calculation method used within Accelrys Materials Studio.
- MD simulation parameters used in initial analysis.
- MD modeling to study the effect of increasing dynamics time duration on the predicted mechanical properties.
- MD modeling to study the effect of increasing cell sizes on the predicted mechanical properties.
- MD modeling to predict the mechanical properties for both hydrated and un-hydrated cementitious materials,
- Comparison of predicted MD mechanical properties with previously published data at nano, micro, and macro scales.
- MD modeling to predict and understand the variation in predicted properties analyzed at higher thermodynamic pressure state conditions.
- Summary of computational resources required for the MD modeling analysis.
- Concluding remarks.

### 3.1 Mechanical Properties

Mechanical properties such as elastic modulus [59], shear modulus [60], bulk modulus [61], and Poisson's ratio [62] are stiffness characteristics of materials that can be determined via experiments. Molecular dynamics analysis provides an effective methodology for computational prediction of such material properties employing material molecular structures, and has been investigated in a wide range of material systems. Mechanical properties as defined by equivalent bulk modulus, shear modulus, the computed elastic modulus, and Poisson's ration are calculated within Accelrys Materials Studio using both stiffness and compliance matrices, and classical mechanics approximations, as discussed next.

- The results and molecular trajectories (positions and velocities) from the dynamic analysis step of MD within Accelrys yield stiffness matrix (C) and compliance matrix (S). Analysis algorithms within Accelrys Materials Studio determine the general anisotropic stiffness matrix coefficients based on the second derivative of the potential energy with respect to lattice strain components given by [32]

$$C_{ij} = \frac{1}{V} \frac{\partial^2 U}{\partial \varepsilon_i \partial \varepsilon_j} \quad (3.1)$$

where:

$\varepsilon_i, \varepsilon_j$  are lattice strain components,

$U$  is potential energy, and  $V$  is simulation cell volume.

- The resulting Elastic stiffness matrix (C) is in general anisotropic as.

$$C_{ij} = \begin{pmatrix} C_{11} & C_{12} & C_{13} & C_{14} & C_{15} & C_{16} \\ C_{21} & C_{22} & C_{23} & C_{24} & C_{25} & C_{26} \\ C_{31} & C_{32} & C_{33} & C_{34} & C_{35} & C_{36} \\ C_{41} & C_{42} & C_{43} & C_{44} & C_{45} & C_{46} \\ C_{51} & C_{52} & C_{53} & C_{54} & C_{55} & C_{56} \\ C_{61} & C_{62} & C_{63} & C_{64} & C_{65} & C_{66} \end{pmatrix} \quad (3.2)$$

- Elastic compliance matrix (S) which is the inverse of the stiffness matrix(C)

$$S_{ij} = \begin{pmatrix} S_{11} & S_{12} & S_{13} & S_{14} & S_{15} & S_{16} \\ S_{21} & S_{22} & S_{23} & S_{24} & S_{25} & S_{26} \\ S_{31} & S_{32} & S_{33} & S_{34} & S_{35} & S_{36} \\ S_{41} & S_{42} & S_{43} & S_{44} & S_{45} & S_{46} \\ S_{51} & S_{52} & S_{53} & S_{54} & S_{55} & S_{56} \\ S_{61} & S_{62} & S_{63} & S_{64} & S_{65} & S_{66} \end{pmatrix} \quad (3.3)$$

- Bulk modulus (K) using Reuss, Voight, and Hill approximations providing bounds for a homogeneous bulk modulus with the predicted bulk modulus values used in comparison is taken to be equal to  $K_{Hill}$ , which is an average value of Reuss and Voight approximations.

$$K_{Voight} = \frac{1}{9}(C_{11} + C_{22} + C_{33} + 2(C_{12} + C_{13} + C_{23})) \quad (3.4)$$

$$K_{Reuss} = (S_{11} + S_{22} + S_{33} + 2(S_{12} + S_{13} + S_{23}))^{-1} \quad (3.5)$$

$$K_{Hill} = \frac{1}{2}(K_{Voight} + K_{Reuss}) \quad (3.6)$$

- Shear modulus (G) using Reuss, Voight, and Hill approximations with the predicted shear modulus used in the comparisons is considered to be equal to  $G_{Hill}$ , an average of the Reuss and Voight shear modulus values.

$$G_{Voight} = \frac{1}{15}(C_{11} + C_{22} + C_{33} + 3(C_{44} + C_{55} + C_{66}) - C_{12} - C_{13} - C_{23}) \quad (3.7)$$

$$G_{Reuss} = \frac{15}{4(S_{11}+S_{22}+S_{33})-2(S_{12}+S_{13}+S_{23})+3(S_{44}+S_{55}+S_{66})} \quad (3.8)$$

$$G_{Hill} = \frac{1}{2}(G_{Voight} + G_{Reuss}) \quad (3.9)$$

- Poisson's ratio ( $\nu$ ) which is the ratio of lateral to longitudinal strains and can be computed from the following equation based on the above bulk and shear modulus values based on isotropic, homogeneous material assumption.

$$\nu = \frac{3K-2G}{6K+2G} \quad (3.10)$$

where:

$K$  is bulk modulus, and

$G$  is shear modulus.

- Elastic modulus ( $E$ ) follows the prior Poisson's ratio approximation and can be computed from the following equation

$$E = 2G(1 + \nu) \quad (3.11)$$

where:

$G$  is shear modulus, and  $\nu$  is Poisson's ratio.

### 3.2 MD Simulation Parameters for Initial Analysis

As discussed in chapter 2, there are few MD simulation parameters and one of the key parameters is the dynamics analysis time duration. Dynamic analysis time has a significant effect on the time averaged predicted mechanical properties. Careful choice of dynamics analysis time will lead to stable and convergent property averages. Therefore, MD analyses study for different dynamics analysis time values of 100, 200, and 300 ps were performed and the results were compared for the cementitious material constituents to ensure enough molecular configurations for better time averages. The computational cost also increases for larger dynamic time durations. The analysis parameters used in initial MD simulation analysis runs for all cementitious material constituents are the same as mentioned in section 2.5.

The crystalline molecular structures of both unhydrated cement components ( $C_3S$ ,  $C_2S$ ) and hydrated cement products (CH, C-S-H Jennite, and C-S-H Tobermorite<sup>14</sup>) were obtained from the American Mineralogist Crystalline Structure Database [13].

Table 3.1 shows the crystalline structure dimensions for all cementitious components employed in the present study.

Table 3.1

*Crystalline Structures Dimensions*

Cell Parameters	C <sub>3</sub> S	C <sub>2</sub> S	CH	Jennite (C-S-H)	Tobermorite 14 (C-S-H)
Space group	P-1	P21/n	P-3m1	P1	BIIb
Space group number	2	14	164	2	15
lattice	Triclinic	Monoclinic	Trigonal	Triclinic	Monoclinic
Cell-a (Å)	11.67	5.48	3.5925	10.576	6.735
Cell-b (Å)	14.24	6.76	3.5925	7.265	7.425
Cell-c (Å)	13.72	9.28	4.905	10.931	27.987
Cell-angle $\alpha$ (Degrees)	105.5	90	90	101.3	90
Cell- angle $\beta$ (Degrees)	94.33	94.33	90	96.98	90
Cell- angle $\gamma$ (Degrees)	90	90	120	109.65	123.25

**3.3 Comparison of Mechanical Properties Predicted from Different MD Analysis Time****Durations**

Using materials studio, the associated predictive mechanical properties from the MD analysis of unhydrated cement components (C<sub>3</sub>S, C<sub>2</sub>S) and hydrated cement products (CH, C-S-H Jennite, and C-S-H Tobermorite14) at atmospheric pressure were obtained. Three different dynamic time duration values were employed in these preliminary MD analysis studies. Table 1 appendix A shows elastic modulus, bulk modulus, and shear modulus for both unhydrated and hydrated cement components obtained from MD analysis for different dynamics time durations.

These property predictions from MD analysis performed for different dynamic durations are shown in Figure 3.1. From this figure it is clear that the dynamic analysis time duration influences the predicted properties, as these are based on time averaged values. Fluctuations and significant variations are seen in some cementitious molecular material structures while others show a reasonable convergence. The accepted dynamic analysis time depends on the material system analyzed. Further long term dynamic duration analysis is needed for further refinement of this. It is to be noted that the computational time significantly increases for longer time duration analysis.

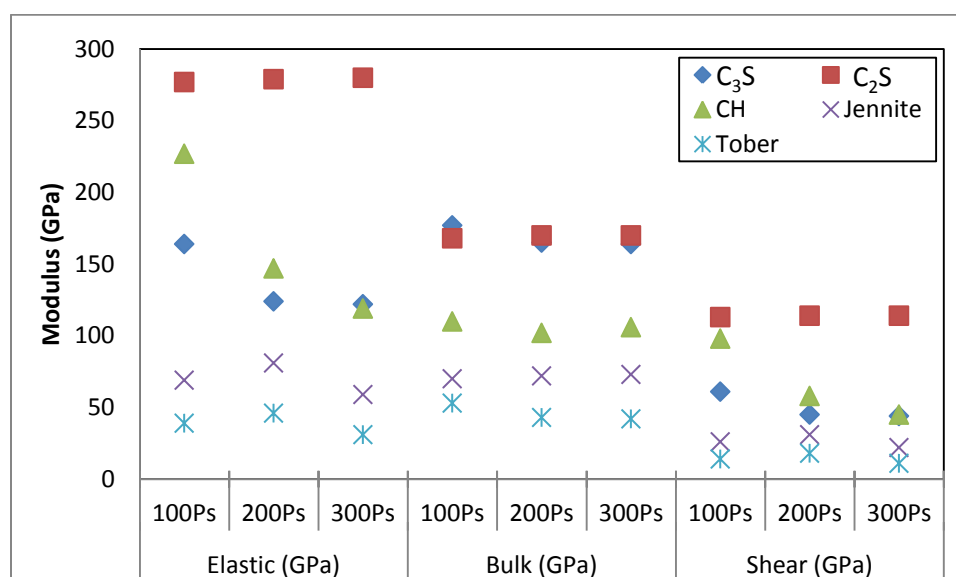


Figure 3.1 Predicted mechanical properties from MD analysis employing different dynamics time durations.

Considering multiple factors involved, it can be inferred that the mechanical properties are nearly equal for most of the cementitious materials. CH mechanical properties results show a decrease in the elastic modulus and shear modulus with the increase in MD analysis time duration. For further models and dynamic analysis the choice of 100 ps was selected as an appropriate value for the dynamics time parameter.

Table 3.2 shows Poisson's ratio comparison for cementitious materials computed from MD analysis performed with different dynamics time durations.

Table 3.2

*Poisson's Ratio at Different Dynamics Time Durations*

Property	Poisson's ratio		
	100 Ps	200 Ps	300 Ps
C <sub>3</sub> S	0.35	0.37	0.37
C <sub>2</sub> S	0.23	0.22	0.22
CH	0.15	0.26	0.31
C-S-H Jennite	0.34	0.31	0.36
C-S-H Tobermorite	0.38	0.32	0.38

### 3.4 Influence of Different Molecular Cell Sizes on the Predicted Mechanical Properties

The size of the molecular structure and the number of unit cell molecular configurations also influence the predicted properties from MD analysis. Though periodic boundary conditions are employed, the boundary effects are higher in the case of single unit cell, while large cell configurations (several unit cells) reduce the boundary effects. They increase the material system size, but making them computationally expensive. Mechanical properties were obtained from MD analysis performed with different cell size models. Three different molecular cell size models formed from the unit cell configurations of the different material systems were studied. Tables (2 – 6) appendix A present the predicted mechanical properties from MD dynamic analysis for 100 ps for cementitious materials components based on these 3 cell volumes, cell size parameters, and number of atoms involved for all three cases of cell volume.



Figure 3.2 presents consolidated mechanical properties comparison for both unhydrated and hydrated cementitious material constituents utilizing different cell sizes. No significant variation is noted in most cases except for CH and  $C_3S$ .

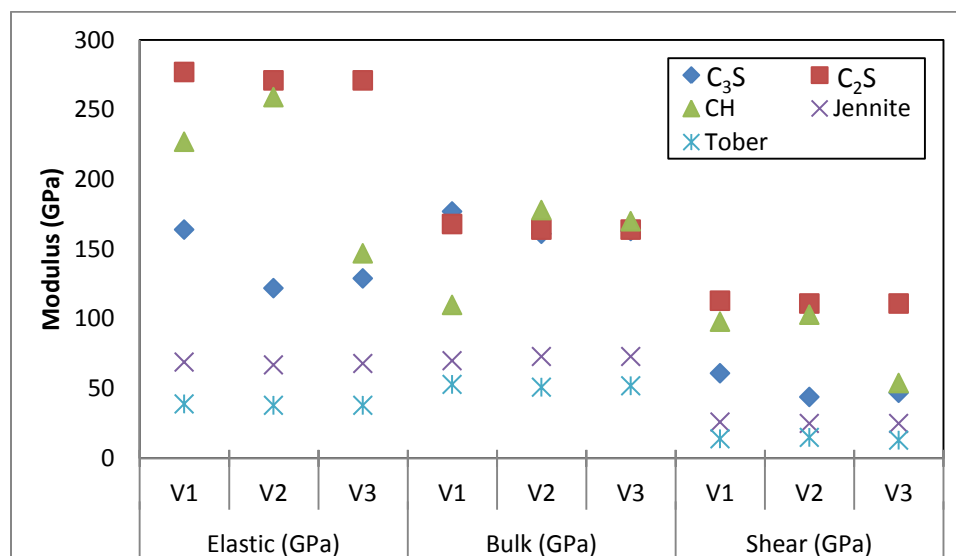


Figure 3.2 Mechanical properties for different cell sizes.

Table 3.3 presents the Poisson's ratio predictions from MD analysis of different cell sizes. There is no significant difference in Poisson's ratio results except for CH structure.

Table 3.3

*Predicted Poisson's Ratio from MD Analysis with Different Cell Sizes*

Property	Poisson's Ratio		
	V1	V2	V3
Cell size			
$C_3S$	0.35	0.37	0.37
$C_2S$	0.23	0.22	0.22
CH	0.23	0.26	0.36
C-S-H Jennite	0.34	0.34	0.34
C-S-H Tobermorite	0.38	0.37	0.37

### 3.5 MD Modeling Analysis for Mechanical Property Predictions

Following the MD simulation parameters as discussed in chapter 2 and the prior section in this chapter, all subsequent MD analysis studies for mechanical property predictions used dynamic times of 100 ps and cell size of 1 unit cell size. Other MD analysis parameters were taken to be the same as presented earlier in chapter 2.

Table 3.4 shows predicted mechanical properties obtained from MD analysis summarized for all cementitious materials at atmospheric pressure.

Table 3.4

#### *Mechanical Properties Results*

Properties	C <sub>3</sub> S	C <sub>2</sub> S	CH	Jennite	Tobermorite
Elastic modulus (GPa)	164	277	227	69	39
Bulk modulus (GPa)	177	168	110	70	53
Shear modulus (GPa)	61	113	98	26	14
Poisson's ratio	0.35	0.23	0.15	0.34	0.38

#### **3.5.1 Comparison of MD analysis predicted mechanical properties for C<sub>3</sub>S and C<sub>2</sub>S.**

Table 3.5 compares the mechanical properties obtained from the present work based on MD analysis and available data from literature for C<sub>3</sub>S molecular structures.

Mechanical property predictions from the current MD analysis are in excellent correlation with prior MD analysis results [63] at atmospheric pressures. The results are also reasonably comparable to the experimental values from nanoindentation experiments, which are generally at a larger material scale than the MD analysis, and other reported data based on resonance frequency tests at micro scale level [24, 25, 26, 28].

Table 3.5

*C<sub>3</sub>S MD Analysis Predictions and Available Literature Data*

Cement Compound	C <sub>3</sub> S				
	Current Nano/molecular scale	Ref. [63] Nano scale (MD)	Ref.[28] Micro scale (Resonance)	Ref.[26, 28] Micro scale (Nanoindentation)	Ref. [24, 25] Macro scale (Resonance)
Elastic (GPa)	164	168	147	135	117.6
Bulk (GPa)	177	180	N/A	N/A	105.2
Shear (GPa)	61	63	N/A	N/A	44.8
Poisson's Ratio	0.35	0.34	0.30	0.31	0.314

Figure 3.3 shows different length scales comparison of C<sub>3</sub>S mechanical properties based on MD analysis and other values from literature.

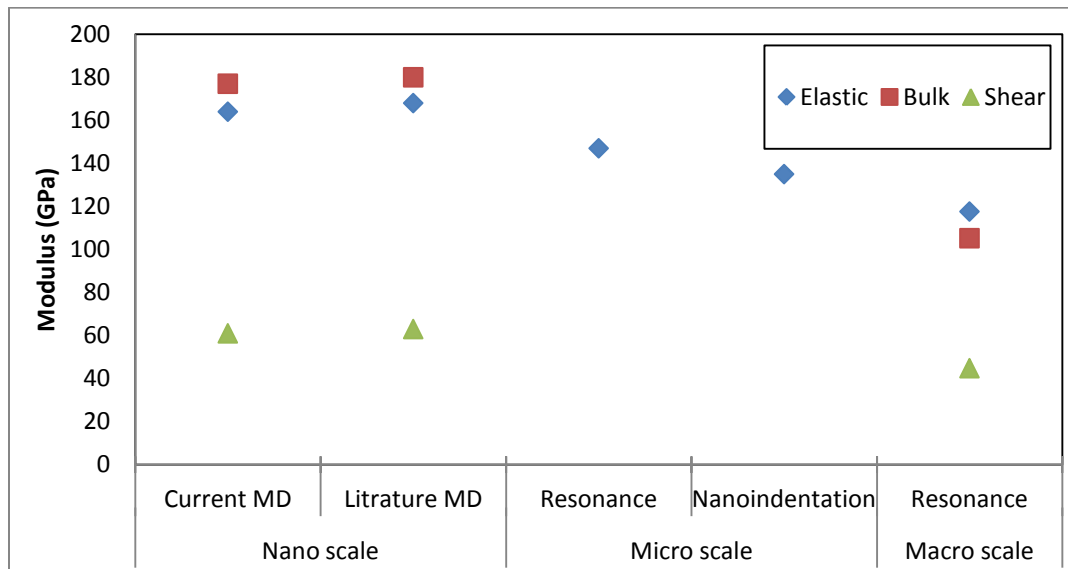


Figure 3.3 C<sub>3</sub>S mechanical properties results comparison.

Table 3.6 and Figure 3.4 show different length scales comparison of  $C_2S$  mechanical properties based on MD analysis and other values from literature.

Table 3.6

$C_2S$  MD Analysis Predictions and Available Literature Data

Cement Compound	$C_2S$				
	Current Nano/molecular scale	Ref. [63] Nano scale (MD)	Ref.[28] Micro scale (Resonance)	Ref.[26, 28] Micro scale (Nanoindentation)	Ref. [24, 25] Macro scale (Resonance)
Elastic (GPa)	277	285	130	140	117.6
Bulk (GPa)	168	177	N/A	N/A	105.2
Shear (GPa)	113	116	N/A	N/A	44.8
Poisson's ratio	0.23	0.23	0.19	0.19	0.314

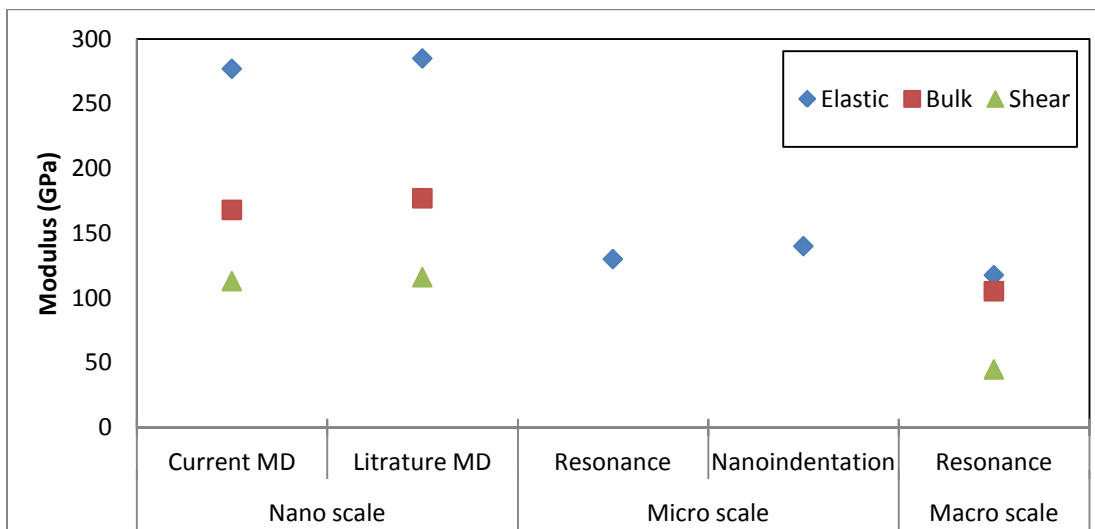


Figure 3.4  $C_2S$  mechanical properties results comparison.

**3.5.2 Hydrated cement CH mechanical properties comparison.** Table 3.7 presents a comparison of predicted mechanical properties from MD analysis with the available literature data for CH. Though the results show excellent correlation with the literature results based on MD analysis, a good difference is seen in comparison to other testing methods involving larger material sizes [63].

Table 3.7

*CH MD Analysis Predictions and Literature Data*

Cement Compound	CH				
	Current Nano scale	Ref. [63] Nano scale (MD)	Ref.[4] Micro scale (Nanoindentation)	Ref.[27, 64] Micro scale (Mathematical Method)	Ref. [24] Macro scale Cement paste (Ultrasonic)
Elastic (GPa)	227	239	38	72.8	15.5 - 18
Bulk (GPa)	110	122	N/A	40	10 - 11
Shear (GPa)	98	90	N/A	16	6 - 7
Poisson's ratio	0.15	0.24	N/A	0.324	0.46 - 0.5

Figure 3.5 shows a graphical comparison of mechanical properties of CH from MD analysis with the data available at larger length scales from literature. Though the predictions from this and past MD analysis are in good agreement, properties based on material at different length scales and associated techniques show a significant deviation.

These property data clearly show the existence of a scale effect in the associated properties of the material systems with the reduced properties reported at micro, meso scales than at molecular scale.

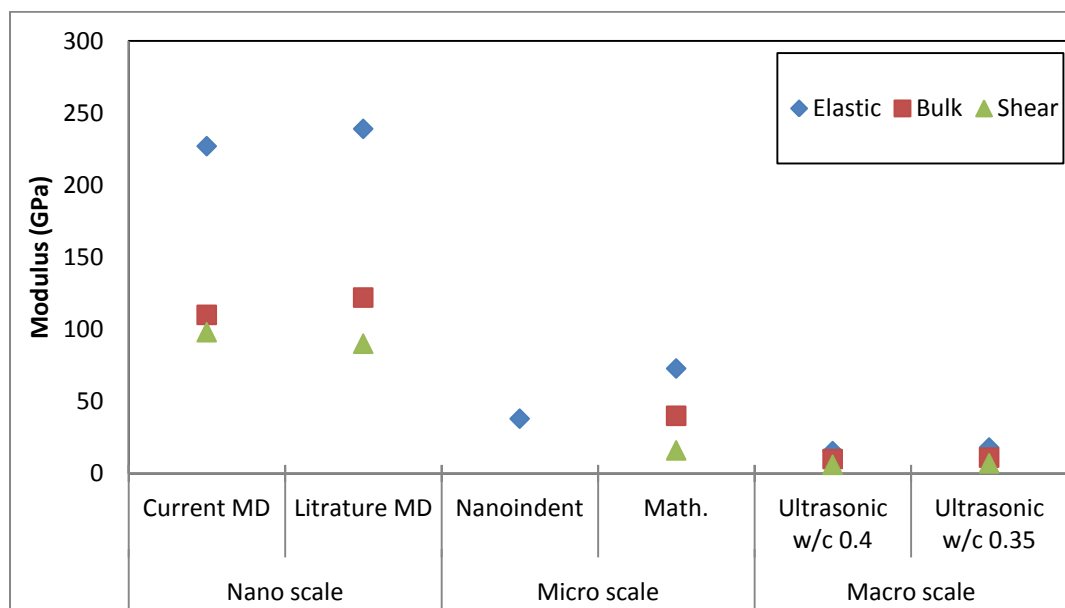


Figure 3.5 CH mechanical properties comparison.

### 3.5.3 C-S-H MD predicted mechanical properties and comparison to literature

**values.** For C-S-H Jennite and Tobermorite 14 structures, the mechanical properties were obtained and compared with available data from both MD models and experimental characterizations at larger scales at atmospheric pressure.

The results for current analysis predictions were in excellent correlation with prior MD analysis results [32] at atmospheric pressures. The results correlate well with both micro scale nano-indentation based averaged experimental values [4, 28] and those based on resonance frequency. As well, the results correlate with NIST model [26] at water/cement ratio of 0.45 and 14 days, or at water/cement ratio of 0.5 and 56 days. Also MD results were compared with macro scale results at water/cement ratio of 0.4 after 24 hours of hydration and at water/cement ratio of 0.35 after 24 hours of hydration [24].

Table 3.8 and Figure 3.6 present the MD analysis predictions of mechanical properties compared to available experimental data for C-S-H Jennite.

Table 3.8

*Jennite C-S-H MD Analysis Mechanical Properties and Literature Data*

Cement	C-S-H Jennite			
Mechanical Properties	Current Nano scale (MD)	Ref. [63] Nano scale (MD)	Ref.[4, 28] Micro scale (Nanoindentation)	Ref. [24] Macro scale (Ultrasonic)
Elastic (GPa)	69	82	22	15.5 - 18
Bulk (GPa)	70	78	15	10 - 11
Shear (GPa)	26	31	9	6 - 7
Poisson's Ratio	0.34	0.33	0.25	0.46 - 0.5

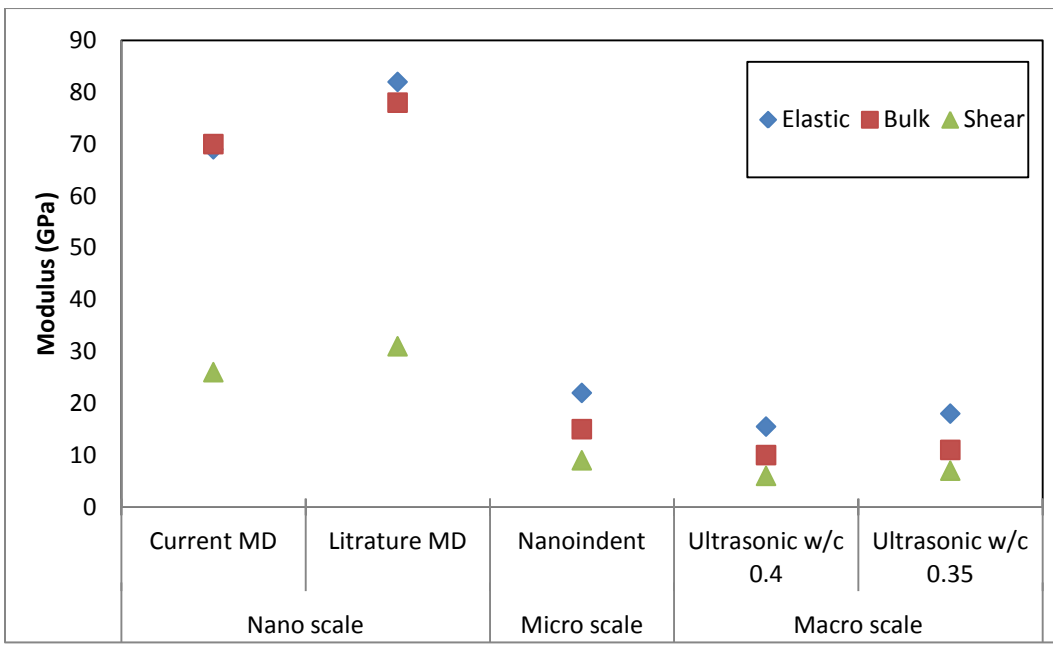


Figure 3.6 C-S-H Jennite mechanical properties comparison.

Table 3.9 and Figure 3.7 present the MD analysis predictions of mechanical properties compared to available experimental data for C-S-H Tobermorite 14.

Table 3.9

*C-S-H Tobermorite 14 Mechanical Properties Comparison*

Cement	C-S-H Tobermorite 14			
	Current Nano scale	Ref. [63] Nano scale (MD)	Ref.[4, 28] Micro scale (Nanoindentation)	Ref. [24] Macro scale (Ultrasonic)
Elastic (GPa)	39	43	22	15.5 - 18
Bulk (GPa)	53	46	15	10 - 11
Shear (GPa)	14	39	9	6 - 7
Poisson's ratio	0.38	0.34	0.25	0.46 - 0.5

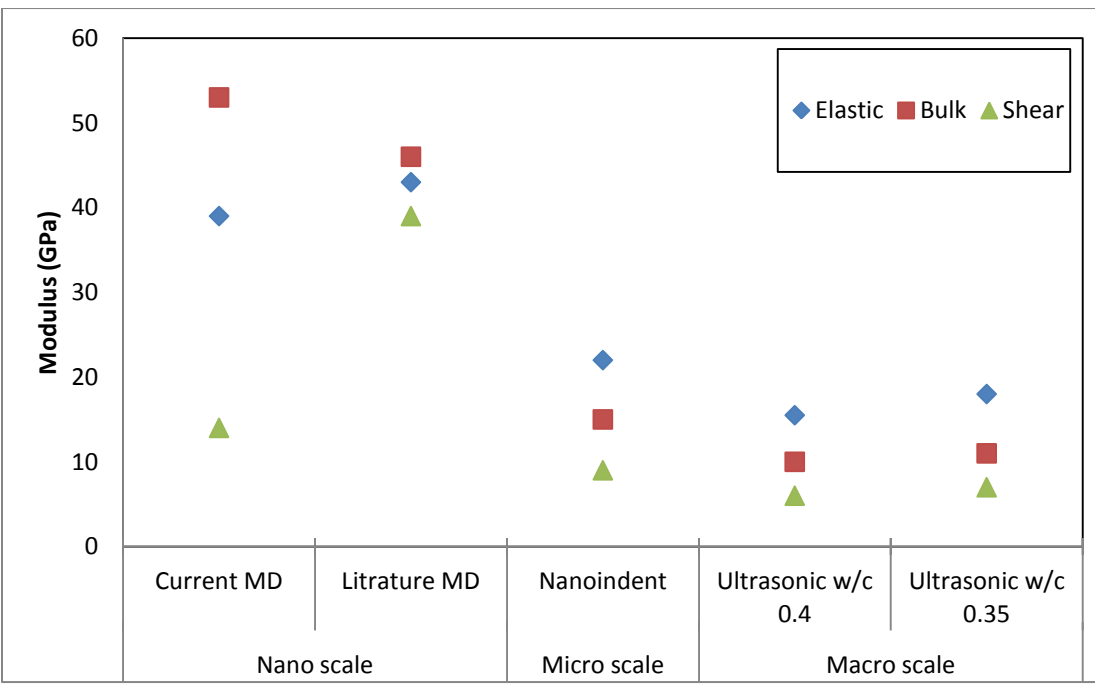


Figure 3.7 Tobermorite 14 mechanical properties comparison.



In all these comparisons presented earlier, MD analysis predictions from the current work were in good agreement with results obtained using MD analysis. However, significant deviations are seen in the properties when compared with experimental data from various experimental characterization methods at larger scales. This can be attributed to the “scale effect” where the nano / molecular level material exhibits higher properties values compared to the properties obtained from larger material sizes.

### **3.6 Property Predictions at Higher Pressure States via MD Analysis**

Material properties and behavior are influenced by variations in thermodynamic state conditions. Higher pressure state conditions are experienced in high strain rate and dynamic behavior of materials under shock and ballistic loading conditions. It is essential to understand potential variations in the mechanical properties of materials under higher pressure state conditions where experimental methods have limitations. Pressure is one of the key factors in MD analysis that can be varied in the defined ensemble. Thus, MD can be effectively used to study the behavior of cementitious materials at higher pressure values. In the present research, MD analysis was employed to predict mechanical properties for cementitious materials under different higher pressures. Several MD analysis simulation runs for a dynamic time of 100 ps were completed for different pressure values of 0.0001, 0.001, 0.01, 0.05, 0.1, 0.2, 0.4, 0.6, 0.8, 1.0, 1.5, and 2.0 GPa. All MD parameters for these studies were the same as in the models to estimate the properties at atmospheric pressure except for the use different ensemble state pressure.

The results from MD analysis of unhydrated cement components ( $C_3S$ ,  $C_2S$ ), and hydrated cement products (CH, C-S-H Jennite and Tobermorite<sup>14</sup>) at different pressure values and the associated predictive mechanical property values obtained are discussed next.

**3.6.1 C<sub>3</sub>S MD analysis of mechanical properties at high pressures.** For C<sub>3</sub>S, thermodynamic pressure state of the Ensemble was modified from 0.0001 to 2.0 GPa with individual simulations completed for each ensemble pressure state. Results show a fluctuation in the elastic modulus, bulk modulus, and shear modulus values with the increase of pressure until about 1.0 GPa in the pressure value range studied. Subsequently, there were no significant changes. Table 7 appendix A and Figure 3.8 show the predicted mechanical properties at different ensemble pressure states.

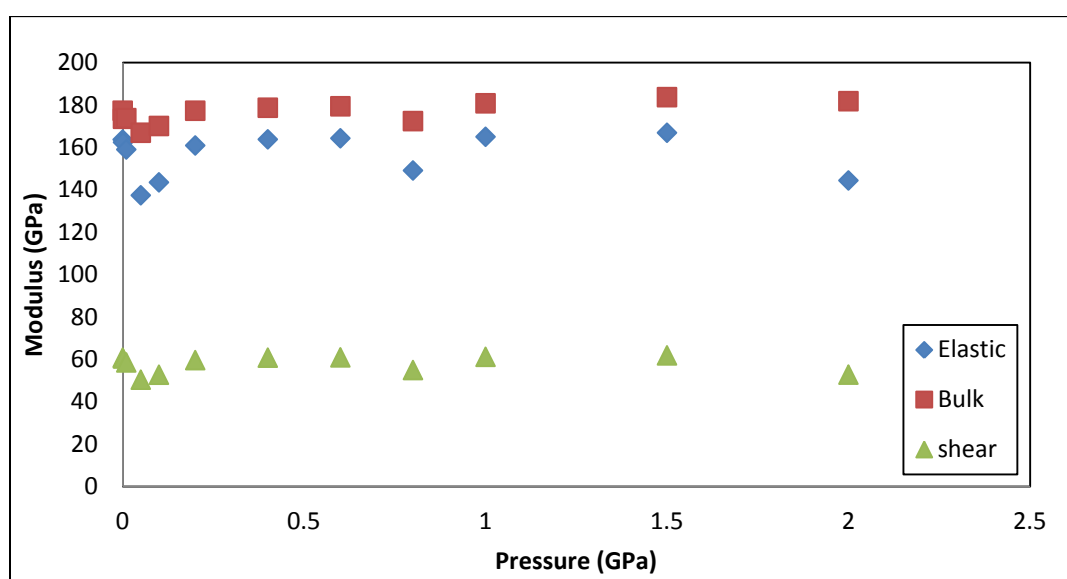


Figure 3.8 C<sub>3</sub>S modulus results at higher pressures.

**3.6.2 C<sub>2</sub>S MD analysis predicted mechanical properties at different pressures.** For C<sub>2</sub>S, elastic modulus, bulk modulus, and shear modulus did not show significant variations in the pressure ranges studied as seen in Figure 3.9 at different ensemble state pressures from the atmospheric pressure to 2.0 GPa. Table 8 appendix A show C<sub>2</sub>S predicted mechanical properties values at various pressures.

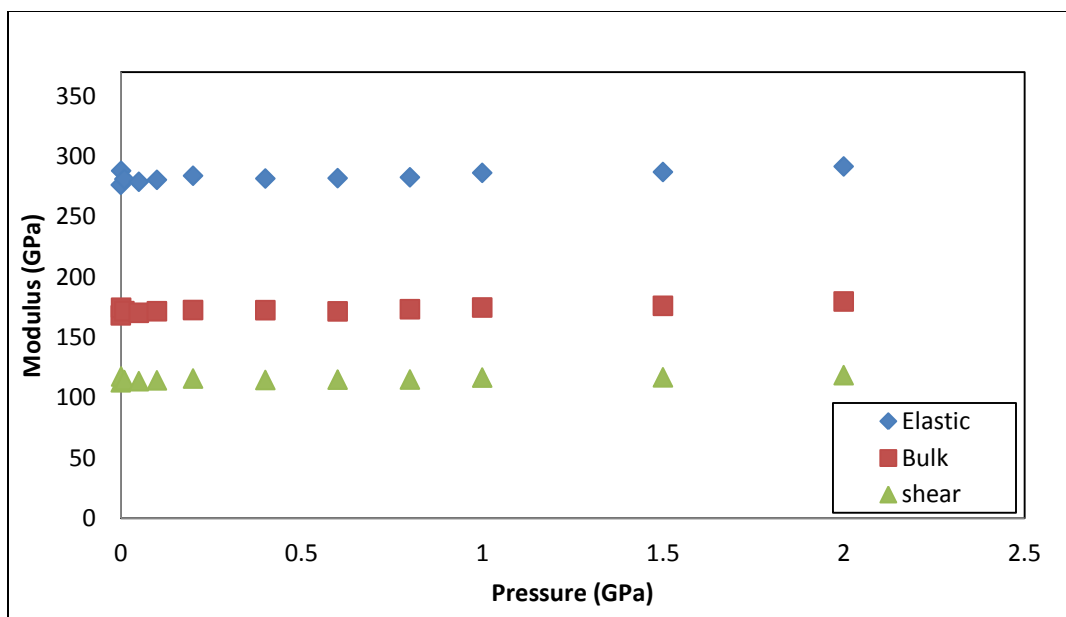


Figure 3.9 C<sub>2</sub>S properties vs. pressure values (0.0001-2.0) GPa.

### 3.6.3 MD analysis of mechanical properties for CH at different ensemble pressures.

For CH, elastic modulus, bulk modulus, and shear modulus results show variations with the increase of the pressure, while there was no significant variation for bulk modulus. Table 9 appendix A and Figure 3.10 show CH predicted mechanical properties at various pressures.

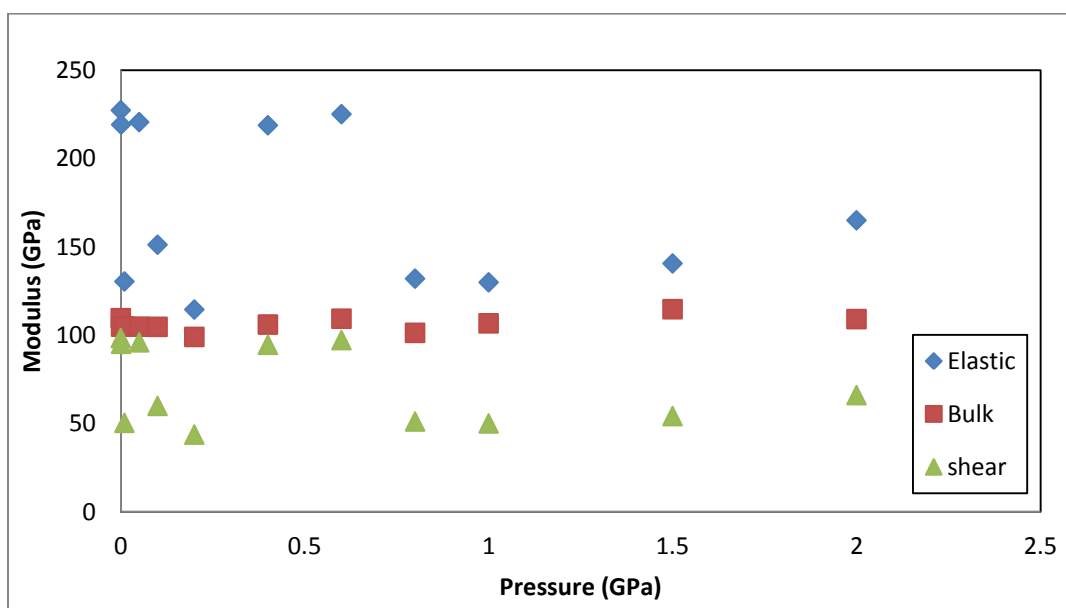


Figure 3.10 MD analysis of predicted properties for CH at various ensemble pressure range.

**3.6.4 C-S-H Jennite MD analysis predicted mechanical properties at various ensemble pressure states.** Table 10 appendix A and Figure 3.11 show C-S-H Jennite mechanical properties at various pressures from the atmospheric pressure to 2.0 GPa.

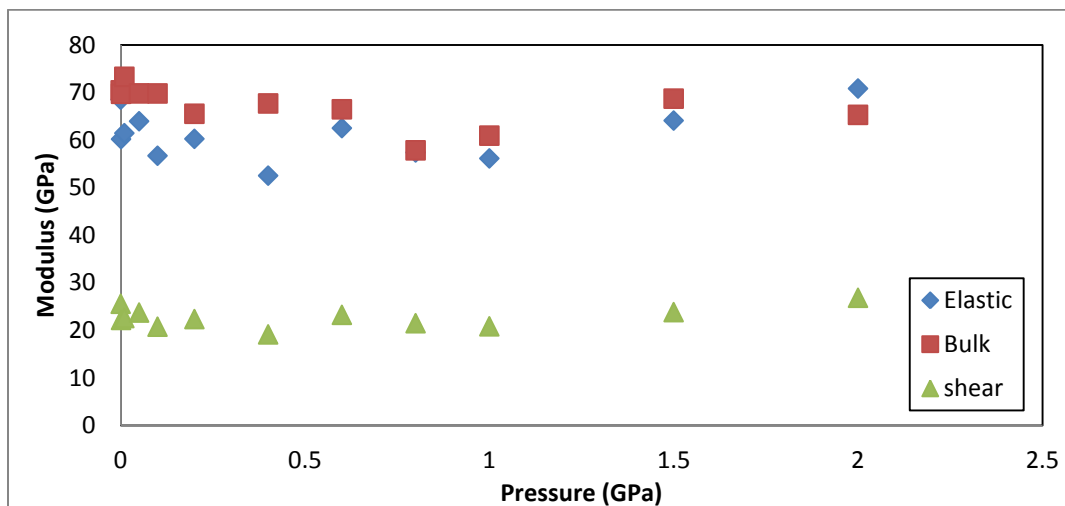


Figure 3.11 C-S-H Jennite mechanical properties vs. pressure.

**3.6.5 MD analysis for predictive mechanical properties for C-S-H Tobermorite 14 at different ensemble pressure states.** Table 11 appendix A and Figure 3.12 show Tobermorite mechanical properties at different pressures. For Tobermorite 14, a decrease of the mechanical properties was found with the increase of the pressures from 0.0001 to 0.1 GPa.

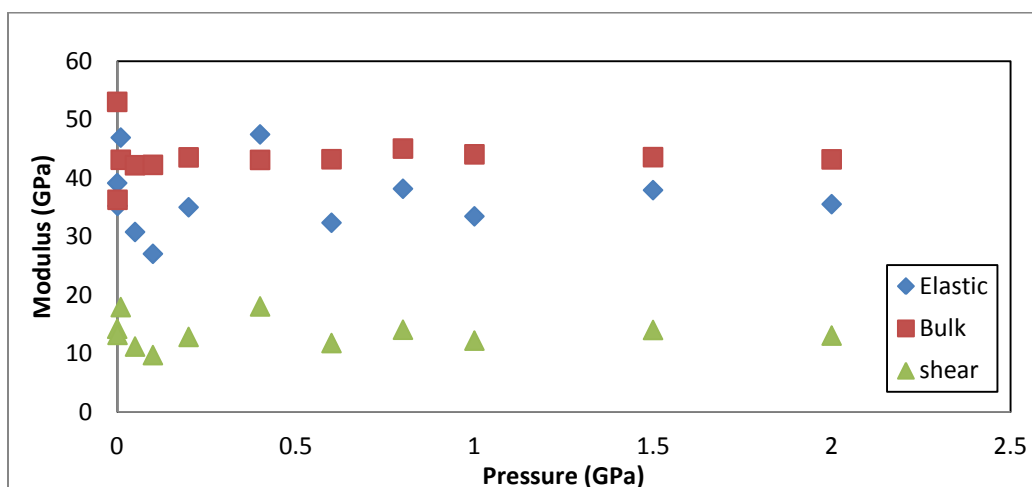


Figure 3.12 C-S-H Tobermorite properties vs. pressure.

**3.6.6 Poisson's ratio at different ensemble pressure states.** Poisson's ratio results demonstrated a fluctuation effect with the change in pressures for  $C_3S$ ,  $C_2S$ , CH, Jennite, and Tobermorite 14. For  $C_3S$ , results almost stable around 0.35. For  $C_2S$ , results were almost stable around 0.22. For CH, results fluctuated between 0.15 and 0.3. For Jennite and Tobermorite 14, results fluctuated between 0.3 and 0.4. Table 12 appendix A and Figure 3.13 shows the Poisson's ratio obtained from MD analysis predictions for cementitious materials at different pressures.

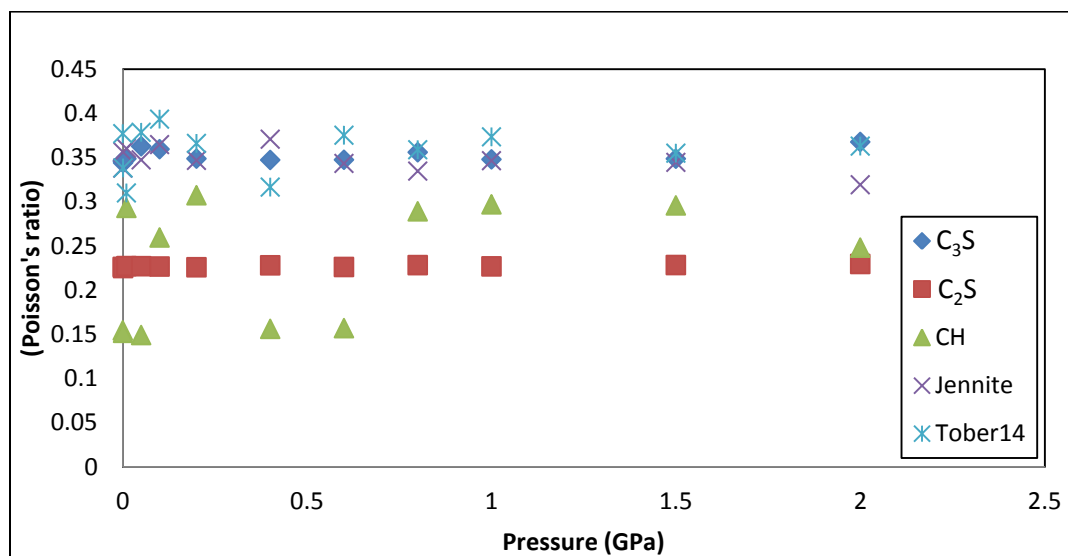


Figure 3.13 Poisson's ratio at different pressure value.

The results presented above have clearly shown that the predicted properties are influenced by the pressure in the system. MD provides an effective method to understand such variations based on the material molecular structures.

High strain rate dynamic loading conditions such as those produced by shock waves, or detonations lead to materials experiencing high pressure conditions. MD modeling provides means to investigate the associated property variations that are essential for the understanding of new material systems. Changes in molecular features impact the behavior of materials and MD also provide means to understand such effects.

MD analysis requires significant computational resources. A brief discussion of the computational resources employed in various modeling analysis studies is presented next.

### 3.7 Computational Resources

For all previous molecular structures discussed in this chapter, the MD modeling analysis runs were performed on an Intel processor based computer using Accelrys Material Studio.

Computation time (s) for different models analysis on the same computing system is presented in Table 3.10 and Table 3.11.

Table 3.10

*Computing Time for Different Pressures*

Pressure (GPa)	C <sub>3</sub> S	C <sub>2</sub> S	CH	Jennite	Tobermorite
0.0001	1600.04	216.97	80.32	567.98	2393.88
0.001	1068.34	223.77	79.59	569.47	2328.83
0.01	1083.66	225.69	82.76	594.99	2439.96
0.05	1081.13	228.49	82.87	587.66	2524.08
0.1	1099.23	221.3	86.22	590.96	2382.99
0.2	1097.03	232.52	76.81	577.27	2473.29
0.4	1057.42	226.64	81.57	583.04	2446
0.6	1130.38	223.99	82.59	585.61	2504.5
0.8	1129.09	224.39	82.84	587.83	2457.37
1	1089.71	219.43	84.74	587.2	2413.43
1.5	1115.14	234.66	84.71	594.1	2485.58
2	1110.31	223.05	83.65	585.5	2490.91

Table 3.11

*Computing Time for Different Cell Sizes and Dynamic Time Models*

Time (s)	V1	V2	V3	(V1) 100 ps	(V1) 200 ps	(V1) 300 ps
C <sub>3</sub> S	1600.04	27006.91	128561.3	1600.04	2115.97	3585.09
C <sub>2</sub> S	216.97	217.03	219.31	216.97	488.18	842.42
CH	80.32	284.17	1075.17	80.32	216.06	314.48
Jennite	567.98	5400.41	47829.89	567.98	1248.07	1730.72
Tober 14	2393.88	15390.56	185564.2	2393.88	4963.8	7279.63

Computational time increases with the increase of the cell sizes because the number of atoms increases. Also, increasing the dynamic time increases the computational time but at a smaller rate than cell sizes variance. For higher pressure models, the computational time fluctuates with increasing of pressure.

### 3.8 Concluding Remarks

MD modeling analysis provides a viable methodology for the prediction of mechanical properties of different cementitious material constituents based on their molecular structures. The present research focused on the study and understanding of the effect of high pressure ensemble states on these predicted mechanical properties. The analysis results clearly indicate that the predicted mechanical properties and structure configuration of cement components and hydrated cement products are influenced by ensemble pressure states.

## CHAPTER 4

### MD Methodology for Mie-Gruneisen EOS Characterization

This chapter presents an overview of the background theory related to the materials dynamic behavior when subjected to propagating shock waves. Also, background discussions on the theory behind Hugoniot curves are presented. This is not meant to be an exhaustive discussion and is included to provide the required background for the MD based computational material modeling methodology for the characterization of Equation of State (EOS) model. Generally, characterization of such EOS requires extensive high strain rate experiments and the specialized material coupons. As noted in prior chapters, fundamental molecular structure and chemistry of a material system defines its properties and behavior. The present work following this philosophy proposes and presents a molecular dynamics modeling based methodology that can be employed to characterize an EOS employing the associated material molecular structure. Such a fully computational based methodology allows one to understand the expected behavior of material systems including the modifications to the molecular structure *a priori* in Materials by Design modeling framework. In addition the variations expected due to changes in the fundamental material molecular structure building upon the new evolving concepts of material genome coupling material science and engineering and mechanics can also be studied. In particular, a proposed MD methodology to obtain the characteristic parameters that characterize and define the Hugoniot curves for a material based on their molecular structures is explained.

The chapter concludes with a complete presentation of the MD analysis methodology involved in material modeling characterization for Mie-Gruneisen EOS model, one of the several EOS material models discussed in literature. The application of this methodology for hydrated



cement material constituent C-S-H Jennite based on its molecular structure is demonstrated in the next chapter.

#### 4.1 Shock Wave Propagation Theory

A shock, shock front, or shock wave is a perturbation propagating through a medium at a speed higher than the speed of sound in that medium that can be in solid, liquid, gas or plasma.

Figure 4.1 illustrates shock wave propagation through medium [65].

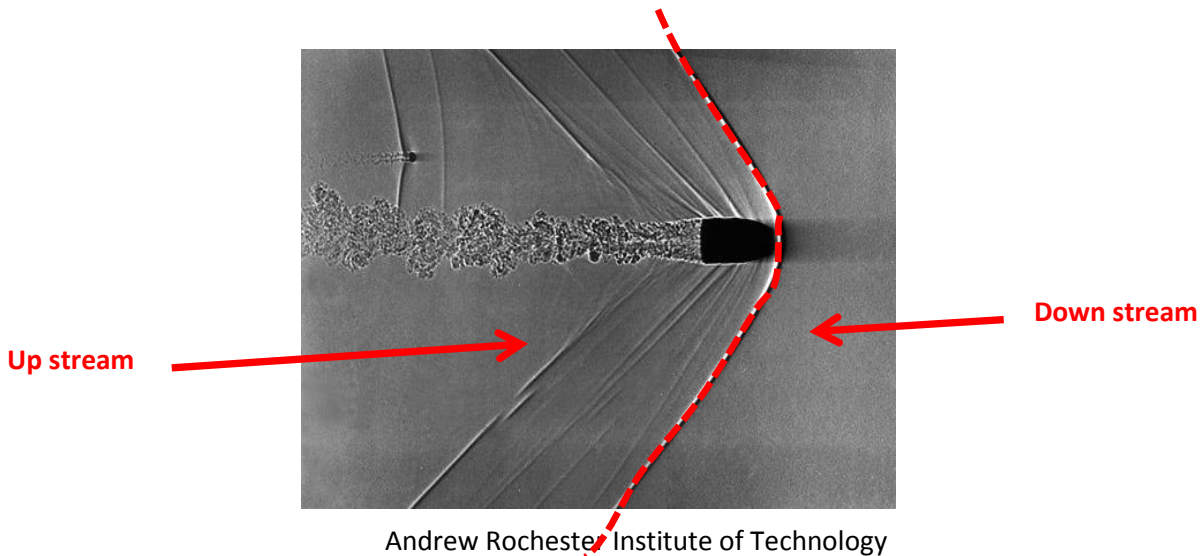


*Figure 4.1* Representation of shock wave propagation through medium.

The propagation of a shock through a material creates two different regions with very distinct properties, one corresponds to the material affected by the passing of the shock (upstream material,  $S^+$ ) and the other corresponding to the material yet to be affected by the shock (downstream material,  $S^-$ ) [66]. During the propagation of a shock through a medium, it is assumed that the only continuous field variable is the displacement. All other field variables such as stress, particle velocity, and mass density are discontinuous.

Upstream material ( $S^+$ ) can be characterized by the following four quantities.

- $(\rho^+)$ : Material density.
- $(t^+)$ : Longitudinal stress.
- $(\epsilon^+)$ : Specific internal energy.
- $(\dot{X}^+)$ : Particle velocity.

Similarly, downstream material( $S^-$ ) can be characterized by the following four quantities.

- $(\rho^-)$ : Material density.
- $(t^-)$ : Longitudinal stress.
- $(\epsilon^-)$ : Specific internal energy.
- $(\dot{X}^-)$ : Particle velocity.

In the case of uniaxial shock propagation, the upstream and downstream quantities along with the shock velocity ( $U_s$ ) form a set of nine variables that describes the effect of any longitudinal shock on the material.

In most cases, the state of the downstream material ( $S^-$ ) that is still not under the influence of propagating shock and the shock velocity are known (corresponding to the unloaded characteristics of the material) which means there are four quantities remaining for a complete characterization of the effect of the shock. The description and solution of these four quantities requires a set of four equations. Three of those equations are the conservation laws (conservation of mass, linear momentum, and energy) across the shock front. For plane longitudinal shocks, these conservation law equations are called Jump equations. The fourth required equation is the equation of state (EOS) which describes the relation between state variables of the material [66].

High strain rate dynamic behavior of materials can be investigated based on the effects produced by the passing of a longitudinal shock wave through materials. Theoretical background

of the governing mathematical equations for the longitudinal shock wave propagation that forms the basis of the molecular dynamics modeling methodology is presented next.

**4.1.1 Continuum mechanics equations.** In continuum mechanics there are two equivalent forms to describe the deformation of a body: Eulerian and Lagrangian descriptions [67].

Eulerian description, also called spatial description, focuses on what happens at a given position during the deformation. Eulerian description thus follows a particular geometric position in the un-deformed body. Lagrangian description, also called material description, focuses on what happens to a given material particle throughout the deformation process. Figure 4.2 schematically shows the reference and current configuration of a deforming body [67].

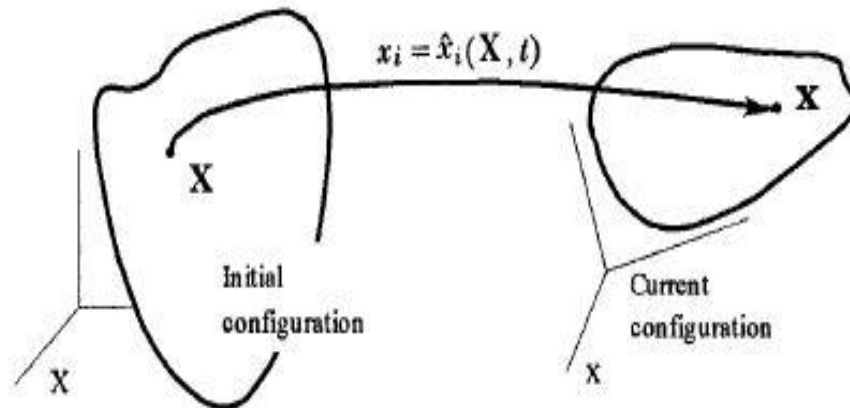


Figure 4.2 Reference and current configurations of a body.

Conservation equations for uniaxial deformation can be presented in Eulerian form by the following differential equations [67]:

- Conservation of mass

$$\frac{\partial \rho}{\partial t} + \frac{\partial}{\partial x}(\rho \dot{x}) = 0.0 \quad (4.1)$$

where:

$\rho$  is the material density,

$\dot{x}$  is the particle velocity,

$x$  is the position, and

$t$  is time.

- Conservation of linear momentum is given by

$$\frac{\partial t_{11}}{\partial x} - \rho \left( \frac{\partial \dot{x}}{\partial t} + \frac{\partial \dot{x}}{\partial x} \dot{x} \right) = -\rho f \quad (4.2)$$

where:

$t_{11}$  is the longitudinal stress, and

$f$  is the external force per unit mass of material.

- Conservation of energy is given by

$$\rho \left( \frac{\partial \varepsilon}{\partial t} + \frac{\partial \varepsilon}{\partial x} \dot{x} \right) - t_{11} \left( \frac{\partial \dot{x}}{\partial x} \right) = -\frac{\partial q}{\partial x} + \rho r \quad (4.3)$$

where:

$q$  is the heat flux vector (the rate of transferred energy out of the system per unit area),

$r$  is the external heat supply (the rate of transferred energy into the system per unit area), and

$\varepsilon$  is the specific internal energy (internal energy per unit mass).

Similarly, conservation equations for uniaxial deformation can be presented in Lagrangian form by the following differential equations [67]:

- Conservation of mass

$$\frac{\partial \dot{x}}{\partial X} - \rho_R \frac{\partial v}{\partial t} = 0.0 \quad (4.4)$$

where:

$\rho_R$  is the reference density, and  $v$  is the volume.

- Conservation of linear momentum is given by

$$\frac{\partial t_{11}}{\partial X} - \rho_R \frac{\partial \dot{x}}{\partial t} = -\rho_R f \quad (4.5)$$

where:

$f$  is the external force per unit mass of material.

- Conservation of energy is given by

$$\rho_R \frac{\partial \varepsilon}{\partial t} - t_{11} \left( \frac{\partial \dot{x}}{\partial X} \right) = -\frac{\partial Q}{\partial X} + \rho_R r \quad (4.6)$$

where:

$Q$  is the Lagrangian heat flux vector.

**4.1.2 Jump equations.** Jump equations represent conservation laws across the propagating longitudinal shock front. They describe the transition between two uniform states across a shock front. When the shock occurs, there are discontinuities in the field variables. Due to these discontinuities, differential forms of the conservation equations, similar to those presented in the previous section, are not applicable [68].

Therefore, an integral form of the conservation laws is needed to describe the effect of a longitudinal shock through a material. The integral forms of conservation laws across the shock front are called Jump equations. Figure 4.3 illustrates the discontinuity between the upstream and downstream sides during longitudinal shock propagation [66].

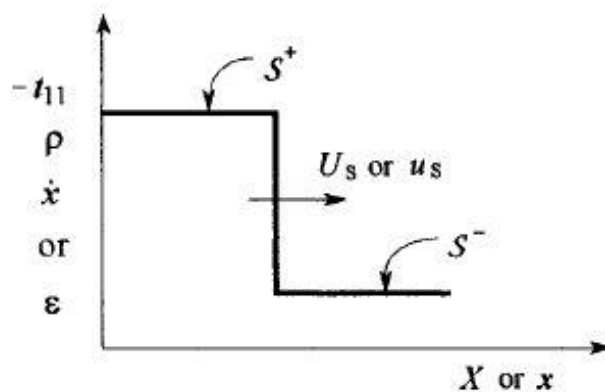


Figure 4.3 Shock transition between uniform states.

Jump equations for plane longitudinal shocks using Eulerian form are given by [66]

$$[[\rho]]u_s = [[\rho\dot{x}]] \quad (4.7)$$

$$[[\rho\dot{x}]]u_s = [[\rho\dot{x}^2 - t_{11}]] \quad (4.8)$$

$$\left[ \left[ \rho \left( \varepsilon + \frac{1}{2} \dot{x}^2 \right) \right] \right] u_s = \left[ \left[ \rho \left( \varepsilon + \frac{1}{2} \dot{x}^2 \right) \dot{x} - t_{11} \dot{x} \right] \right] \quad (4.9)$$

where:

$u_s$  is the shock velocity in Eulerian description,

$[[\xi]]$  Denotes the Jump in the field variable between the upstream and downstream side ( $[[\xi]] = \xi^+ - \xi^-$ ),

$\xi^+$  is final/upstream value, and

$\xi^-$  is initial/downstream value.

Jump equations for plane longitudinal shocks using Lagrangian form are given by [66]

$$\rho_R U_s [[-v]] = [[\dot{x}]] \quad (4.10)$$

$$\rho_R U_s [[\dot{x}]] = [[-t_{11}]] \quad (4.11)$$

$$\rho_R U_s \left[ \left[ \left( \varepsilon + \frac{1}{2} \dot{x}^2 \right) \right] \right] = [[t_{11} \dot{x}]] \quad (4.12)$$

where:

$U_s$  is the shock velocity in Lagrangian description, and

$\rho_R$  is the reference density.

Downstream parameters for quiescent materials are:

$\dot{x}$  is particle velocity is equal to zero,

$t_{11}^-$  is the longitudinal stress, it is known at downstream side,

$\varepsilon^-$  is the specific internal energy, it is known at downstream side, and

$\rho^-$  is material density, it is known at downstream side.

Jump equations for quiescent materials plane longitudinal shocks using Eulerian description are thus given by [66]:

$$\rho^+ = \frac{\rho^- u_S}{u_S - \dot{x}^+} \quad (4.13)$$

$$\llbracket -t_{11} \rrbracket = \rho^- \dot{x}^+ u_S \quad (4.14)$$

$$\llbracket \varepsilon \rrbracket = \frac{1}{2} (\dot{x}^+)^2 + \frac{1}{\rho^- u_S} (-t_{11}^-) \dot{x}^+ \quad (4.15)$$

Jump equations for quiescent materials plane longitudinal shocks using Lagrangian description are given by [66]:

$$\rho^+ = \frac{\rho^- U_S \rho_R}{\rho_R U_S - \rho^- \dot{x}^+} \quad (4.16)$$

$$\llbracket -t_{11} \rrbracket = \rho_R \dot{x}^+ U_S \quad (4.17)$$

$$\llbracket \varepsilon \rrbracket = \frac{1}{2} (\dot{x}^+)^2 + \frac{1}{\rho_R U_S} (-t_{11}^-) \dot{x}^+ \quad (4.18)$$

**4.1.3 Equation of state.** EOS is a mathematical relation between state variables of a material such as pressure (P), temperature (T), and specific volume ( $v$ ). The EOS of a material along with the Jump equations, form a set of equations that can explain the effect of the propagation of a shock through a material, and is required to characterize the adiabatic changes experienced in the thermodynamic states.

Some of the most widely used EOS for solids cited in the literature are:

- Bulk modulus (K), also called incompressibility, which is the ability of the material to withstand changes in volume under uniform isothermal compression. Bulk modulus is considered to be the simplest isothermal EOS[34], and it can be expressed as follows

$$K = -V \left( \frac{\partial P}{\partial V} \right)_T \quad (4.19)$$

where:

$V$  is the volume,

$\left(\frac{\partial P}{\partial V}\right)_T$  is the volume derivative of pressure at constant temperature.

This equation is only valid for  $P < K$  and for a linearly increasing  $K$

$$K = K_o + K_o' P \quad (4.20)$$

where:

$K_o$  is bulk modulus at atmospheric pressure, and

$K_o'$  is the pressure derivative of the bulk modulus.

$$K_o' = \frac{\partial K}{\partial P} \quad (4.21)$$

- Murnaghan EOS[35] is based on the assumption that the bulk modulus and pressure are linearly related. This EOS is widely used and known to reproduce both P-V data and the correct values of the room pressure bulk modulus for compressive strain up to about 10%. A general form of this EOS is given by

$$V = V_o (1 + K'P / K_o) \quad (4.22)$$

where:

$K'$  is the pressure derivative of the bulk modulus  $\frac{\partial K}{\partial P}$ .

- The Birch-Murnaghan EOS[36] is one of the most widely used EOS by mineralogists.

The general equation based on the Eulerian strain ( $f_E$ ) is given by

$$P = 3k_o f_E (1 + 2f_E)^{\frac{5}{2}} \left(1 + \frac{3}{2}(k' - 4)f_E + \frac{3}{2}(k_o k'' + (k' - 4)(k' - 3) + \frac{35}{9})f_E^2\right) \quad (4.23)$$

where:

$f_E$  is the Eulerian strain,

$K_o'$  is the pressure derivative of the bulk modulus and set to be equal 4,

$k'$  is used when  $\frac{\partial K}{\partial P}$  varies significantly with pressure, and

$k''$  is used for extremely condensed materials and is given by,



$$k'' = \frac{-1}{k_0} ((3 - k')(4 - k') + \frac{35}{9}) \quad (4.24)$$

- Mie-Gruneisen EOS [38] is the relation between pressure, internal energy, and specific volume. The Gruneisen model is a general form of Mie-Gruneisen EOS and describes the effect of changing the volume on the vibrational properties.

Gruneisen model can be expressed as

$$\gamma = V \left( \frac{dp}{de} \right)_V \quad (4.25)$$

where:

$V$  is volume,  $p$  is pressure,

$e$  is specific internal energy,

$\gamma$  is the Gruneisen parameter, and

$\frac{dp}{de}$  is the energy derivative of the pressure.

In the above equation, assuming that  $\gamma$  is independent of  $(p, e)$ , by integration the Gruneisen model yields

$$p - p_o = \frac{\gamma}{V} (e - e_o) \quad (4.26)$$

where:

$p_o$  is the pressure at reference state, usually the atmospheric and room temperature state of the material

$e_o$  is the internal energy at reference state.

In this work, a MD modeling analysis methodology proposed characterizes the Mie-Gruneisen EOS and demonstrated in cementitious materials for C-S-H Jennite molecular structure. MD simulation models and analysis methodology presented characterize the various parameters associated with Mie-Gruneisen EOS.

Mie-Gruneisen EOS [38] was used because it describes the relationship between pressure, volume, and internal energy, and is an important material characterization model needed to understand the high strain rate behavior in materials. These parameters that characterize the representative material EOS along with Jump equations are required for the analysis of high strain rate behavior of materials that are associated with longitudinal shock wave propagation.

## 4.2 Hugoniot Curves

Jump equations discussed in the previous section do not contain any information about the constitutive behavior of the material. The behavior of materials subjected to shock wave can be characterized using Hugoniot curves. Hugoniot curves provide information about the relationship between two thermodynamic properties of material while it is subjected to the propagation of a shock [66].

In the case of longitudinal shock propagation, the Hugoniot curves are presented in terms of five quantities: specific volume  $v$ , longitudinal stress  $t_{11}$ , particle velocity  $\dot{x}$ , specific internal energy  $\varepsilon$ , and shock velocity  $u_s$  or  $U_s$ . Some of the Hugoniot curves defined and discussed in literature are  $(t_{11} - v)$  or  $(P - v)$ ,  $(t_{11} - \dot{x})$ , and  $(\dot{x} - u_s)$ . Hugoniot curves can be transformed from one set of variables to another using the Jump equations. With additional thermodynamic information, temperature and entropy Jumps can also be determined for shock wave propagation[66]. The MD modeling methodology proposed and presented in this work focuses on the  $(t_{11} - v)$  and  $(P - v)$  Hugoniot curves. The mathematical background related to the Hugoniot relationship that is employed for the present MD modeling methodology is presented next.

**4.2.1 Pressure-specific volume Hugoniot.** The development of the pressure vs. specific volume Hugoniot curve, based on Mie-Gruneisen EOS, is presented next. The mathematical model equations are presented following discussions in the literature [47].

Integrating the Mie-Gruneisen equation assuming a constant  $\gamma$  parameter, yields [38]:

$$p^H = p^{iso} + \frac{\gamma}{v} (e^H - e^{iso}) \quad (4.27)$$

As discussed in reference [47], Rankine-Hugoniot equation is given by

$$e^H - e^R = \frac{1}{2} p^H (v_R - v) \quad (4.28)$$

And from both equations, it can be deduced

$$p^H = \frac{p^{iso} + \frac{\gamma}{v} (e^R - e^{iso})}{1 - \frac{\gamma}{2v} (v_R - v)} \quad (4.29)$$

In all the above equations

$p^H$  is Hugoniot pressure,

$p^{iso}$  is the isothermal pressure,

$v$  is specific volume,

$v_R$  is reference specific volume,

$e^R$  is reference internal energy,

$e^{iso}$  is isothermal internal energy, and

$\gamma$  is Gruneisen parameter.

**4.2.2 Longitudinal stress-specific volume Hugoniot.** Longitudinal stress vs. specific volume Hugoniot can be determined from the following equations, following the discussions in the literature [47, 66].

The relationship between pressure and stress tensor diagonal terms is given by:

$$P = \frac{1}{3} (t_{11} + t_{22} + t_{33}) \quad (4.30)$$

$$t_{ij} = -P\delta_{ij} + t'_{ij} \quad (4.31)$$

where:

$t'_{ij}$  is stress deviator tensor, and  $\delta_{ij} = 1$  when  $i = j$ , 0.0 otherwise.

For uniaxial strain state,

$$t_{22} = t_{33} \quad (4.32)$$

$$\tau_{max} = \frac{1}{2}(t_{11} - t_{22}) \quad (4.33)$$

$$t_{11} = -P - \frac{4}{3}\tau_{max} \quad (4.34)$$

where:

$\tau_{max}$  is the maximum shear stress. For confined materials under shock conditions the stress

Based on the above discussions, the development and characterization of Hugoniot curves for a material system based on Mie-Gruneisen EOS requires the following parameters:

- $P^H$  : Non-isothermal Hugoniot pressure,
- $\gamma$  : Mie – Gruneisen parameter, and
- $\tau_{max}$  : Shear strength of the material at associated thermodynamic states.

The stress state developed in a material undergoing the passage of a shock is very high.

Therefore in all likelihood the shear stress will overcome the shear strength of the material, especially for brittle materials. However, since the material is confined failure due to shear stress will not occur. For that reason in the modeling approach presented here the maximum shear stress is replaced by the shear strength of the material.

The proposed MD material modeling methodology based on material molecular structures for these above parameters that characterize the Mie-Gruneisen EOS and subsequently the associated Hugoniot relations is presented next.

**4.2.3 Proposed material model.** The shocked state of the material can be represented in the form of Hugoniot curves as discussed above which are a simpler form of the EOS[66]. The main result from the proposed material model is the longitudinal stress vs. specific volume Hugoniot curve. This curve along with the Jump equations can be used to determine the change of the thermodynamic properties of the material due the passing of a shock.

The objective is to characterize and estimate the material parameters associated with the Mie-Gruneisen EOS, Longitudinal stress – specific volume Hugoniot. Based on the mathematical modeling discussions presented earlier, a full description of the axial stress – specific volume Hugoniot requires four quantities. These are: isothermal pressure – specific volume curve, isothermal energy – specific volume curve, Gruneisen parameter, and the shear strength of the material. Based on the governing material model equations discussed in earlier sections, adiabatic Hugoniot pressure ( $P^H - v$  relationship) can be obtained from isothermal pressure – specific volume, energy – specific volume data and Gruneisen parameter values. The longitudinal stress Hugoniot ( $t_{11} - v$ ) can be estimated using the Hugoniot pressure values and the ultimate isothermal shear strength.

In the present work, all the required baseline parameters such as isothermal pressure, Gruneisen parameter and ultimate shear strength parameter for a material are obtained from material molecular structures and MD modeling analysis methodology. This is achieved through three separate MD modeling analysis runs denoted by MD#1, MD#2, and MD#3.

Figure 4.4 presents a flow chart of the MD modeling methodology that determines the principal unknown factors and subsequent quantities. The details of these MD modeling analysis runs are discussed next.

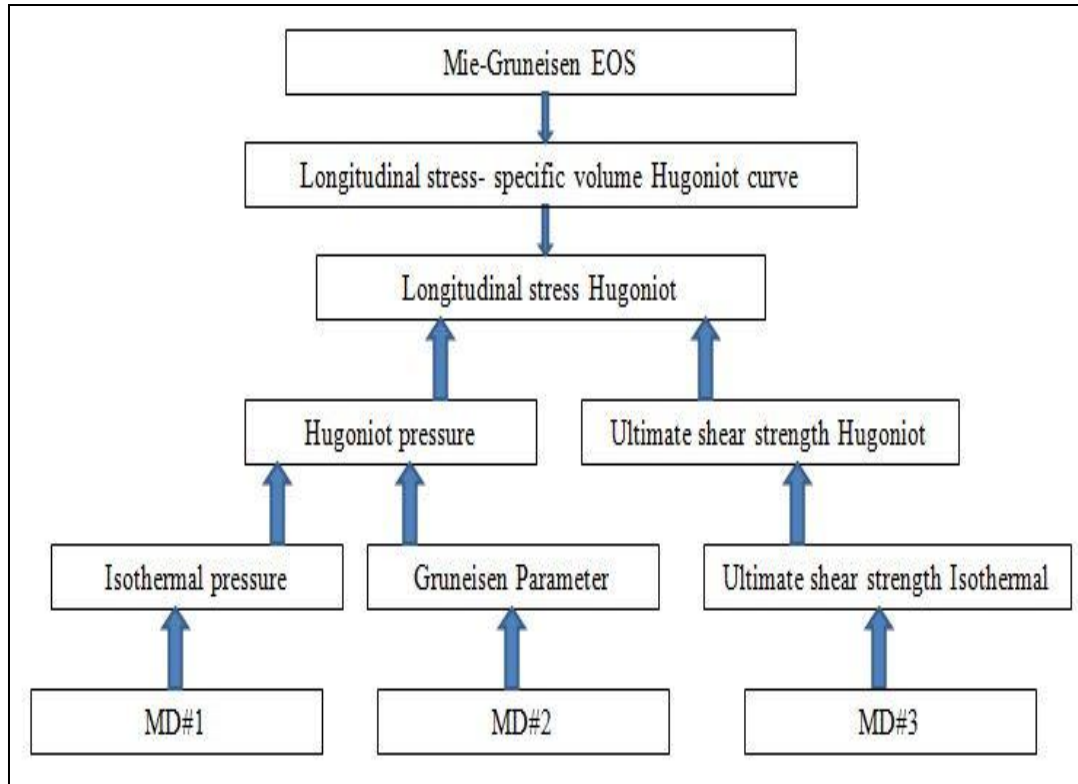


Figure 4.4 Material model flow chart.

The MD modeling method consists of three separate MD modeling analysis runs.

- MD#1 is an isothermal compression MD modeling analysis to obtain the pressure vs. specific volume and the internal energy vs. specific volume isothermal relationships.
- MD#2 is a MD modeling analysis to estimate the Gruneisen parameter. This is performed by using MD analysis to obtain internal energy – pressure relationship. This parameter is then used, along with the results of MD#1, to obtain the pressure vs. specific volume Hugoniot relationship as discussed in section 4.2.1.
- MD#3 is a MD modeling analysis to estimate the material ultimate shear strength value employing material molecular structures. This estimated value from MD modeling analysis at various thermodynamic pressure states can be used with the pressure vs.

specific volume Hugoniot relationship to obtain the longitudinal stress vs. specific volume Hugoniot relationship, as outlined in section 4.2.2.

The final result from the proposed MD modeling methodology is longitudinal stress vs. specific volume Hugoniot relationship. All these material modeling have been developed solely based on material molecular structure.

### **4.3 Prior MD Modeling Analysis**

The proposed MD modeling methodology couples and adapts some of the MD modeling analysis approaches discussed in literature. Limited work exists on the MD modeling analysis of shock wave behavior in material molecular structures. Grujicic et al [39], studied the shock wave behavior at molecular scale in soda lime glass. Their MD modeling analysis resulted in a computationally determined shock Hugoniot.

In another work, Grujicic et al [47], developed a multi length scale modeling of high pressure induced phase transformations in soda lime glass using molecular modeling at room temperature. They computationally determined shock Hugoniot by creating MD models to develop isothermal pressure vs. specific volume relation employing MD modeling analysis and material molecular structures. This work also followed the use of Mie-Gruneisen EOS to develop Hugoniot pressure vs. specific volume curve. They also used MD modeling of simple shear test.

The shear strength obtained from MD shear testing was subsequently used to obtain the longitudinal stress vs. specific volume Hugoniot curve using equation (4.34).

Figure 4.5 shows a representation of the MD model shear test at the molecular scale.

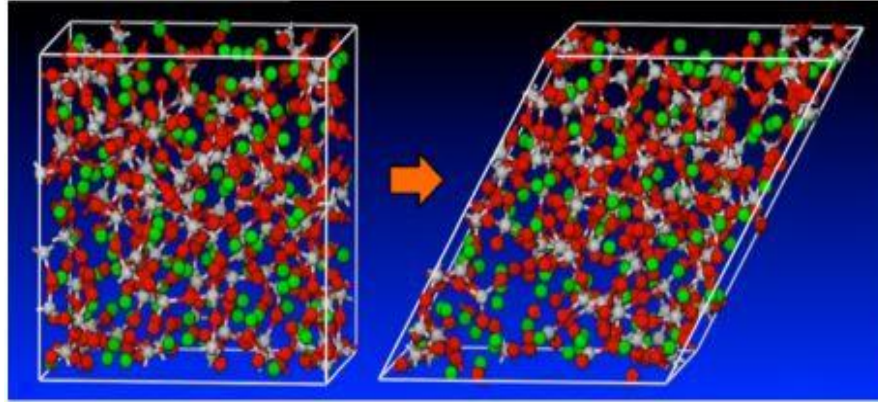


Figure 4.5 Shear test at the molecular scale.

The present methodology for cementitious material molecular structures adapts and follows the tenets of these research works from the literature. The application of MD modeling analysis for the characterization of a Mie-Gruneisen EOS for cementitious material structures have not been investigated earlier and is focused in the present work. In the case of cementitious materials, Ronald et al [69], used MD modeling analysis to simulate the stress strain behavior of C-S-H model, employing a NVT ensemble, temperature of 300K and shear strain increment of 0.005, that resulted in a MD analysis based shear stress – strain behavior shown in Figure 4.6.

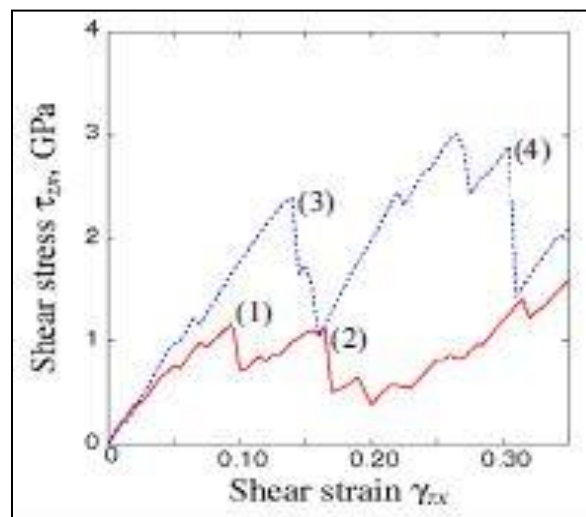


Figure 4.6 Shear stress – strain variation [69].



In other related work, Arther Paskin et al [70] used the MD technique to study and simulate longitudinal shock waves in solid materials. The Hugoniot relations were used to convert shock and particle velocities into pressure and volume relationships.

#### 4.4 Current MD Analysis Methodology

In the present work, as discussed in section 4.2.3, using MD modeling analysis capabilities of Material Studio Accelrys, three different computational MD modeling analyses were developed and conducted. These models determine the parameters and characterize the high strain rate behavior through the Mie Gruneisen EOS material model. These three MD modeling analyses are:

1. MD#1- isothermal compression MD modeling analysis,
2. MD#2 - Estimation of the Gruneisen Parameter MD modeling analysis, and
3. MD#3 – Estimation of the shear strength MD modeling analysis.

**4.4.1 MD#1 Isothermal compression MD modeling analysis.** This MD model was developed to obtain the isothermal relationships pressure vs. specific volume and internal energy vs. specific volume. To obtain the isothermal relationships several MD analysis runs at gradually increasing pressures are setup and the corresponding pressure, internal energy, and specific volumes are obtained. A NPT ensemble was employed in all analysis. This MD modeling analysis methodology, accomplished by employing the computational analysis capabilities of Materials Studio Accelrys, is as follows.

- Obtain the most stable molecular structure via Smart minimization method.
- Obtain the pressure – specific volume variation employing a series of NPT ensemble analysis. This was achieved as follows: A dynamic run for the system was performed by gradually incrementing the pressure of the molecular system. The pressure value was

increased from atmospheric pressure (0.0001) GPa to (5.0) GPa at increments of 0.1 GPa. The final molecular structure at the end of each increment pressure step was used as the initial structure for the next pressure step. Each pressure increment consists of two dynamic analysis steps, namely, a relaxation step and equilibration step. The relaxation step in the MD modeling analysis was performed by using NPT ensemble for 0.5 ps. This initial relaxation step is to allow the structure to relax around the desired incremental pressure value. The equilibrium analysis also used NPT ensemble for a period of 10 ps to allow the structure to reach a stable average pressure value.

- Output values from each pressure increment of the NPT analysis that includes temperature, pressure, density, total energy, and stress are obtained. A time average of the output values were calculated over the last 5 ps of each equilibrium pressure step. These average values were used in further analysis to develop the two sets of data corresponding to isothermal pressure and specific energy vs. specific volume.

Figure 4.7 shows schematic representation of the gradually increasing pressure profile in the several NPT ensemble MD analysis studies performed for MD#1.

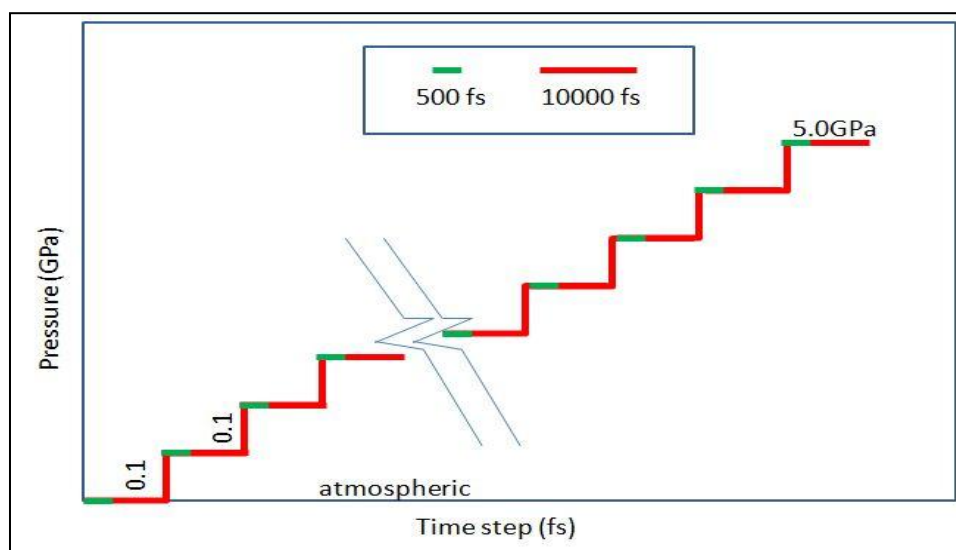


Figure 4.7 Schematic of NPT dynamic pressure profile for MD#1.

Figure 4.8 shows the flow chart of the MD modeling analysis methodology followed for the MD#1. Several steps in the flow chart are performed by setting the MD dynamic analysis in a Script file that automatically completed the sequence of MD analysis steps involved.

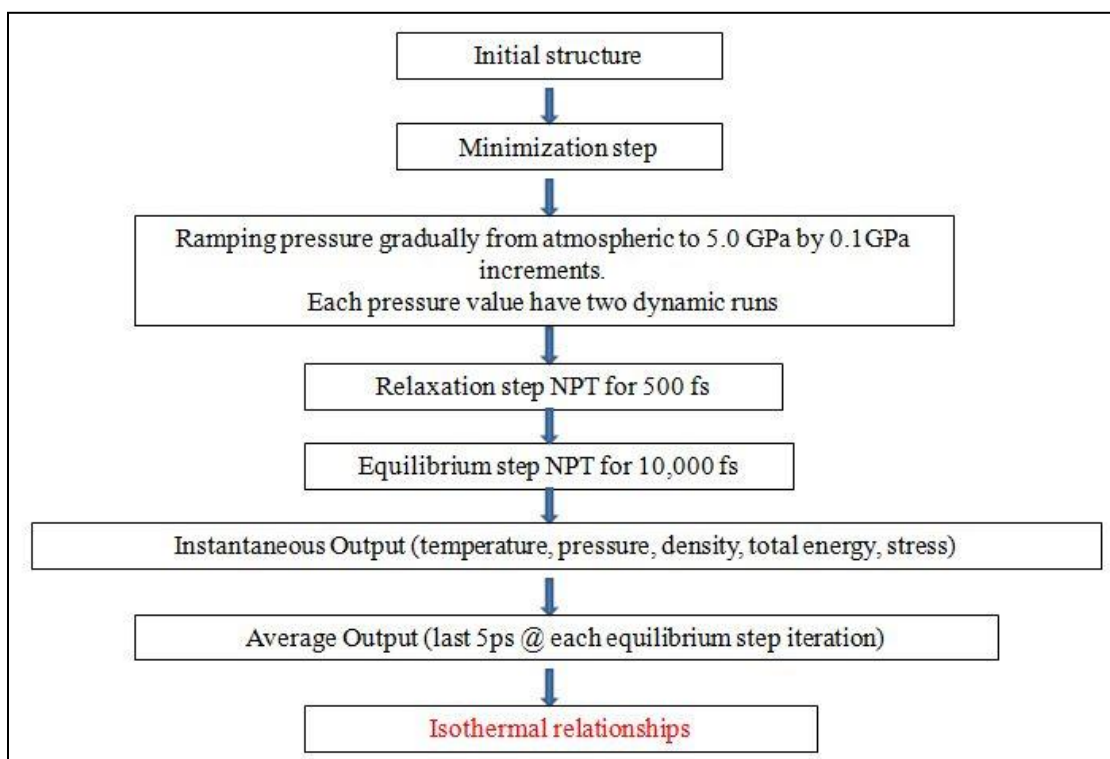


Figure 4.8 Flow Chart: MD #1 - Isothermal compression MD modeling analysis.

**4.4.2 MD#2 Estimation of Gruneisen parameter MD modeling analysis.** As discussed earlier, Gruneisen parameter ( $\gamma$ ) relates the change in internal energy to the change in pressure at a specific volume. This change in internal energy and pressure can be obtained from the change in any thermodynamic property other than specific volume. This can be achieved through a series of MD analysis using a Canonical NVT ensemble and equilibrating the molecular system at different temperatures for each specific volume.

In the present work, MD Dynamic modeling analysis runs for the molecular structures were set up using NVT ensemble at different temperature values (200, 300, 400, 500, 600, and 700) K for 100 ps. This analysis was done for a molecular system with the specific volume

corresponding to the atmospheric pressure based on the assumption that the quantity  $(\gamma/v)$  is constant [67]. The corresponding pressure values from the MD modeling analysis and the associated energy values were compiled to obtain the relationship between pressure and energy at each temperature value and a constant specific volume.

The average of the pressure and internal energy over the last 5 ps of each NVT run were used to create the pressure – internal energy relationship from which the Gruneisen parameter was estimated. A flow chart for the MD #2 analysis is shown in Figure 4.9. All the computations required were completed using a script file that enabled an automatic setup of the several MD analysis required.

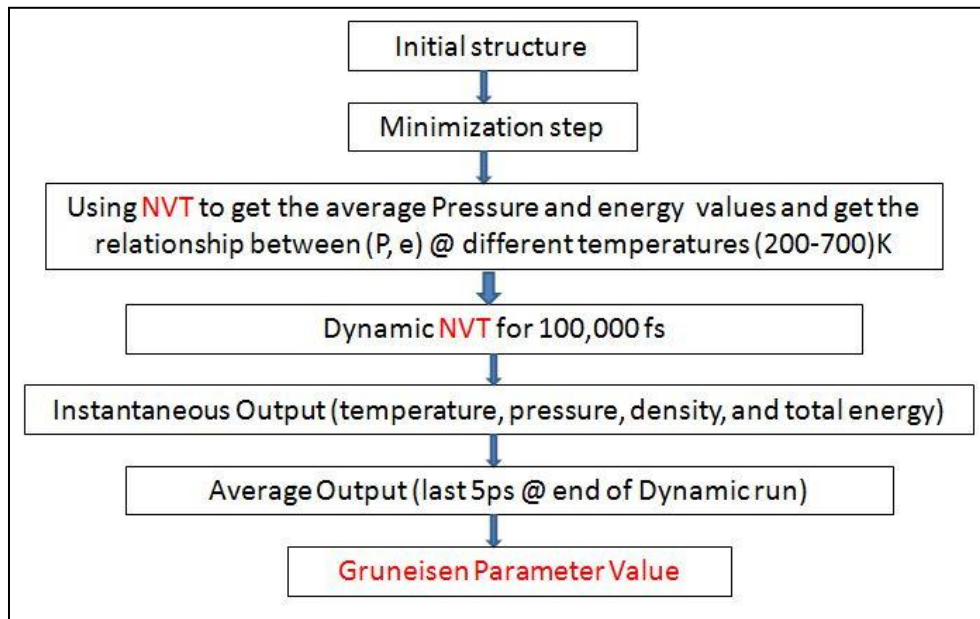


Figure 4.9 Flow Chart: MD#2 - Gruneisen parameter MD modeling analysis.

The slope of the pressure – energy relationship is equal to  $(\gamma/v)$  [42]. This slope as computed from the reference state is used for all specific volumes.

$$\frac{\gamma_R}{v_R} = \frac{\gamma(v)}{v} \quad (4.35)$$

where:

$\gamma_R$  is Gruneisen parameter at reference state,

$v_R$  is specific volume at reference state,

$v$  is specific volume, and

$\gamma(v)$  is Gruneisen parameter at  $v$  state.

Gruneisen parameter at reference state can be calculated from the following equation [42]

$$\gamma_R = \frac{\Delta P}{\Delta E} v_R \quad (4.36)$$

where:

$\gamma_R$  is Gruneisen parameter,

$\Delta P/\Delta E$  is and the slope of the  $\Delta P/\Delta E$  curve.

**4.4.3 MD#3 Estimation of ultimate shear strength MD modeling analysis.** This MD modeling analysis methodology estimates the shear strength based on the application of geometrical deformation of the molecular MD cell structure. This MD model can be set up as follows.

- The initial molecular structure corresponds to each specific volume considered in the analysis. Each pressure increment of MD#1 provides the required initial structure.
- Relaxation step based on employing NPT ensemble for 20ps at a temperature of 10K and atmospheric pressure to generate a minimally stressed structure.
- Geometry deformation to emulate shearing of the molecular MD cells. This is achieved by increasing the triclinic lattice gamma angle (Table 3.1) gradually at increments of 0.2 degrees (0.0035 rad) up to 15 degrees (0.2618 rad) and also changing triclinic lattice b dimension (Table 3.1). A total of 75 shearing deformation increments were performed and the corresponding stress and strain values were obtained. Figure 4.10 shows the schematics of shear deformation of the cell box containing the atomic structure.

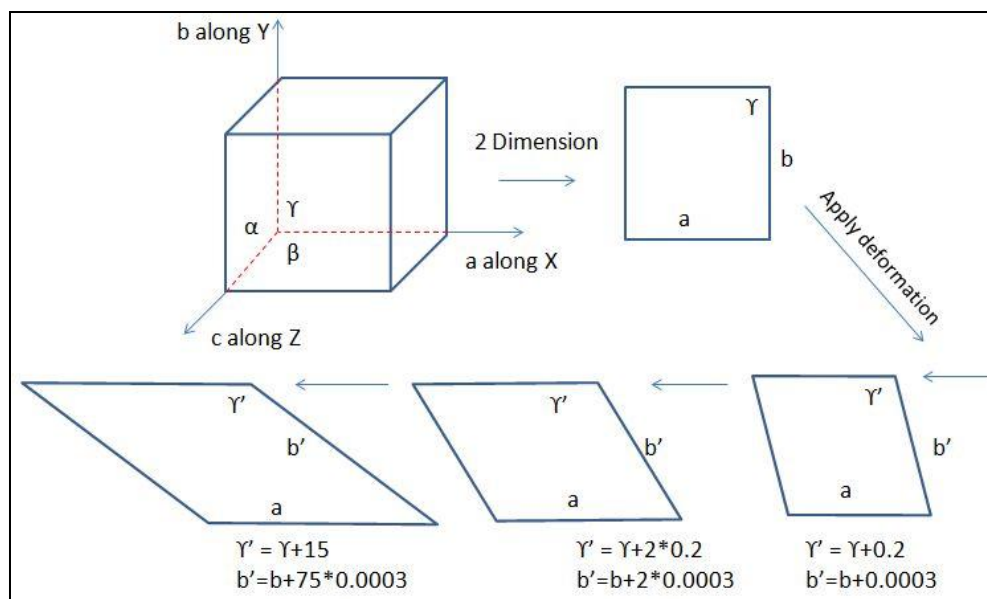


Figure 4.10 Schematics of shear deformation.

- For each deformed cell box in MD modeling analysis, Smart minimization method was employed to achieve the most stable structure.
- A dynamic MD analysis was completed by using NVT ensemble for 10 ps to allow the structure to reach a stable average temperature value.
- Obtain output values from the modeling analysis after each shearing increment during the dynamic analysis. Shear stress and strain values during the dynamic MD analysis were obtained and averaged value over the last 5 ps. These average values from MD modeling analysis were used to develop the stress strain curve and obtain the ultimate shear strength value  $\tau_{max}$  that corresponds to each specific volume considered in MD#1.

Figure 4.11 illustrates the flow chart of the MD modeling analysis steps involved in the estimation of the shear strength. All MD analysis steps were completed using a script file that can set and execute the different steps involved in the dynamic analysis.

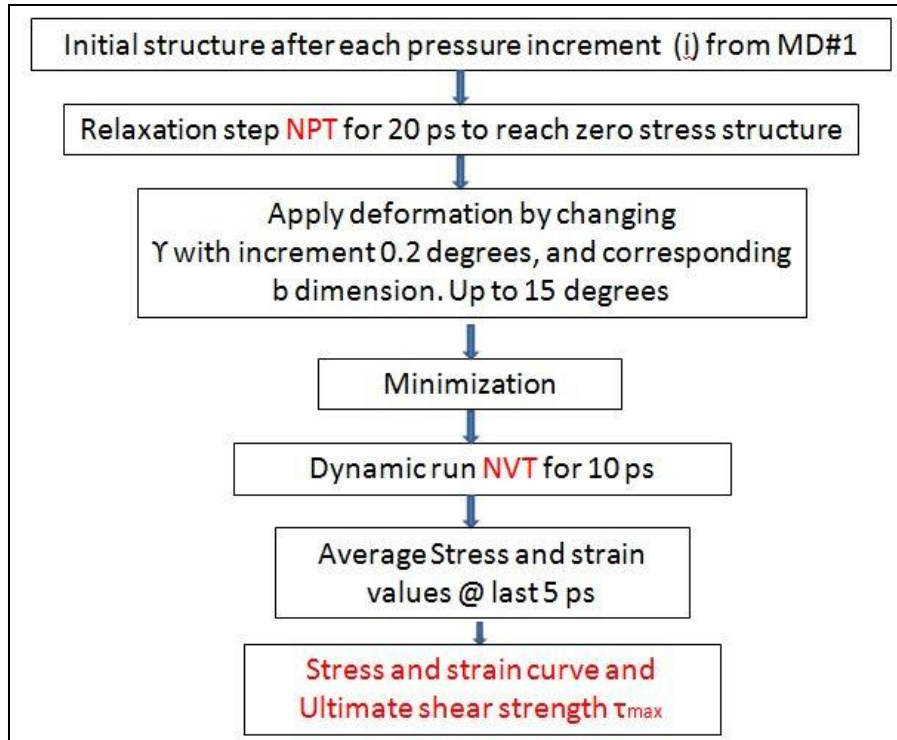


Figure 4.11 Flow Chart: MD #3 -Ultimate shear strength MD modeling analysis.

#### 4.5 Concluding Remarks

As discussed in the flow chart in section 4.2.3, the results from the three MD analysis, MD#1, MD#2, and MD#3, provide the required data to computationally obtain the  $(t_{11} - v)$  Hugoniot curve that characterizes the Mie Gruneisen EOS material model. The MD modeling methodology proposed here obtains this characterization employing only virtual material molecular structures. The application of the proposed MD modeling methodology to characterize the Mie Gruneisen EOS model is demonstrated for the C-S-H Jennite molecular structure in chapter 5. This is only for the demonstration of the computational material modeling methodology and its effectiveness. Further refinement of the MD analysis method parameters and verification of the modeling results through other means are still required.

## CHAPTER 5

### MD Prediction of Mie-Gruneisen EOS Model for C-S-H Jennite

In this chapter, MD modeling analysis methodology discussed in chapter 4 is employed, applied to and demonstrated for C-S-H Jennite molecular structure. Initial structure for C-S-H Jennite representation that is used in the present work as noted earlier was obtained from the American Mineralogist Crystalline Structure Database [13]. This structure is based on Bonaccorsi et al [17]. Figure 5.1 shows one unit cell C-S-H Jennite molecular crystalline structure that was employed in the MD modeling analysis. A total of 68 atoms are present in this molecular structure.

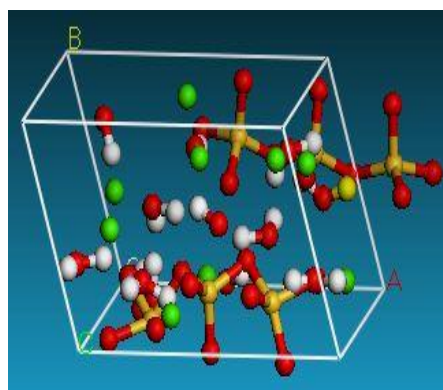


*Figure 5.1* C-S-H Jennite crystalline structure.

The details and current results from the three MD analysis steps and the corresponding Hugoniot curve are presented next. Discussions are presented in the following subsections.

- MD#1: Isothermal compression MD modeling analysis.
- MD#2: Gruneisen parameter MD modeling analysis.
- MD#3: shear strength MD modeling analysis results.
- Longitudinal stress vs. specific volume Hugoniot curve development based on the results from the above three MD modeling analysis.
- Conclusions.



## 5.1 MD#1 Isothermal Compression Modeling Analysis

Isothermal compression MD modeling analysis was performed using one unit cell C-S-H Jennite structure. MD simulation parameters used for C-S-H Jennite molecular structure are.

- Jennite cell size: (10.576x7.265x10.931) Å
- lattice angles are ( $\alpha = 101.3$ ,  $\beta = 96.98$ ,  $\gamma = 109.65$ )
- number of atoms: 68 atoms
- force field: COMPASS
- Molecular Tools: Discover
- Energy minimization: smart minimization
- MD ensemble: NPT
- temperature: 298 K
- Temperature control: Anderson
- Pressure values: gradually increasing from 0.0001 GPa to 5.0 GPa by 0.1 GPa increment
- Pressure control: Parrinello
- Time step: 1.0 femto second (fs)
- Dynamics time: 0.5 ps followed by 10 ps as discussed earlier
- Cutoff distance: 9.5 Å
- PBC: on

Dynamic run was performed on C-S-H Jennite molecular structure as discussed in section 4.4.1 by gradually incrementing the pressure from 0.0001 to 5.0 GPa with an increment of 0.1 GPa. The outputs of dynamic run after each pressure increment were obtained. These outputs include energy, pressure, and density values at every time step.

The averages of these quantities over the last 5ps of the dynamic run at each pressure step were calculated. The pressure – specific volume and internal energy – specific volume isothermal relationships are the main results from the MD#1 analysis. These results are subsequently used in the equation (4.29) to obtain Hugoniot pressure values. Figure 5.2 and Figure 5.3 show pressure vs. specific volume and energy vs. specific volume respectively. The internal energy is the total energy of the system divided by the molecular mass.

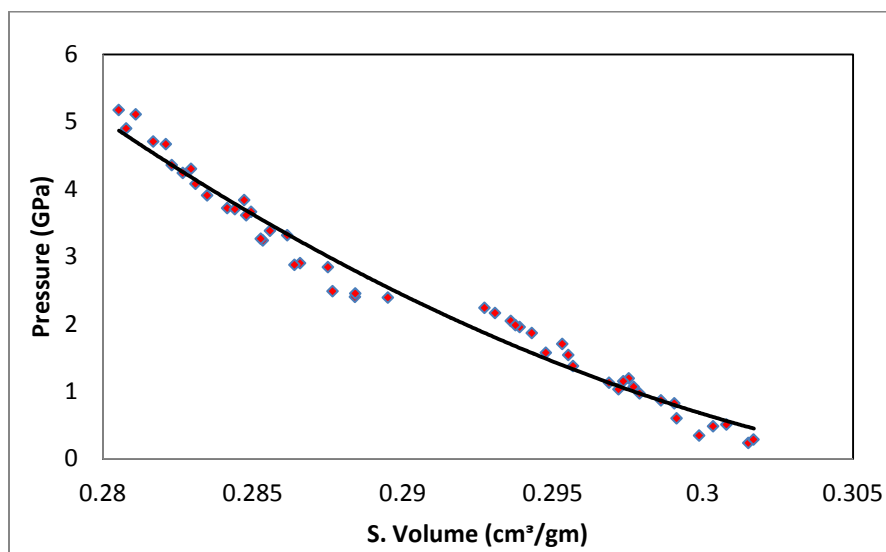


Figure 5.2 Isothermal pressure specific curve relationship.

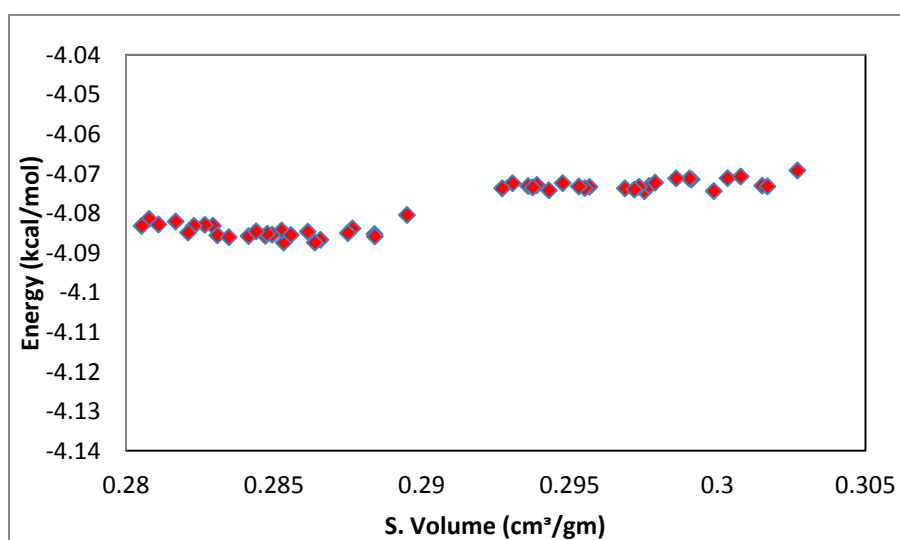


Figure 5.3 Isothermal energy vs. specific volume relationship.

## 5.2 MD#2 Estimation of Gruneisen Parameter MD Modeling Analysis

Gruneisen parameter experiment was performed using one unit cell C-S-H Jennite structure. MD simulation parameters used for C-S-H Jennite molecular structure are the same as discussed in section 5.1 except for the following parameters MD ensemble: NVT, temperature: (200-700) K, and dynamics time: 100 ps.

As discussed earlier, several MD modeling analysis at various temperatures were completed employing NVT ensemble and the relationship between pressure and internal energy at constant volume for different temperature values (100, 200, 300, 400, 500, 600, and 700) K were obtained. The change of the pressure  $\Delta P$  and  $\Delta E$  were calculated by comparing the previous pressure and internal energy values with the pressure and internal energy at reference temperature of 300 K. As mention in section 4.4.2 the Gruneisen parameter at reference state can be determined from the slope of  $\frac{\Delta P}{\Delta E} = \frac{\gamma_R}{v_R}$  [42, 67]. Gruneisen parameter determined by MD was compared with literature values [37, 45]. Figure 5.4 shows the relationship between pressure and energy.

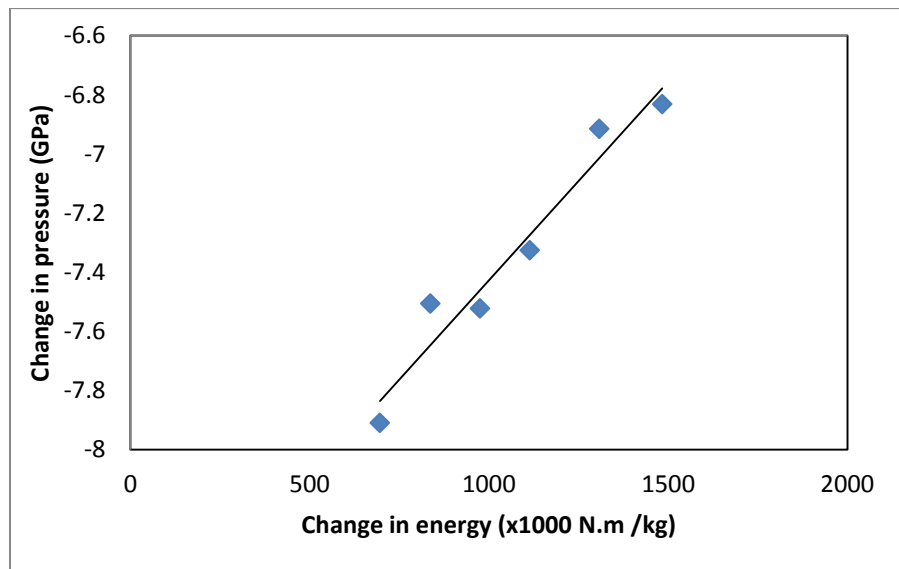


Figure 5.4 Determination of Gruneisen parameter.

An expression for the Gruneisen parameter defined in literature is based on using Leant Equation [45] given by

$$\gamma_D = 1.5 \left( \frac{B}{\rho V^2} \right) \quad (5.1)$$

where:

B is the bulk modulus; a value of 66 GPa as obtained from MD analysis from chapter 3 is employed for this estimation,

$\rho$  is density 2.325 gm/cm<sup>3</sup>, and

V is the speed of sound (3200-3600) m/sec.

Another expression defined in the literature for Gruneisen parameter is based on using Belomestnykh [45] Equation

$$\gamma_D = 1.5 \left( \frac{1+\mu}{2-3\mu} \right) \quad (5.2)$$

where:

$\mu$  is Poisson's ratio (0.15 - 0.5).

Mazzatesta et al [37], have found different Gruneisen parameter values for mortar and cement paste samples. These values were determined experimentally using ultrasonic method, and also depend on the porosity of the samples. The values from these empirical equations, experimental methods as stated above and the present MD modeling analysis values are compared.

Figure 5.5 shows the comparison of the Gruneisen parameter value obtained from the literature with the value obtained from MD#2. The comparison show that the Gruneisen parameter value obtained by the present work is between the experimental and empirical values.

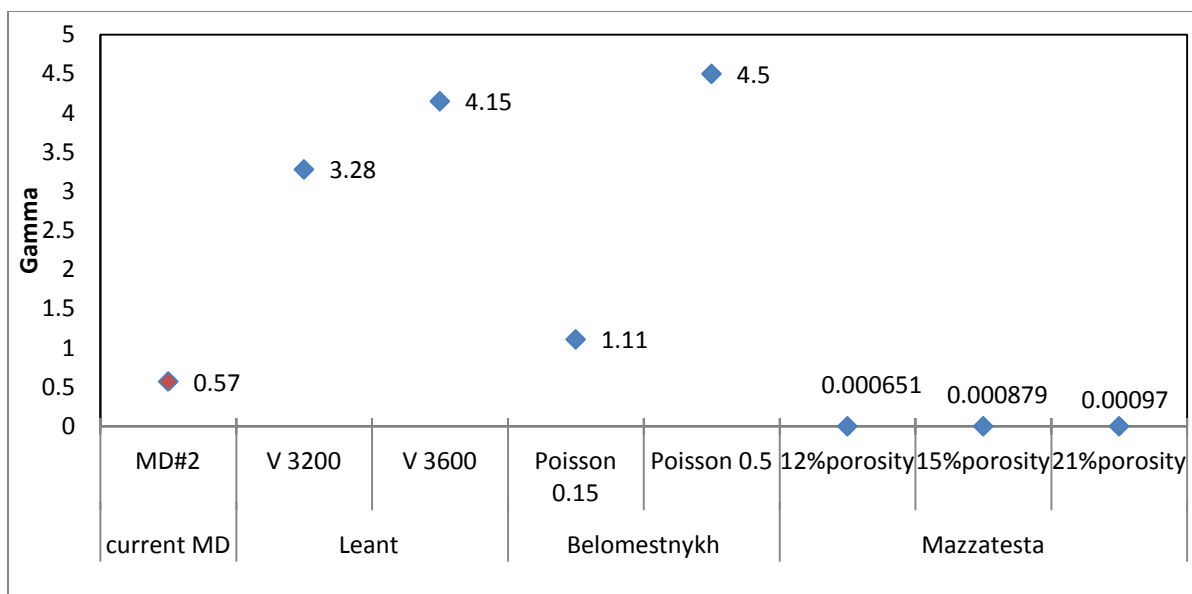


Figure 5.5 Comparison of Gruneisen parameter.

The main outcome from MD#2 modeling analysis is the quantity  $\left(\frac{\gamma_R}{v_R}\right)$ . This value along with the outcomes obtained from the MD#1 modeling analysis will complete all the required data needed in the equation (4.29) for the Hugoniot pressure. The pressure vs. specific volume Hugoniot curve was obtained and it is presented in Figure 5.6.

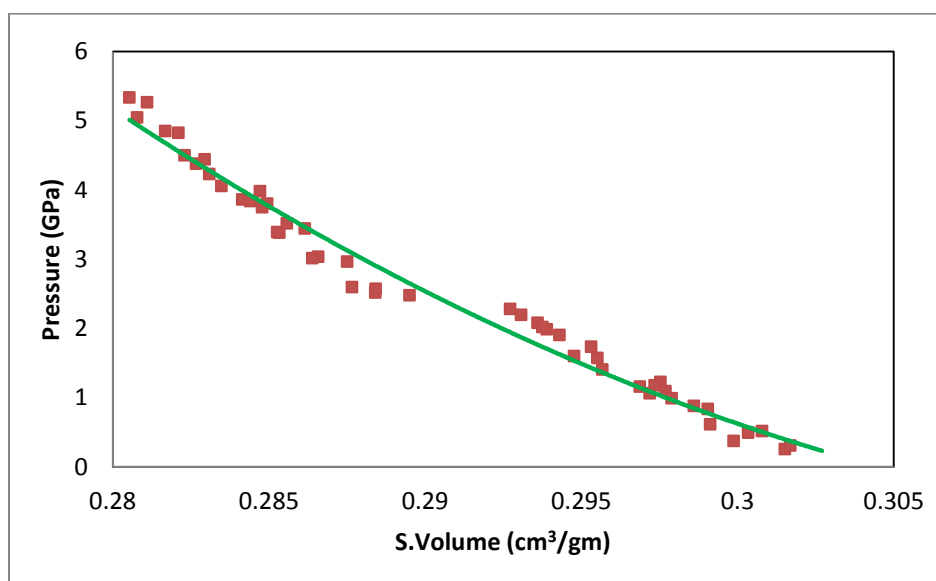


Figure 5.6 Hugoniot pressure vs. specific volume.

Figure 5.7 shows a comparison between the isothermal and Hugoniot pressure vs. specific volume curves. There is minor change noticeable between the isothermal and Hugoniot pressure.

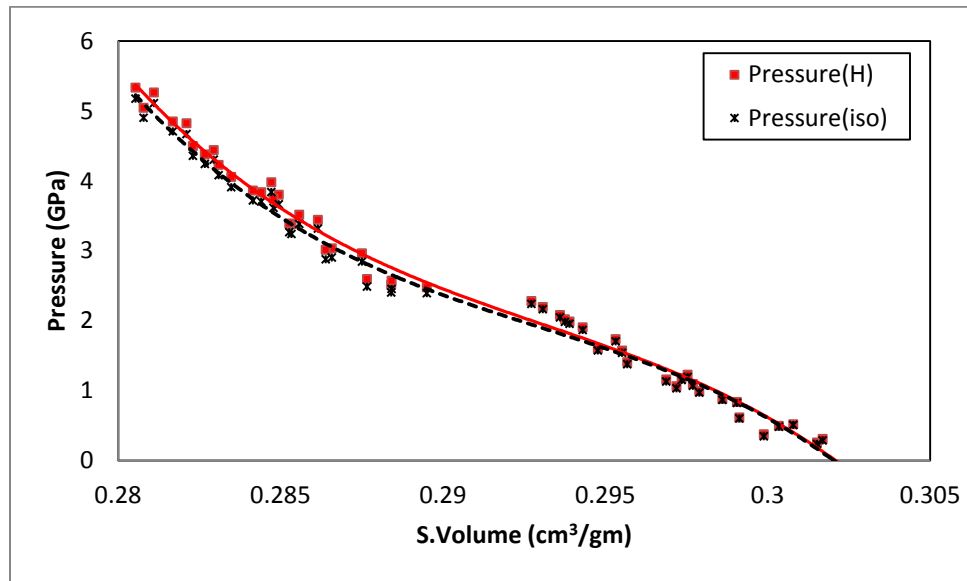


Figure 5.7 Comparison between Isothermal and Hugoniot pressure vs. specific volume.

### 5.3 MD#3 Estimation of Shear Strength MD Modeling Analysis

The shear strength MD modeling analysis was performed using one unit cell C-S-H Jennite structure. MD simulation parameters used are the same as discussed in section 5.1 except for the following parameters.

First, for the relaxation step:

- MD ensemble: NPT,
- Temperature: 10 K,
- Pressure: 0.0001 GPa, and
- Dynamics time: 20 ps

Second, for the dynamic run step:

- MD ensemble: NVT,
- Temperature: 300 K, and
- Dynamics time: 10 ps.

Following the procedure discussed in section 4.4.1, a total of fifty final structures could be obtained from the isothermal compression model MD#1 corresponding to the fifty pressure increments. These structures could be used as the initial structures for MD#3 to obtain the shear stress –strain results and the corresponding ultimate shear strength as discussed in section 4.4.3.

Due to the large number of MD simulation analysis to be performed and the computational cost, in this work, an average value of the ultimate shear strength was estimated based on a sampling of six stress – strain curves. The structures used were obtained from MD#1 at pressure increments 0.1, 0.2, 2.5, 2.6, 4.9, and 5.0 GPa. MD#3 modeling analysis was performed on each one of these six initial structures as discussed in section 4.4.3, resulting in six stress-strain curves. Figure 5.8 presents the stress-strain plots corresponding to each structure. The ultimate shear strength value for each curve was obtained as the highest stress value of each curve.

Table 5.1 shows the obtained ultimate shear strength values and their average value. This average was used as the  $\tau_{max}$  in the analysis described in equation (4.34) section 4.2.2.

Table 5.1

*C-S-H Jennite Ultimate Shear Strength Values for Different Molecular Structures*

Structure	0.1 GPa	0.2 GPa	2.5 GPa	2.6 GPa	4.9 GPa	5.0 GPa	average
Shear strength (GPa)	2.65	2.28	4.18	4.48	4.13	4.82	3.69

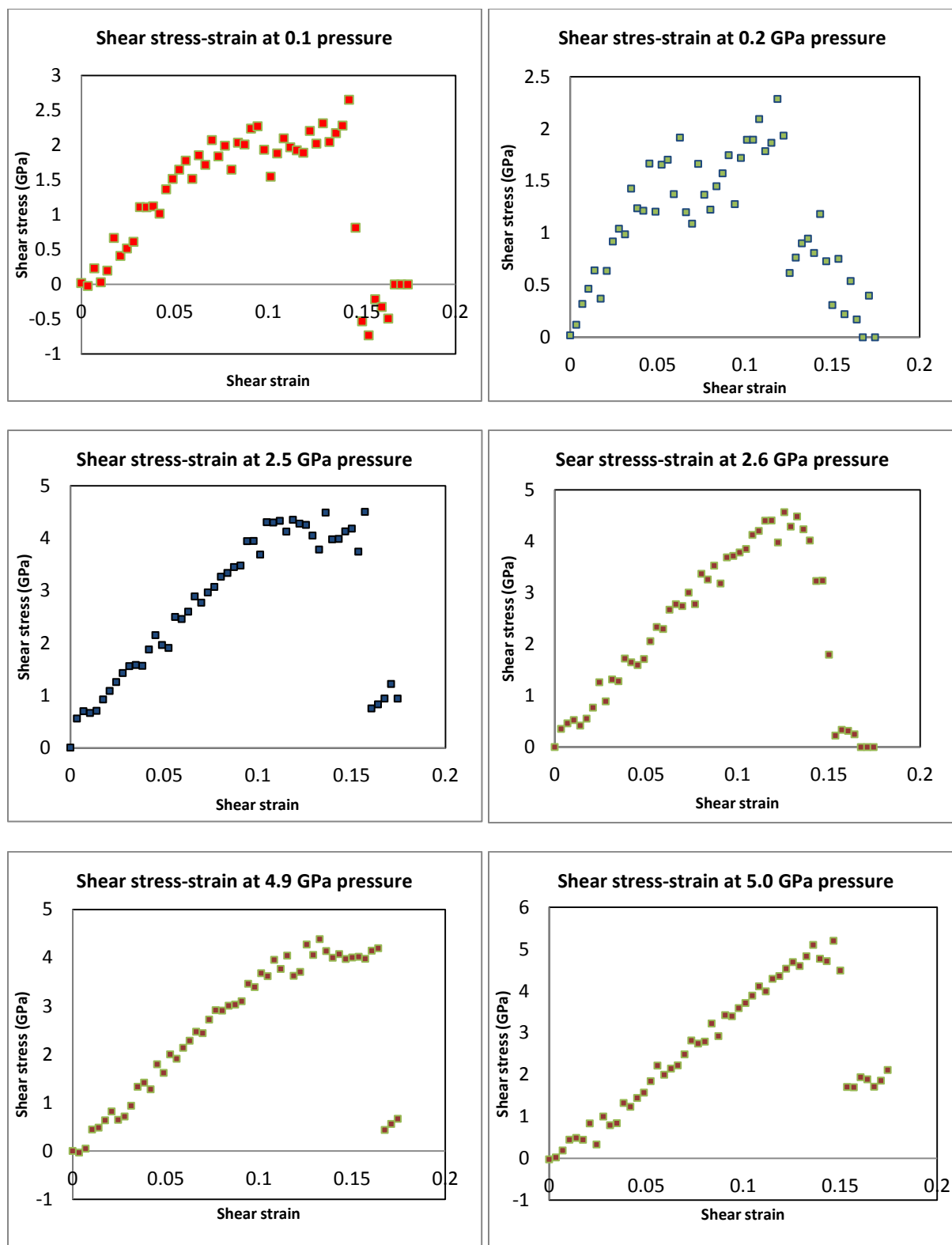


Figure 5.8 Shear stress-strain curves for different pressure increment structures.



#### 5.4 Longitudinal Stress vs. Specific Volume Hugoniot Curve

The main result for MD#3 is the average material's ultimate shear strength value. This value along with the pressure Hugoniot values obtained from section 5.2 were used in the equation (4.34) discussed in section 4.2.2 to obtain the Hugoniot longitudinal stress values, and the longitudinal stress vs. specific volume Hugoniot curve. This curve is the main result outcome from the proposed MD modeling analysis methodology as outlined in MD#1, MD#2, and MD#3. This curve along with the Jump equations can be used to study the effects of the passing of a shock through a material. Figure 5.9 presents the corresponding longitudinal stress vs. specific volume Hugoniot curve obtained using only the CSH molecular structure.

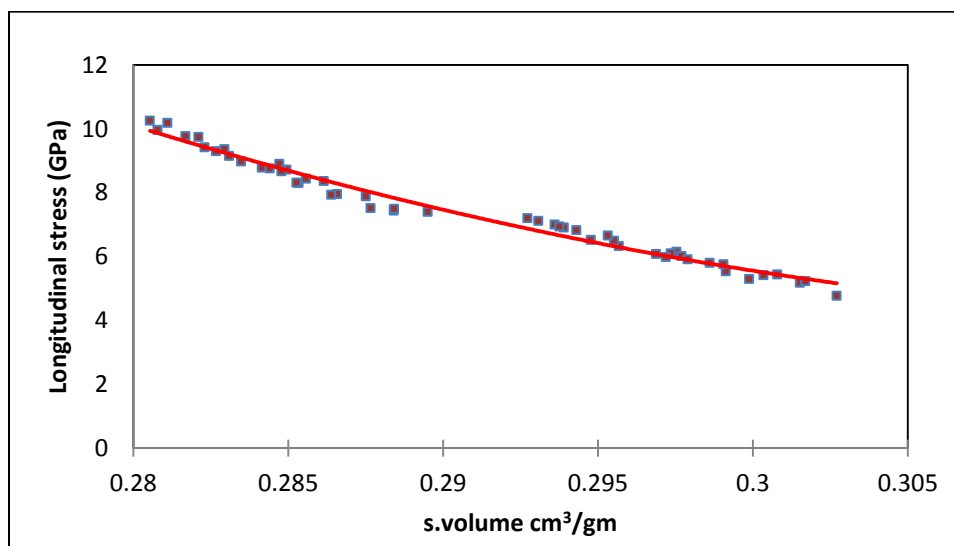


Figure 5.9 C-S-H Jennite longitudinal stress - specific volume Hugoniot curve.

#### 5.5 MD#1 Modeling Analysis for Larger C-S-H Jennite Structure

The size of the molecular system impacts the analysis results and the parameters associated with MD modeling. To understand the size effect of C-S-H Jennite molecular structure, isothermal compression MD modeling analysis was extended to using four unit cells

C-S-H Jennite structure. The corresponding Jennite cell size was  $(42.30 \times 29.06 \times 43.72) \text{ \AA}$ , and the number of atoms used was 4352 atoms.

Available memory from single processor computers employed in most of earlier analysis were insufficient to perform the dynamic run for this large molecular model. Therefore, a parallel script code using BTCL was developed to submit this model to a multi-processor system (named Hermes) at North Carolina A&T State University. BTCL is Accelrys Material Studio command language. Further investigations are in process to run MD#2 and MD#3 for C-S-H Jennite four unit cells molecular structure. A comparison between the present C-S-H Jennite four unit cell molecular structure and the current one unit cell results are conducted to study and understand the effect of structure size.

Figure 5.10 shows C-S-H Jennite four unit cells molecular structure.

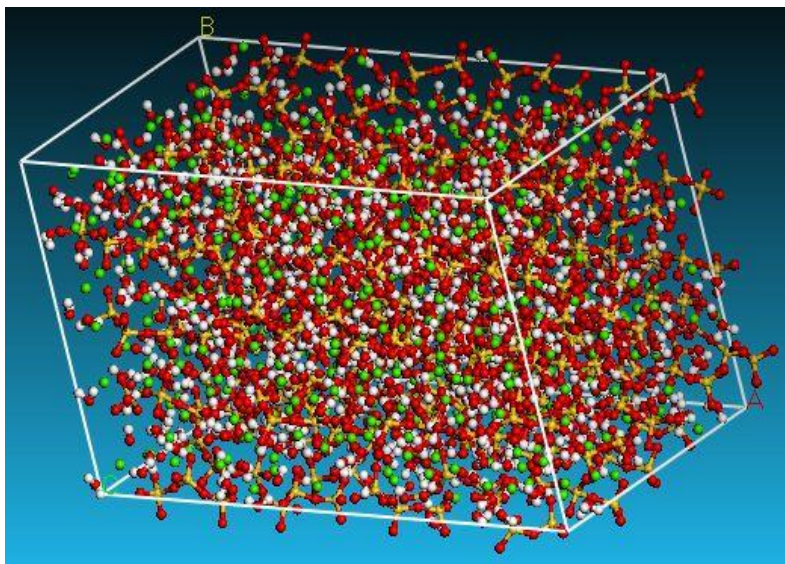


*Figure 5.10* Four unit cells C-S-H Jennite molecular structure.

Isothermal relationships from MD#1 modeling analysis are presented next. Figure 5.11 shows isothermal pressure vs. specific volume and Figure 5.12 shows isothermal energy vs. specific volume for this larger MD model.

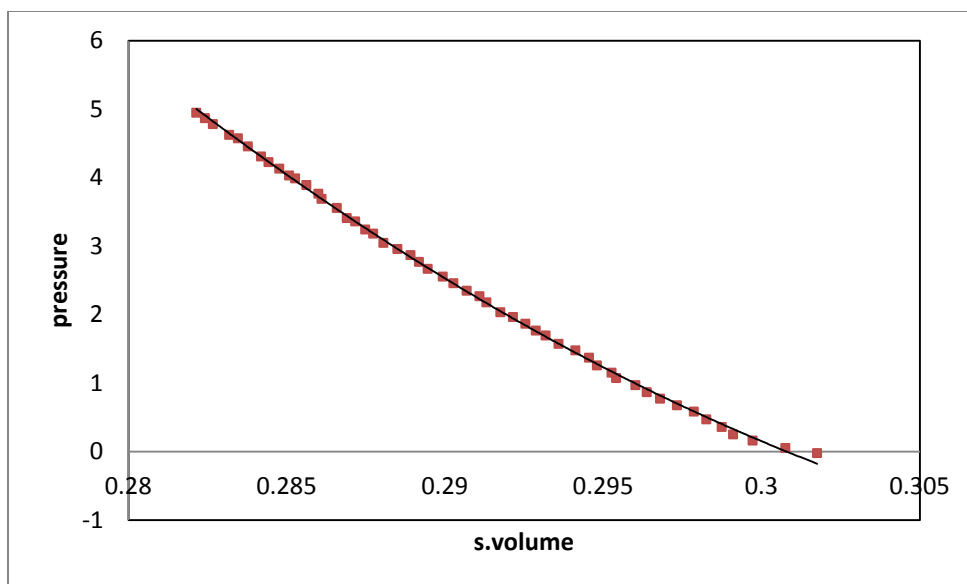


Figure 5.11 Isothermal pressure vs. specific curve relationship.

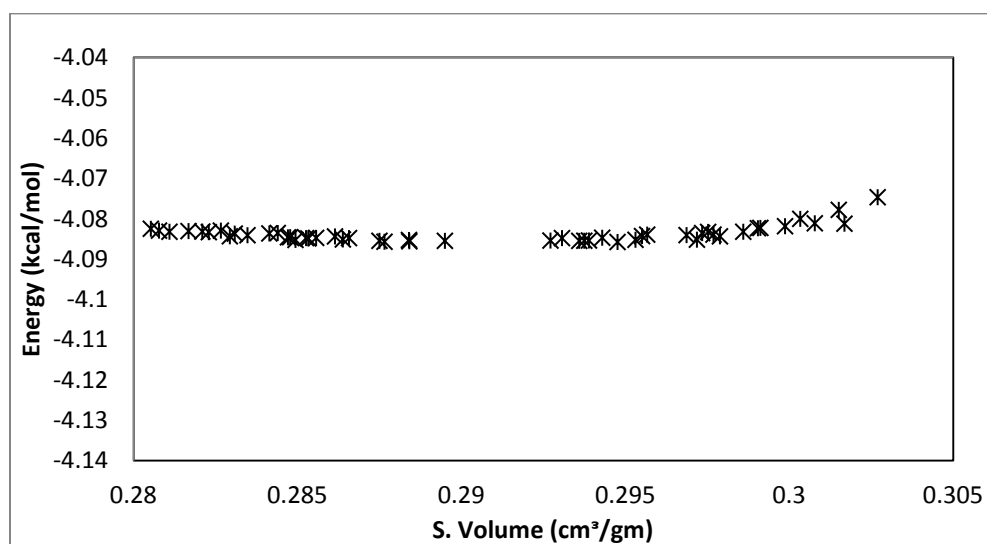


Figure 5.12 Isothermal energy vs. specific curve relationship.

The internal energy plotted above is the total energy of the system divided by the molecular mass.

Figures 5.13 and 5.14 present a comparison between the pressure vs. specific volume and internal energy vs. specific volume for C-S-H Jennite modeled using system sizes corresponding to 1x1x1 unit cells and 4x4x4 unit cells. It can be noticed that the overall behavior of both

systems is very similar. However the smaller system displays a pseudo jump in the internal energy that does not appear in the larger system. This justifies the need of applying this modeling methodology using larger system to guarantee that size effects are minimized.

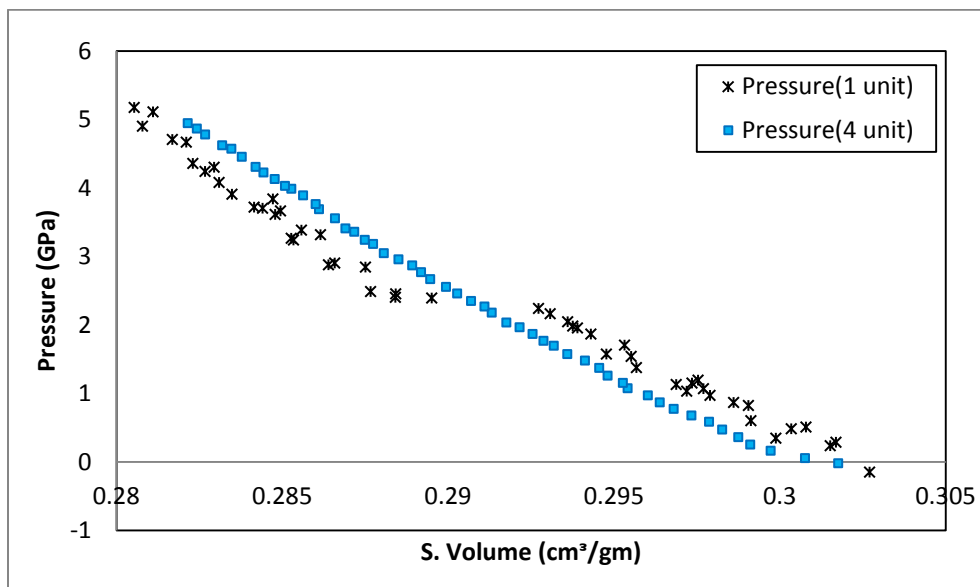


Figure 5.13 Isothermal pressure vs. specific volume relation for C-S-H Jennite structures modeled using 1x1x1 unit cell and 4x4x4 unit cell.

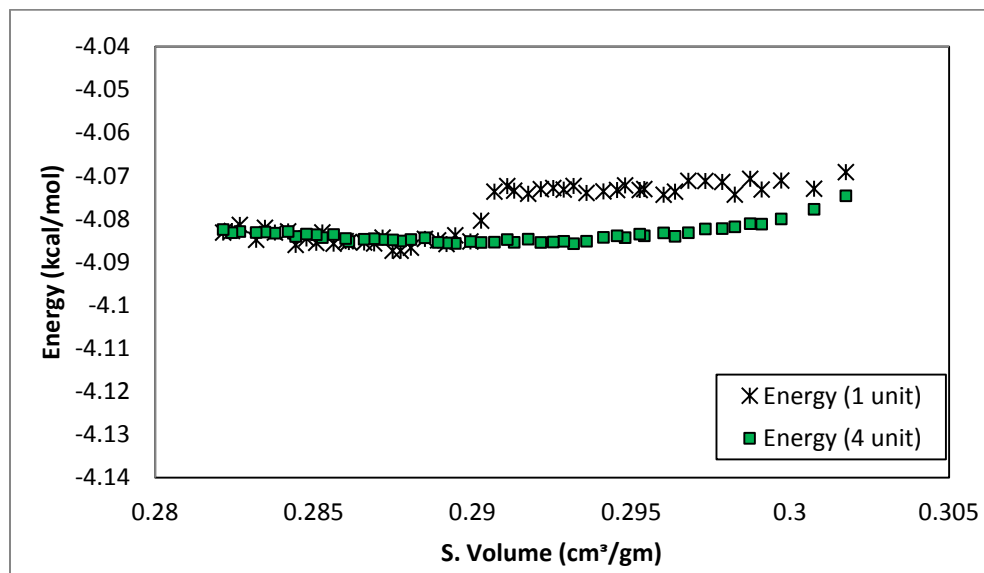


Figure 5.14 Isothermal internal energy vs. specific volume relation for C-S-H Jennite structures modeled using 1x1x1 unit cell and 4x4x4 unit cell.

## 5.6 Concluding Remarks

Chapter 5 demonstrated the application and effectiveness of the proposed MD modeling methodology discussed in chapter 4 for C-S-H Jennite molecular structure.

This proposed MD modeling methodology can be employed for other material systems with the correct selection of MD parameters. The results clearly show that the MD modeling methodology is an effective method for computationally determining the required parameters to estimate the Hugoniot of a material system.

It is to be noted that the high strain rate material Hugoniot curves obtained for C-S-H Jennite in this study have been obtained based on MD molecular structures only, and serve as an effective method for the characterization of EOS. However further studies are needed to guarantee that size effects, dynamic time effects, and the potential effect of the initial structures are carefully understood. Verifications and validations of the present modeling results are also needed.

## CHAPTER 6

### Conclusion

#### 6.1 Concluding Remarks

A summary of the conclusions from the present study are

- Molecular Dynamics MD modeling analysis is an effective method for studying and understanding the behavior of materials at the molecular level and the associated effects due to molecular structural changes and chemistry of the material system.
- MD modeling analysis used to predict the mechanical properties for unhydrated  $C_3S$  and  $C_2S$ , and hydrated CH, C-S-H Jennite representation, and C-S-H Tobermorite 14 representation at molecular scale level at atmospheric pressure.
- MD modeling analysis is effective in predicting the mechanical properties for both unhydrated and hydrated cementitious materials under varying thermodynamic higher pressures using the corresponding molecular ensemble pressures.
- A MD modeling Analysis Methodology was proposed to characterize material behavior, and to study and understand the behavior of materials subjected to shock wave propagation, other high velocity impact and high strain rate. This MD modeling analysis based material model characterizing the Mie Gruneisen Equation of State model were built from:
  - MD modeling analysis to study the isothermal compression deformation and develop isothermal pressure vs. specific volume relations,
  - MD modeling analysis to obtain Gruneisen parameter associated with Mie-Gruneisen EOS state modeling, and

- MD modeling analysis to obtain the shear strength value by modeling geometric shear deformation and generating shear stress vs. shear strain curve. The MD modeling analysis based shear strength value was employed in the development of the axial stress vs. specific volume Hugoniot curve. An average value from six sampling points is employed in this work for the determination of longitudinal stress. Further refinement would require large scale models and performing these analyses for a longer dynamic time.
- Proposed MD modeling Methodology was applied and demonstrated for C-S-H Jennite representation and showed the capability and effectiveness to obtain the associated Hugoniot curves.
- Proposed MD modeling Methodology for the Hugoniot curves is based only on the material molecular structure and could be used for any material with the appropriate material molecular structures and associated MD analysis parameters.

### **6.3 Future Directions**

- Develop and investigate larger molecular model configurations over longer dynamic analysis time with the use of larger memory and massively parallel computing systems.
- Develop and investigate larger molecular models which combine both hydrated and unhydrated cementitious materials with different percentages.
- Utilize the proposed MD modeling Methodology to develop the Hugoniot curves for all cementitious materials constituents  $C_3S$ ,  $C_2S$ , CH, and C-S-H Tobermorite 14, and refine the present study for CSH Jennite.
- Investigate the effect of material additions, modified molecular structure and the variations in material chemistry.

## References

1. Allen, A.J., J.J. Thomas, and H.M. Jennings, *Composition and density of nanoscale calcium-silicate-hydrate in cement*. Nat Mater, 2007. **6**(4): p. 311-6.
2. *United States Geological Survey Cement*. USGS Mineral, 2011.
3. Construction, C.E.-M.f.C., *CEMENTITIOUS MATERIALS FOR CONCRETE*. ACI Education Bulletin E3-01, 2001. **Supersedes E3-83**.
4. Constantinides, G. and F.-J. Ulm, *The effect of two types of C-S-H on the elasticity of cement-based materials: Results from nanoindentation and micromechanical modeling*. Cement and Concrete Research, 2004. **34**(1): p. 67-80.
5. R. Panneer Selvam, V.J.S., Shanique Murray and Kevin Hall, H., *Potential Application of Nanotechnology on Cement Based Materials*. MBTC DOT 2095/3004, 2009.
6. C01, A.I.C., *Standard Specification for Portland Cement*. ASTM C150, April 15, 2012.
7. Wu, W., *MULTISCALE MODELING AND SIMULATION OF CONCRETE AND ITS CONSTITUENT MATERIALS: FROM NANO TO CONTINUUM*. The University of Mississippi, 2008.
8. Kazuyori Urabe, T.S., and Minoru Iwashima, *Superstructure in a Triclinic Phase of Tricalcium Silicate*. 1999.
9. Golovastikov, N.I., Matveeva, R.G., and Belov, N.V., *Crystal structure of the tricalcium silicate  $3CaO \cdot SiO_2 = C_3S$* . Sov. Phys. Crystallogr., 1975. **20** (4), **441**.
10. Mideley, C., *The crystal structure of dicalcium silicate*. Acta Cryst., 1952. **5**, **307-312**.
11. Harutyunyan, V.S., et al., *Investigation of early growth of calcium hydroxide crystals in cement solution by soft X-ray transmission microscopy*. Journal of Materials Science, 2009. **44**(4): p. 962-969.
12. Henderson, D.M., & Gutowsky, H.S., *A nuclear magnetic resonance determination of the hydrogen positions in Ca*. American mineralogist, , 1962. **47**, **1231-1251**.
13. Database, A.M.C.S., *Database, A.M.C.S.*
14. R. Panneer Selvam, K.D.H., Vikramraja Janakiram Subramani, and Shanique J. Murray, *Application of Nanoscience Modeling to Understand the Atomic Structure of C-S-H*. Nanotechnology in Civil Infrastructure, pp. 85–102., 2011.
15. Thomas, J.J., H.M. Jennings, and A.J. Allen, *Relationships between Composition and Density of Tobermorite, Jennite, and Nanoscale CaO–SiO<sub>2</sub>–H<sub>2</sub>O*. The Journal of Physical Chemistry C, 2010. **114**(17): p. 7594-7601.
16. Jorge S. Dolado, M.G., Jan Hamaekers and Frederik Heber, *The nano-branched structure of cementitious calcium-silicate-hydrate gel*. Institutue for Numerical Simulation, 2010.
17. Bonaccorsi, E., S. Merlino, and H.F.W. Taylor, *The crystal structure of jennite,  $Ca_9Si_6O_{18}(OH)_6 \cdot 8H_2O$* . Cement and Concrete Research, 2004. **34**(9): p. 1481-1488.
18. Bonaccorsi, E., S. Merlino, and A.R. Kampf, *The Crystal Structure of Tobermorite 14 A (Plombierite), a C-S-H Phase*. Journal of the American Ceramic Society, 2005. **88**(3): p. 505-512.
19. Roberto Gomperts, E.R., and Milan Mehta, *Enabling Technologies for Innovative New Materials*. AMERICAN LABORATORY Volume 37, Number 22, 2005.
20. Dolado, J.S. and K. van Breugel, *Recent advances in modeling for cementitious materials*. Cement and Concrete Research, 2011. **41**(7): p. 711-726.



21. Gang Lu, E.K., *Overview of Multiscale Simulations of Materials*. Department of Physics and Division of Engineering and Applied Science, Harvard University, Cambridge, Massachusetts, USA, 2005. **Volume X: Pages (1–33)**(CHAPTER 22).
22. Schrodinger, E., *An Undulatory theory oh the Mechanics of Atoms and Molecules*. The Physical Review, Vol. 28,No.6, 1926.
23. Edward J. Garboczi and Dale P. Bentz "*Computational and Mathematical Models of Microstructural Evolution*".
24. Boumiz, A., C. Vernet, and F.C. Tenoudji, *Mechanical properties of cement pastes and mortars at early ages: Evolution with time and degree of hydration*. Advanced Cement Based Materials, 1996. **3**(3–4): p. 94-106.
25. Boumiz, A.S., D; Vernet, C, *Modelling the development of the elastic moduli as a function of the hydration degree of cement pastes and mortars* 2nd International RILEM Workshop on Hydration and Setting Location: DIJON, FRANCE Date: JUN 11-13, 1997, 1997.
26. Haecker, C.J., et al., *Modeling the linear elastic properties of Portland cement paste*. Cement and Concrete Research, 2005. **35**(10): p. 1948-1960.
27. Monteiro, P.J.M. and C.T. Chang, *The elastic moduli of calcium hydroxide*. Cement and Concrete Research, 1995. **25**(8): p. 1605-1609.
28. Velez, K., et al., *Determination by nanoindentation of elastic modulus and hardness of pure constituents of Portland cement clinker*. Cement and Concrete Research, 2001. **31**(4): p. 555-561.
29. Ahmed Al-Ostaz a, W.W., A. H.-D. Chengc, C. R. Songd, *A molecular dynamics and microporomechanics study on the mechanical properties of major constituents of hydrated cement I*. Journal of Cement and Concrete Research, 2008., 2008.
30. Wu, W., et al., *Computation of Elastic Properties of Portland Cement Using Molecular Dynamics*. JOURNAL OF NANOMECHANICS AND MICROMECHANICS, 2011. **1**(2): p. 84-90.
31. Hall, K.D., et al., *Molecular Dynamics to Understand the Mechanical Behavior of Cement Paste*. Transportation Research Record: Journal of the Transportation Research Board, 2010. **2142**(-1): p. 75-82.
32. Accelrys, *Material studio online help manual*.
33. SCIENCE, L.A., *shock wave Vs sound wave*. Spring/Summer 1985.
34. Thomas, S.-M., *Equations of state*. university of Nevada Las Vegas, 2012.
35. Murnaghan, F.D., *THE COMPRESSIBILITY OF MEDIA UNDER EXTREME PRESSURES*. DEPARTMENT OF MATHEMATICS, THE JOHNS HOPKINS UNIVERSITY, 1944. **30,1944**.
36. BIRCH, F., *Finite Elastic Strain of Cubic Crystals*. Harvard University, Cambridge, Massachusetts, 1947. **71,11**.
37. A.D. Mazzatesta, M.R., H.Sidhu, E.A.Lindgren, *Equation of state of cementitious materials by ultrasonic methodology*. Materials Science and Engineering A251 (1998) 121–128, 1998.
38. Mie-Gruneisen, *Equation of State*.
39. Grujicic, M., et al., *Molecular-level analysis of shock-wave physics and derivation of the Hugoniot relations for soda-lime glass*. Journal of Materials Science, 2011. **46**(22): p. 7298-7312.

40. N.L.Vocadlo, G.D.P., *The Grüneisen parameter via lattice dynamics computer calculations*. Physics of the Earth and Planetary Interiors, 82(1994) 261—270 Elsevier Science B.V., 1993.
41. L. VOCADLO, J.P.P., AND G.D. PRICE, *Grüneisen parameters and isothermal equations of state*. American Mineralogist, Volume 85, 2000.
42. Holt, A. and M. Ross, *Calculations of the Grüneisen Parameter for Some Models of the Solid*. Physical Review B, 1970. **1**(6): p. 2700-2705.
43. Paul Harris, e.a.P.A.D., New Jersey, *SOME PHYSICS OF THE GRUNEISEN PARAMETER*. National Technical Information Service U. S. DEPARTMENT OF COMMERCE, 1972.
44. Preston, L.B.a.D.L., *An Analytic Model of the Grüneisen Parameter at All Densities* Leonid Burakovsky and Dean L. Preston. Los Alamos National Laboratory, 2002.
45. Sanditov, D.S., et al., *On the Grüneisen parameter for crystals and glasses*. Technical Physics, 2009. **54**(3): p. 385-388.
46. Alder, B.J. and T.E. Wainwright, *Studies in Molecular Dynamics. I. General Method*. THE JOURNAL OF CHEMICAL PHYSICS, 1959. **31**(2): p. 459.
47. Grujicic, M., et al., *Multi-Length Scale Modeling of High-Pressure-Induced Phase Transformations in Soda-Lime Glass*. Journal of Materials Engineering and Performance, 2010. **20**(7): p. 1144-1156.
48. Sun, H., *COMPASS: An ab Initio Force-Field Optimized for Condensed-Phase Applications Overview with Details on Alkane and Benzene Compounds*. Molecular Simulations Inc., 9685 Scranton Road, San Diego, California, 1998.
49. Lennard-Jones, J.E., *On the Determination of Molecular Fields*. Proc. R. Soc. Lond, 1924. **A 106 (738): 463–477**, .
50. Haile, J.M., *Molecular Dynamics Simulation: Elementary Methods*. 2001.
51. Cygan, R.T., *Molecular Modeling in Mineralogy*. Sandia National Laboratories, 2001. **vol.39-2001**.
52. Lee, J.G., *Computational Materials Science*, ed. T.F. Group 2012.
53. Ercolessi, F., *A molecular dynamics primer*. University of Udine, Italy, 1997.
54. Theodorou, D.N. and U.W. Suter, *ATOMISTIC MODELING OF MECHANICAL-PROPERTIES OF POLYMERIC GLASSES*. Macromolecules, 1986. **19**(1): p. 139-154.
55. H. J. C. Berendsen, J.P.M.P., W. F. van Gunsteren, A. DiNola, and J. R. Haak, *Molecular dynamics with coupling to an external bath* Journal of Chemical Physics, 1984. **Volume 81**(issu 8).
56. Nose, S., *A MOLECULAR-DYNAMICS METHOD FOR SIMULATIONS IN THE CANONICAL ENSEMBLE* Molecular Physics, 1984. **52**(2): p. 255-268.
57. Hoover, W.G., *Canonical dynamics: Equilibrium phase-space distributions*. Physical Review A, 1985. **31**(3): p. 1695-1697.
58. Parrinello, M. and A. Rahman, *Polymorphic transitions in single crystals: A new molecular dynamics method*. Journal of Applied Physics, 1981. **52**(12): p. 7182-7190.
59. Nic, M.J., J.; Kosata, B. IUPAC Compendium of Chemical Terminology . "modulus of elasticity (Young's modulus), E". 2006.
60. Nic, M.J., J.; Kosata, B., IUPAC Compendium of Chemical Terminology "shear modulus, G". 2006.
61. University., h.G.S., "Bulk Elastic Properties". hyperphysics. Georgia State University.
62. Wisconsin, R.L.u.o., *Poisson's ratio*.

63. Weidong Wu, A.A.-O., M. Alexander H.-D. Cheng, M. and Chung R. Song, M., *Computation of Elastic Properties of Portland Cement Using Molecular Dynamics*. JOURNAL OF NANOMECHANICS AND MICROMECHANICS, 2011. **ASCE / JUNE 2011 Vol. 1, No. 2,**
64. Holuj, F., M. Drozdowski, and M. Czajkowski, *Brillouin spectrum of Ca(OH)<sub>2</sub>*. Solid State Communications, 1985. **56**(12): p. 1019-1021.
65. davidhazy, A., Rochester Institute of Technology.
66. L.Davison, Y.H., *Shock Wave and High Pressure Phenomena*, ed. L. Davison. Vol. chapter 3. 2008
67. Lee Davison, Y.H., *Fundamentals of Shock Wave Propagation in Solids*. Vol. chapter 2. 2008.
68. Henderson, L.F., *General Laws for Propagation of Shock Waves through Matter*. 2001.
69. Pellenq, R.J., et al., *A realistic molecular model of cement hydrates*. Proc Natl Acad Sci U S A, 2009. **106**(38): p. 16102-7.
70. Paskin, A., *Molecular Dynamic Simulations of Shock Waves in a Three-Dimensional Solid*. Journal of Applied Physics, 1972. **43**(4): p. 1605.

## Appendix A

Table 1

*Comparison of Mechanical Property Variations Obtained from Different MD Dynamics Time Analysis*

Mechanical property	Elastic (GPa)		
Cement component	100ps	200ps	300ps
C <sub>3</sub> S	164	124	122
C <sub>2</sub> S	277	279	280
CH	227	147	119
C-S-H Jennite	69	81	59
C-S-H Tobermorite 14	39	46	31
Mechanical property	Bulk (GPa)		
C <sub>3</sub> S	177	165	164
C <sub>2</sub> S	168	170	170
CH	110	102	106
C-S-H Jennite	70	72	73
C-S-H Tobermorite 14	53	43	42
Mechanical property	Shear (GPa)		
C <sub>3</sub> S	61	45	44
C <sub>2</sub> S	113	114	114
CH	98	58	45
C-S-H Jennite	26	31	22
C-S-H Tobermorite 14	14	18	11

Table 2

*C<sub>3</sub>S Mechanical Properties for Various Cell Sizes (Geometric and Molecular Data for the Cell Structures are also Listed)*

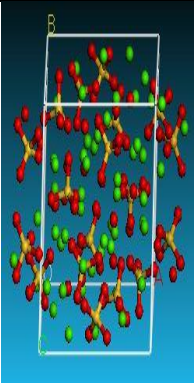
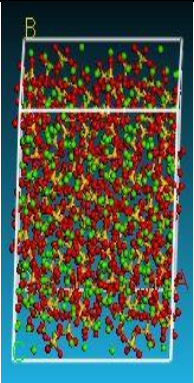
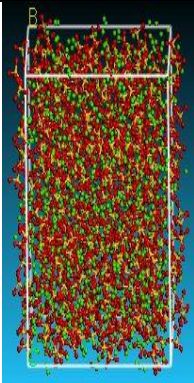
System	C <sub>3</sub> S		
Model	V1	V2	V3
Number of atoms	162	1296	4374
Cell-a (Å)	11.67	23.34	35.01
Cell-b (Å)	14.24	28.48	42.72
Cell-c (Å)	13.72	27.44	41.16
Cell- $\alpha$ (Degrees)	105.5	105.5	105.5
Cell- $\beta$ (Degrees)	94.33	94.33	94.33
Cell- $\gamma$ (Degrees)	90	90	90
Volume (Å <sup>3</sup> )	2280	18240	61560
Molecular structure			
Elastic modulus (GPa)	164	122	129
Bulk modulus (GPa)	177	161	163
Shear modulus (GPa)	61	44	47
Poisson's ratio	0.35	0.37	0.37

Table 3

*C<sub>2</sub>S Mechanical Properties for Various Cell Sizes (Geometric and Molecular Data for the Cell Structures are also Listed)*

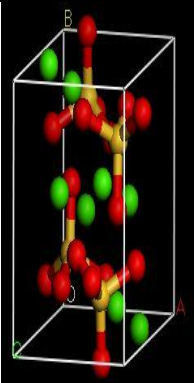
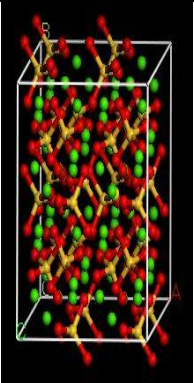
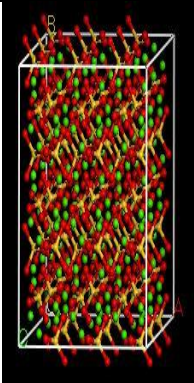
System	C <sub>2</sub> S		
	V1	V2	V3
Model	V1	V2	V3
Number of atoms	28	224	756
Cell-a (Å)	5.48	10.96	16.44
Cell-b (Å)	6.76	13.52	20.28
Cell-c (Å)	9.28	18.56	27.84
Cell- $\alpha$ (Degrees)	90	90	90
Cell- $\beta$ (Degrees)	94.33	94.33	94.33
Cell- $\gamma$ (Degrees)	90	90	90
Volume (Å <sup>3</sup> )	344	2750.2	9282
Molecular structure			
Elastic modulus (GPa)	277	271	271
Bulk modulus (GPa)	168	164	164
Shear modulus (GPa)	113	111	111
Poisson's ratio	0.23	0.22	0.22

Table 4

*CH Mechanical Properties for Various Cell Sizes (Geometric and Molecular Data for the Cell Structures are also Listed)*

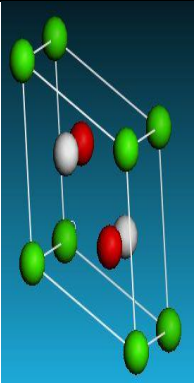
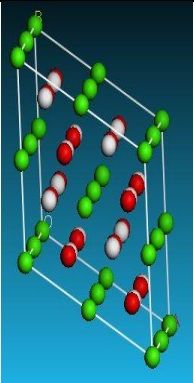
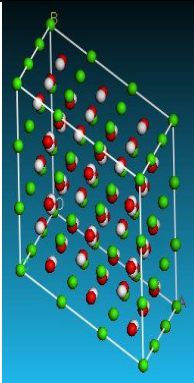
System	CH		
	V1	V2	V3
Model	V1	V2	V3
Number of atoms	5	40	135
Cell-a (Å)	3.59	7.18	10.77
Cell-b (Å)	3.59	7.18	10.77
Cell-c (Å)	4.90	9.81	14.72
Cell- $\alpha$ (Degrees)	90	90	90
Cell- $\beta$ (Degrees)	90	90	90
Cell- $\gamma$ (Degrees)	120	120	120
Volume (Å <sup>3</sup> )	63	505.21	1705
Molecular structure			
Elastic modulus (GPa)	227	259	147
Bulk modulus (GPa)	110	178	170
Shear modulus (GPa)	98	103	54
Poisson's ratio	0.15	0.26	0.36

Table 5

*C-S-H Jennite Mechanical Properties for Various Cell Sizes (Geometric and Molecular Data for the Cell Structures are also Listed)*

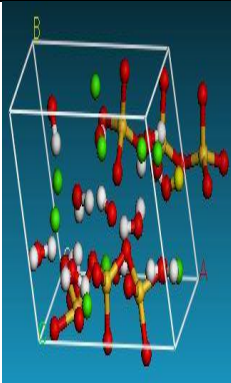
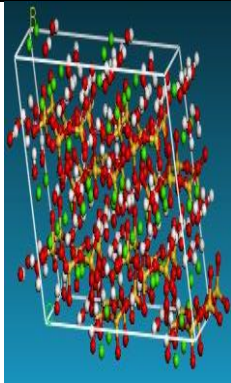
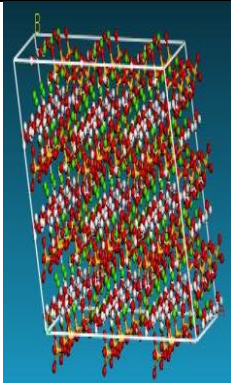
System	C-S-H Jennite		
Model	V1	V2	V3
Number of atoms	68	544	1836
Cell-a (Å)	10.58	21.18	31.74
Cell-b (Å)	7.26	14.52	21.78
Cell-c (Å)	10.93	21.86	32.79
Cell- $\alpha$ (Degrees)	101.3	101.3	101.3
Cell- $\beta$ (Degrees)	96.98	96.98	96.98
Cell- $\gamma$ (Degrees)	109.65	109.65	109.65
Volume (Å <sup>3</sup> )	840	6719	22677
Molecular structure			
Elastic modulus (GPa)	69	67	68
Bulk modulus (GPa)	70	73	73
Shear modulus (GPa)	26	25	25
Poisson's ratio	0.34	0.34	0.34



Table 6

*C-S-H Tobermorite 14 Mechanical Properties for Various Cell Sizes (Geometric and Molecular Data for the Cell Structures are also Listed)*

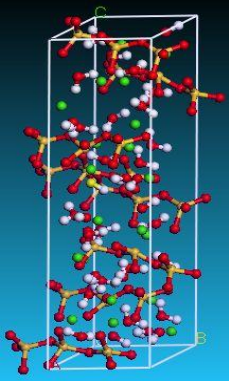
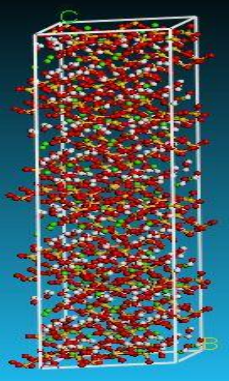
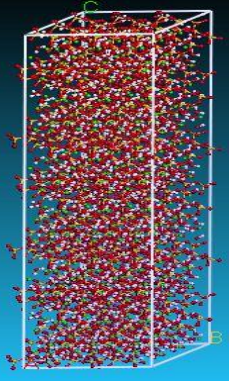
System	C-S-H Tobermorite 14		
Model	V1	V2	V3
Number of atoms	224	1792	6048
Cell-a (Å)	6.735	13.47	20.21
Cell-b (Å)	7.425	14.85	22.27
Cell-c (Å)	27.987	55.97	83.96
Cell- $\alpha$ (Degrees)	90	90	90
Cell- $\beta$ (Degrees)	90	90	90
Cell- $\gamma$ (Degrees)	123.25	123.25	123.25
Volume (Å <sup>3</sup> )	1400	11196	37788
Molecular structure			
Elastic modulus (GPa)	39	38	38
Bulk modulus (GPa)	53	51	52
Shear modulus (GPa)	14	15	13
Poisson's ratio	0.38	0.37	0.37

Table 7

*C<sub>3</sub>S MD Analysis Predicted Mechanical Properties at Different Ensemble State Pressures*

Pressure (GPa)	Elastic	Bulk	shear	Poisson
0.0001	163.7	177.3	60.81	0.3461
0.001	162.4	173.5	60.41	0.344
0.01	159	173.8	58.56	0.3486
0.05	137.4	166.9	50.43	0.3627
0.1	143.5	170.1	52.77	0.3594
0.2	160.9	177.3	59.65	0.3487
0.4	163.8	178.7	60.81	0.3472
0.6	164.3	179.4	60.96	0.3474
0.8	149.1	172.4	54.97	0.3559
1	165	180.8	61.21	0.3479
1.5	166.9	183.7	61.89	0.3486
2	144.4	181.8	52.81	0.3676

Table 8

*C<sub>2</sub>S Mechanical Properties at Different Pressures*

Pressure (GPa)	Elastic	Bulk	shear	Poisson
0.0001	276.5	168.3	112.8	0.2262
0.001	288.2	174.6	117.6	0.2249
0.01	281.3	171.8	114.6	0.2271
0.05	279.1	170.4	113.7	0.227
0.1	280.7	171.7	114.4	0.2266
0.2	284.1	172.7	115.9	0.2258
0.4	281.8	172.6	114.7	0.228
0.6	282.1	171.6	115.0	0.2261
0.8	282.8	173.4	115.1	0.2282
1	286.5	174.8	116.7	0.2268
1.5	287.2	176.2	116.9	0.2283
2	291.8	179.8	118.7	0.2295

Table 9

*CH Mechanical Properties at Various Pressures*

Pressure (GPa)	Elastic	Bulk	Shear	Poisson
0.0001	227.4	109.7	98.47	0.1545
0.001	219.3	104.9	95.22	0.1516
0.01	130.5	105	50.46	0.293
0.05	220.7	104.9	96.05	0.1491
0.1	151.3	104.8	60.06	0.2595
0.2	114.6	99.1	43.82	0.3073
0.4	218.9	106.1	94.66	0.1561
0.6	225.2	109.4	97.32	0.1569
0.8	132.1	101.4	51.23	0.2891
1	130	106.8	50.13	0.297
1.5	140.7	114.8	54.29	0.2958

Table 10

*C-S-H Jennite Mechanical Properties at Various Pressures*

Pressure (GPa)	Elastic	Bulk	Shear	Poisson
0.0001	68.51	70.47	25.6	0.338
0.001	60.22	69.75	22.2	0.3561
0.01	61.47	73.32	22.59	0.3603
0.05	63.98	69.83	23.75	0.3473
0.1	56.72	69.82	20.78	0.3646
0.2	60.28	65.55	22.38	0.3467
0.4	52.54	67.72	19.16	0.3707
0.6	62.53	66.49	23.27	0.3433
0.8	57.41	57.86	21.51	0.3346
1	56.16	60.95	20.86	0.3464
1.5	64.12	68.73	23.84	0.3445
2	70.86	65.32	26.86	0.3192

Table 11

*C-S-H Tobermorite 14 Mechanical Properties vs. Pressure*

Pressure (GPa)	Elastic	Bulk	shear	Poisson
0.0001	39.14	53.04	14.21	0.377
0.001	35.23	36.28	13.16	0.3382
0.01	46.93	43.13	17.91	0.3099
0.05	30.77	42.19	11.16	0.3785
0.1	27.03	42.26	9.697	0.3934
0.2	35.00	43.54	12.81	0.366
0.4	47.47	43.11	18.03	0.3165
0.6	32.35	43.22	11.76	0.3752
0.8	38.17	45.05	14.04	0.3588
1	33.45	44.06	12.18	0.3734
1.5	37.93	43.58	14.00	0.3549
2	35.53	43.2	13.04	0.3629

Table 12

*Cementitious Materials Poisson's Ratio vs. Pressure*

Pressure (GPa)	C <sub>3</sub> S	C <sub>2</sub> S	CH	Jennite	Tober 14
0.0001	0.3461	0.2262	0.1545	0.338	0.377
0.001	0.344	0.2249	0.1516	0.3561	0.3382
0.01	0.3486	0.2271	0.293	0.3603	0.3099
0.1	0.3594	0.2856	0.2595	0.3646	0.35
1	0.3479	0.2268	0.297	0.3464	0.3734
1.5	0.3486	0.2283	0.2958	0.3445	0.3549
2.0	0.3676	0.2295	0.248	0.3192	0.3629